Department of Mechanics, Mathematics and Management
MECHANICAL AND MANAGEMENT ENGINEERING
Ph.D. Program
SSD: ING-IND/08–FLUID MACHINES
ING-INF/07– ELECTRICAL AND ELECTRONIC MEASUREMENTS

Final Dissertation

Advanced Sensors for Diesel Engines

---

by
Dr. Pietro Pappalardi

Supervisors:

Prof. F. Attivissimo

Prof. S.M. Camporeale

Ing. N. Medoro

Coordinator of Ph.D Program:
Prof. G.P. Demelio

Course n°32, 01/04/2017-15/08/2020

LIBERATORIA PER L'ARCHIVIAZIONE DELLA TESI DI DOTTORATO

Al Magnifico Rettore
del Politecnico di Bari

Il sottoscritto PIETRO PAPPALARDI nato ad ALTAMURA (BA) il 17/05/1989
residente a GRAVINA IN PUGLIA (BA) in via LIVORNO 1 e-mail pietro.pappalardi@poliba.it

iscritto al terzo anno di Corso di Dottorato di Ricerca in INGEGNERIA MECCANICA E GESTIONALE ciclo XXXII

ed essendo stato ammesso a sostenere l'esame finale con la prevista discussione della tesi dal titolo:

ADVANCED SENSORS FOR DIESEL ENGINES

DICHIARA

1) di essere consapevole che, ai sensi del D.P.R. n. 445 del 28.12.2000, le dichiarazioni mendaci, la falsità negli atti e l'uso di atti falsi sono puniti ai sensi del codice penale e delle Leggi speciali in materia, e che nel caso ricorressero dette ipotesi, decade fin dall'inizio e senza necessità di nessuna formalità dai benefici conseguenti al provvedimento emanato sulla base di tali dichiarazioni;
2) di essere iscritto al Corso di Dottorato di ricerca INGEGNERIA MECCANICA E GESTIONALE ciclo XXXII, corso attivato ai sensi del "*Regolamento dei Corsi di Dottorato di ricerca del Politecnico di Bari"*, emanato con D.R. n.286 del 01.07.2013;
3) di essere pienamente a conoscenza delle disposizioni contenute nel predetto Regolamento in merito alla procedura di deposito, pubblicazione e autoarchiviazione della tesi di dottorato nell'Archivio Istituzionale ad accesso aperto alla letteratura scientifica;
4) di essere consapevole che attraverso l'autoarchiviazione delle tesi nell'Archivio Istituzionale ad accesso aperto alla letteratura scientifica del Politecnico di Bari (IRIS-POLIBA), l'Ateneo archivierà e renderà consultabile in rete (nel rispetto della Policy di Ateneo di cui al D.R. 642 del 13.11.2015) il testo completo della tesi di dottorato, fatta salva la possibilità di sottoscrizione di apposite licenze per le relative condizioni di utilizzo (di cui al sito http://www.creativecommons.it/Licenze), e fatte salve, altresì, le eventuali esigenze di "embargo", legate a strette considerazioni sulla tutelabilità e sfruttamento industriale/commerciale dei contenuti della tesi, da rappresentarsi mediante compilazione e sottoscrizione del modulo in calce (Richiesta di embargo);
5) che la tesi da depositare in IRIS-POLIBA, in formato digitale (PDF/A) sarà del tutto identica a quelle **consegnate**/inviate/da inviarsi ai componenti della commissione per l'esame finale e a qualsiasi altra copia depositata presso gli Uffici del Politecnico di Bari in forma cartacea o digitale, ovvero a quella da discutere in sede di esame finale, a quella da depositare, a cura dell'Ateneo, presso le Biblioteche Nazionali Centrali di Roma e Firenze e presso tutti gli Uffici competenti per legge al momento del deposito stesso, e che di conseguenza va esclusa qualsiasi responsabilità del Politecnico di Bari per quanto riguarda eventuali errori, imprecisioni o omissioni nei contenuti della tesi;
6) che il contenuto e l'organizzazione della tesi è opera originale realizzata dal sottoscritto e non compromette in alcun modo i diritti di terzi, ivi compresi quelli relativi alla sicurezza dei dati personali; che pertanto il Politecnico di Bari ed i suoi funzionari sono in ogni caso esenti da responsabilità di qualsivoglia natura: civile, amministrativa e penale e saranno dal sottoscritto tenuti indenni da qualsiasi richiesta o rivendicazione da parte di terzi;
7) che il contenuto della tesi non infrange in alcun modo il diritto d'Autore né gli obblighi connessi alla salvaguardia di diritti morali od economici di altri autori o di altri aventi diritto, sia per testi, immagini, foto, tabelle, o altre parti di cui la tesi è composta.

Luogo e data BARI, 27/10/2020 Firma Pietro Pappalardi

Il sottoscritto, con l'autoarchiviazione della propria tesi di dottorato nell'Archivio Istituzionale ad accesso aperto del Politecnico di Bari (POLIBA-IRIS), pur mantenendo su di essa tutti i diritti d'autore, morali ed economici, ai sensi della normativa vigente (Legge 633/1941 e ss.mm.ii.),

CONCEDE

- al Politecnico di Bari il permesso di trasferire l'opera su qualsiasi supporto e di convertirla in qualsiasi formato al fine di una corretta conservazione nel tempo. Il Politecnico di Bari garantisce che non verrà effettuata alcuna modifica al contenuto e alla struttura dell'opera.
- al Politecnico di Bari la possibilità di riprodurre l'opera in più di una copia per fini di sicurezza, back-up e conservazione.

Luogo e data BARI, 27/10/2020 Firma Pietro Pappalardi

Politecnico
di Bari

Course n°32, 01/04/2017-15/08/2020

Department of Mechanics, Mathematics and Management
MECHANICAL AND MANAGEMENT ENGINEERING
Ph.D. Program
SSD: ING-IND/08–FLUID MACHINES
ING-INF/07– ELECTRICAL AND ELECTRONIC MEASUREMENTS

Final Dissertation

Advanced Sensors for Diesel Engines

by
Dr. Pietro Pappalardi

Referees:

Prof. Paolo Carlucci

Prof. Andrea Cataldo

Supervisors:

Prof. Filippo Attivissimo

Prof. S.M. Camporeale

Ing. N. Medoro

Coordinator of Ph.D Program:

Prof. G.P. Demelio

Course n°32, 01/04/2017-15/08/2020

Acknowledgements

Questo dottorato di ricerca rappresenta la massima espressione di multidisciplinarità, in cui ho avuto la fortuna di ampliare il mio raggio d'azione al di fuori della mia caratterizzazione e contaminarmi al punto di dare una dimensione più completa alla parola ingegnere.

Ringrazio il Professore Camporeale per la sua presenza costante e per il supporto tecnico e intellettuale fornitomi in questo percorso.
Ringrazio il Professore Demelio per la sua premura e disponibilità nel ruolo di Coordinatore dei dottorandi.
Ringrazio tutto il team Bosch di CVIT, in particolare l'Ing. Nello Medoro, per il supporto, il training e le conoscenze messe a disposizione nel mio periodo in azienda.
Ringrazio il team Bosch di Schwieberdingen, con cui, sebbene abbia collaborato principalmente in smart working, mi hanno garantito tutto il necessario per poter usufruire delle loro capacità, grazie al confronto continuo con l'Ing. Jan Lino Hanus.

Un sincero, vero e profondo grazie al Gruppo di Misure Elettriche ed Elettroniche. Mi avete adottato e mi avete trasmesso la vostra passione, la vostra conoscenza e la vostra dedizione. Mi avete fatto sentire a casa e arricchito in maniera totale.
Grazie Attilio, sei stato tecnicamente impeccabile in ogni confronto, un supporto prezioso e fondamentale in questo percorso. Un grande amico. Grazie.
Grazie Francesco per i continui confronti e per aver dato una dimensione al significato di ingegnere. Sei l'ingegnere più completo che abbia mai visto.
Grazie Maurizio per la serietà, la disponibilità e l'attenzione che hai sempre avuto verso me stesso e il mio lavoro.
Grazie Prof. Cavone. Oltre alle conoscenze che mi ha trasmesso, conserverò ogni suo consiglio e ogni sua risata.
Ed infine grazie di cuore al Professore Attivissimo. È un grande Professore con uno spirito innovativo. Di lei ho ammirato subito la diplomazia e l'intelligenza con cui affronta il suo ruolo ed i suoi infiniti impegni. Personalmente, Lei è il tutor che ogni dottorando dovrebbe avere per crescere. Grazie perché Lei è stato in tutto questo percorso, un monumento umano

A mio Padre,

esempio indissolubile di una forza di volontà inesauribile.

Diventare almeno metà dell'uomo che sei,

è stata, è e sarà sempre, la mia più grande ambizione.

ABSTRACT

Department of Mechanics, Mathematics and Management

Doctor of Philosophy

Advanced Sensors for Diesel Engines

by

Dr. Pietro Pappalardi

This thesis describes the work inherent in the development of a diesel quality sensor. The work is carried out within an industrial doctorate in partnership with Bosch and aims to constantly monitor the quality of the fuel used in most heavy vehicles, but not only. The reason that drives Bosch to this type of measurement is the deterioration of the diesel fuel pump due to the use of poor-quality fuel.

The final objective is, therefore, the prototyping of an in-line detection system, that is placed on the pipelines for the distribution of diesel, in the pre-feeding system, next to the tank.

Different solutions have been explored and analyzed to find the technique that guaranteed the detection of water in diesel. Microwave and optical techniques have been compared, simulated and analyzed. Several prototypes were made and compared with each other, highlighting good results.

“Life is like riding a bicycle: if you want to stay in balance you have to move”

Albert Einstein

Summary

List of Figures

List of Tables

List of Abbreviations

S_{11}: Input-reflection coefficient (return of signal a_1 to input at port 1)
S_{22}: Output-reflection coefficient (return of signal a_2 to output at port 2)
S_{21}: Forward-transmission coefficient (transmission through to port 2)
S_{12}: Reverse-transmission coefficient (transmission through to port 1)
DUT: Device Under Test
ε: Complex (Relative) Scalar Permittivity
ε': Relative Dielectric Constant
$\varepsilon'' = tan\delta$: Loss Factor
ε_0: Free Space Permittivity
E: Electric Field
D_f: Electric Flux Density
ε_b: Bulk Relative Permittivity
ε_i: Individual Relative Permittivity Values for Each Phase
Φ_i: Volume Fraction of each Phase
TAN: Total Acid Number
T = Transmittance
I: Transmitted Intensity
I_0: Original Intensity
A: Absorbance
Z_0: Characteristic Impedance
D: Inner Diameter of the Shield
d: Diameter of the Core
ε_D: Relative Permittivity of Pure Diesel
ε_W: Relative Permittivity of Water
ρ: Concentration of Water in the Analyte
f_{mnl}: Resonant Frequency
p_{nm}: Value of the Bessel Function for the TE or TM Modes
r: Radius of the Cavity
h: Height of the Cavity
E(t): Electromotive Force
E: Induced Electromotive Force
B: Magnetic Field Intensity
x(t): Vibration Displacement
l_c: Length of the Sensor
I: Exciting Current
N: Number of Turns of the Exciting Coil
L: Half of the Coil Length
R: radius of Coil
x: Distance from Coil Center in Longitudinal Direction
f: Exciting Frequency
N_0: Number of Turns of the Detection Coil
R_a: Radius of the Particle
μ_r: Particle Permeability

INTRODUCTION

Non sono più lo stesso di un secondo fa
Nel mio caso, fidati, pure un secondo fa
Al mattino la mia voce roca brontola
Dice mettici una croce sopra Golgota
And if you call my name
I don't recognize it
If I look at my face
I don't recognize it

Prosopagnosia – Caparezza

The internal combustion engine is a heat engine that converts the chemical energy of a fuel into mechanical energy, usually made available on a rotating output shaft. The liquid fuel used to operate "compression ignition (CI)" engines, is diesel and, recently, biodiesel, or mixtures of the two. Diesel fuel is obtained from crude oil. Crude oil consists of a mixture of hydrocarbons (hydrogen and carbon) and compounds such as benzene, pentane, hexane, heptane, toluene, propane and butane. The type of hydrocarbons obtained will vary based on the original geographic location of the crude oil. Diesel fuel is a complex mixture of liquid hydrocarbons obtained by the fractionation of crude oil. It is used as fuel for diesel engines and injected directly into the combustion chamber after being brought to high pressure and temperature values for compression. The term biodiesel (or more specifically Fatty Acid Methyl Esters), on the other hand, covers a variety of materials from vegetable oils, fats or recycled cooking oils or animal fat. It is obtained by a process of transesterification of fatty acids of vegetable origin with ethyl or methyl alcohol. In a diesel engine fuel system, fuel performs three functions: it provides chemical energy to be transformed into mechanical energy, lubricates precision parts in the fuel system components and cools the metal surfaces that operate in frictional conditions.

The properties or characteristics of diesel fuel must meet these three conditions for the engine to operate reliably. The main properties of diesel fuel that affect engine performance are developable thermal energy, density, specific weight, flash point, volatility, cetane number, viscosity, electrical permittivity, sulphur content, fungi, bacterial contaminants, oxidation and water. The main contaminant that influences the quality of diesel fuel is water which can cause a reduction in the detonation power, a reduction in the efficiency of the engine, corrosion in the fuel system (pumps, injectors) and erosion and clogging of the filter. The admissible quantities are indicated by current regulations.

Fuel control, therefore, is a part of the maintenance operations aimed at extending the life of the engine and is necessary because the developments in diesel, aimed at greater protection of the environment, have led to greater use of biofuels that have physical and chemical properties other than conventional fuels. The analysis of fluids guarantees the optimization of vehicle performance, the prevention of breakdowns, the reduction of emissions and prevents damage to the common rail technology or at least extends its operating life. The problem of dirty diesel has never been completely solved, but only improved with the common rail considering that, the operating pressures are such that the diesel must be of high quality.

The techniques used today to determine the quantity of water are the centrifugal methods and the coulometric titration method of Karl Fischer, which are laboratory techniques. For in-line fuel monitoring, the most promising measurement techniques are resonant cavity dielectric technology,

spectroscopic techniques (UV-Vis, NIR, FT-IR, fluorescence and Raman), interdigitated capacitive sensing technology, ultrasonic and microwave technology. The creation of an automatic system for the optimal management of automotive engines represents a priority topic in the panorama of international industrial research. Vehicle performance depends not only on engine quality but also on fuel characteristics. In this perspective, the on-line measurement of the physical and chemical properties of the fuel and the use of additional functions are essential to face a very competitive market. The use, for that purpose, of optical or microwave technologies seems to be the right way to create a low-cost, precise and real-time measurement detection system.

This research project aims at developing sensors for the analysis of traditional fuel and biofuel, integrated into the fuel system of diesel engines of commercial vehicles and cars. Bosch is the company where the research activity will be carried out. Bosch develops components of the common rail system intended for use on commercial and automotive vehicles, including an innovative electric pump with a controlled delivery. The flow control, carried out using electronic speed regulation, ensures that the flow rate processed by the Diesel injection system downstream of the pre-feed pump can be "dosed" according to the exact fuel requirement in different operating conditions of the engine. This brings advantages in terms of lower fuel consumption, less wear and greater simplicity of the hydraulic circuit for supplying and recycling the fuel since the ducts and filters are sized on a flow rate that is the minimum necessary. This technological change is one of those that are gradually leading to a greater "hybridization" of the diesel engine, through greater use of accessories controlled by electronic devices instead of being connected to the crankshaft, to improve engine performance thanks to electronic control accessories. For years the company has been developing and optimizing the pump in question and intends to increase its potential through additional functions aimed at protecting the engine and improving its efficiency. The research topic will, therefore, concern the development and integration of these "smart functions", the most important of which is the ability to accurately and continuously evaluate the possible presence of water in the fuel. To achieve this goal, a low-cost sensor integrated into the electric pre-supply pump was designed that can detect anomalies in the diesel fuel and deviations from normal operating conditions that achieve a fair compromise between low costs and high reliability required in commercial vehicles, non-contact detection, good precision and reliability, adaptive detection in a wide dynamic range, on-line and on-board monitoring and, finally, supports the implementation of the entire measurement chain in an autonomous embedded system. The research project proposed here, therefore, is intended to be a contribution to improving the performance of vehicles and reducing consumption and harmful emissions into the air. The idea is to develop a device for real-time monitoring of diesel fuel, an objective that with the sensors on the market today it is not possible to pursue both for technological and complexity reasons; indeed, the aggressive nature of diesel fuel, a mixture of aliphatic hydrocarbons and paraffin, on the

one hand, renders the traditional methods based on contact transduction completely unusable, on the other, for safety reasons it is badly reconciled with traditional techniques based on electrical methods and/or magnetic ones. One aspect of the research will, therefore, be the identification of the best technology, which achieves a compromise between low costs and the high reliability required in commercial vehicles. Since the device in question will have to be marketed both in Europe and North America, where diesel fuel has higher purity characteristics and in East Asia, where the concentration of impurities is several orders of magnitude higher, it will be necessary to create a sensor with variable detection in a rather wide dynamic range to favour the absorption effect in the first case and the diffusion effect in the second. Due to the substantial differences in the composition of the diesel fuel in the various areas of the globe and its consequent quality, the pre-feed pumps need to adapt their operation to optimize the engine performance, depending on the type of diesel fuel, to minimize the exhaust gas and to protect the engine components. The sensors located in the tank, of potentiometric or float type, albeit expensive, do not allow to monitor the quality of the fuel but allow only to measure the level. To overcome these limitations, capacitive sensors are being studied that can measure not only the fuel level in the tank but also the possible stratification of the fuel caused by the presence of additives. The main limitation of this technology is that the measurements are carried out by contact with a highly aggressive product (this is even more true for biodiesel) which in the long run produces corrosions on the sensitive parts of the sensor, severely limiting the useful life period.

The innovation of the research will, therefore, concern not only the reduction of costs, but also the resistance in difficult working conditions due to the type of fuel and, especially in commercial vehicles, to vibrations and operating temperatures. The sensor, the result of the research, will present advanced features as it will have to meet the requirements of being real-time, non-contact, low cost, with variable detectivity and with a modular system that can be integrated into the power supply system. Among the various innovative measurement systems that can be possibly developed, those based on non-contact optical methods are particularly interesting because they would allow to avoid the corrosion of the system and to detect the presence of even very small quantities of impurities and contaminants, to avoid damage to the engine, increase combustion efficiency and reduce air pollution.

The ***first chapter*** briefly describes the fuel used in Diesel engines and the contaminants that, most of all, affect the quality of the fuel, with attention to water and metal contamination.

The ***second chapter*** lists the detection techniques that have been explored to achieve the goal, with specific regard to techniques based on microwaves and measurement of permittivity, for the identification of water in diesel. Moreover, in the same chapter a different technique are described to identify solid particles.

The ***third chapter*** describes the mathematical models present in the literature to describe the permittivity for water determination and the inductance for metal determination.

The ***fourth chapter*** reports the preparation and characterization of the samples of diesel-water mixtures used to define an empirical mathematical model for the design, modeling and simulation of the prototypes which will be described and analyzed in the ***fifth chapter***. In the same chapter, the debris sensor will be modeling and simulated for qualitative analyses.

The ***sixth chapter*** reports the experimental results obtained from the prototypes made by comparing the sensitivity and quantitative results of each of them.

The realization of these two sensors aims to broaden the overview of the creation of an intelligent sensor system for a more complete monitoring of diesel quality.

CHAPTER 1

Io sono il disco, non chi lo canta
Sto in una gabbia e mi avvilisco
Il futuro sopprime colui che negli occhi lo guarda
È un basilisco
…
Cerco me stesso, quindi un supporto che ormai nessuno può darmi.

Prisoner 709 - Caparezza

"Never forget your humanity and respect the dignity of other men"

Robert Bosch

CONTAMINANTS IN DIESEL FUEL

1.1 Diesel Engine

Internal combustion engines are driving machines, which aim to convert the largest possible part of the energy released by burning fuels into the machine itself into mechanical work. Diesel engine is one of the most efficient thermal machines. Its efficiency considers fuel consumption for the purpose of determining consumption costs [1]. Besides fuel efficiency, Heavy Duty (HD) diesel engine offers increased reliability and durability. Internal combustion engines have the great advantage with respect to external combustion engines, like steam plants, of having eliminated heat exchangers both between the combustion products and the working fluid and between the latter and the environment. The result is a limitation for the characteristics of the fuels, which must ensure the completion of the combustion process in the appropriate ways and times. On the other hand, however, there a substantial simplification of the system and the elimination of losses inherent in the heat transfer between two fluids with a finished area exchanger. Consequently, due to their simplicity, compactness and high power/weight ratio, these motors quickly established themselves as propulsion systems for transport vehicles and as power generators. In internal combustion engines, the thermal energy that is transformed into mechanical work is provided by the chemical reactions of oxidation of the fuel with the oxygen of the air. These reactions take place in the same engine cylinder and must be completed in a very short time, releasing as much thermal energy as possible, without leaving too much residue and producing toxic substances [2].

Diesel engines have long been the workhorse of industry. Favored for their high torque output, durability, exceptional fuel economy and ability to provide power under a wide range of conditions, diesels are the dominant engines used in applications such as trucking, construction, farming, and mining. They are also extensively used for stationary power generation and marine propulsion and in passenger vehicles in many regions of the world. Thanks to significant improvements in diesel engine

performance, injection technology and exhaust gas aftertreatment devices, particulate matter and nitrogen oxide emissions have been reduced so that diesels are poised to achieve good standards on emissions [1]. Diesel engines are like gasoline engines in many ways. Both are internal combustion engines and most versions of them use a four-stroke cycle [3].

1.2 Diesel Fuel

Diesel fuel is a complex mixture of liquid hydrocarbons obtained by fractionation of crude oil. It is used as fuel for diesel engines and injected directly into the combustion chamber after having been brought to high values pressure for compression. Diesel fuels are the fuels used in diesel or compression ignition engines. In diesel engines, the air is compressed to a high temperature before the fuel is injected into the cylinder to ignite. Compared to spark-ignition engines, a diesel engine is cost-effective because of its operating advantages, greater efficiency, high power output, and fuel economy under all loads. However, it has disadvantages of noise and emissions of particulates and nitrogen oxides (NO*x*). Three grades of diesel fuels are in common use:

- land diesel fuels, used in trucks, buses, trains, or other land transportation vehicles that have a high variation of speed and load.
- marine diesel fuels used in ships that have variable speed but relatively high and uniform load.
- plant diesel fuels used in electric power generation plants that have low or medium speed with the heavy load.

Hence, the quality of diesel fuels depends on the performance requirements of the engines. Today, many diesel fuels are derived from petroleum, although some may come from other fossil fuel resources such as coal liquefaction fractions and through synthesis, such as Fischer-Tropsch distillates. The quality of diesel fuels can vary significantly owing to differences in the crude oils from which the fuels are derived and the refinery process streams from which they are blended.

Analysis of a representative diesel fuel shows that the main components of diesel fuels are saturated and aromatic hydrocarbons. The saturated hydrocarbons dominant in diesel fuels include normal paraffin, iso-paraffins, and cycloparaffins (naphthenes). Normal paraffin has high cetane numbers and are desirable molecules in diesel fuels for combustion. High-boiling normal paraffin, however, cause cold-flow problems if present in excess. Other than isoprenoid hydrocarbons such as pristane

and phytane, most of the iso-paraffins in diesel fuels are mono and dimethyl alkanes, predominantly with branch points near the ends of the alkyl backbone. The remaining saturated hydrocarbons are mainly 1-ring to 3-ring cycloparaffins. The 4- and 5-ring cycloparaffins, such as steranes and hopanes, are rarely present. Aromatic compounds are mainly benzenes, tetralins, indenes, naphthalenes, biphenyls, acenaphthenes, fluorenes, acenaphthalenes, phenanthrenes, anthracenes, and naphthenophenanthrenes. Diaromatic hydrocarbons are generally the most abundant aromatic components in diesel fuels. Trace amounts of PAHs (3C-ring aromatic compounds) such as chrysenes, pyrenes, benzanthracenes, and perylenes can also be present. The most common sulfur compounds are benzothiophenes and dibenzothiophenes. Trace amounts of nitrogen compounds include indoles, carbazoles, quinolines, acridines, and phenanthridines. The oxygen compounds most often reported in diesel fuels are phenols and dibenzofurans. Formulated diesel fuels also contain small amounts of additives, such as cetane improvers, antioxidants, corrosion inhibitors, metal deactivators, dispersants, detergents, lubricity agents, demulsifiers, and cold-flow improvers, to improve storage stability and performance. Many physical and chemical properties of diesel fuel are related to its composition [3], [4].

In general, suitable fuels should meet the following requirements: abundant availability, ease of preparation, low cost and respect for the environment, high calorific value per unit of mass and volume and ease of transport and storage, quick start-up and development of the combustion process, with any ambient temperature. complete combustion without toxic products and absence of carbon deposits on the walls of the combustion chamber and corrosive products.

1.3 Standards for Fuel Control

Fuels are elements with stored potential energy, which by combustion can be released and transformed into different types of mechanical energy. Even though they are met in all three states (liquid, gaseous and solid), the most used ones in vehicles are the liquid fuels. Some of the advantages of liquid fuels are that they can be easy to handle, transport and they can take the shape of any type of container. It is generally acknowledged that fuels have a set of parameters. Lots of them are also mentioned in standards and legislation [5]. The fuel system consists of tank, pump, filter and injectors or carburetor, and has the function of bringing fuel to the engine when necessary. Each component must work perfectly to ensure optimal performance and reliability. The fuel should lubricate precision components and cool metal surfaces that operate under friction conditions so that the engine operates reliably. Fuel control is a part of the maintenance operations carried out with the aim of extending the life of the engine and reducing the environmental pollution. However, the problem of dirty diesel

has not yet been completely solved but only improved with the introduction of the common rail, whose scheme is described in Figure 1.1. It needs working pressures that, nonetheless, require the use of high-quality diesel.

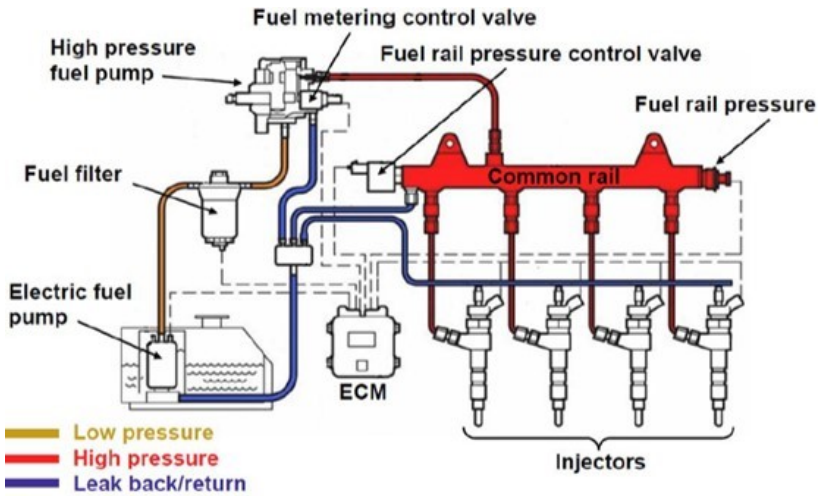

Figure 1.1. Components Overview (example: Bosch EDC 16).

The EN 590 [5] standard prescribes the characteristics that diesel fuel must have to be sold in the European Union and in many other European countries. Setting aside the basic chemical and physical characteristics, the contaminants covered by the standard are different, however, it is utopian to think of developing a system that takes them all into consideration.

Indeed, in agreement with Bosch, the industrial partner of this research, the aim of this work is evaluating the concentration of water in the diesel fuel, as water is primarily responsible for the corrosion of the pipes and the early malfunction of the pre-feed pump. A proof of concept of a measurement system that monitors the concentration of water is required as part of the design of the new pre-feed pump which will be produced and marketed by Bosch soon. In particular, the maximum limit for the concentration of water in diesel fuel is just 200 ppm. Conventionally, and as required also by ISO 12937 [6], the measurements of water concentration in diesel fuel are carried out with the Karl Fischer titration method. However, this technique is unsuitable for online monitoring applications because it requires bulky equipment.

1.4 Water Contamination

Water is commonly found in diesel fuel, due mainly to condensation, handling and environmental conditions. While water is always present in diesel fuel, it is more pronounced in humid areas and

marine applications. However, today's High-Pressure Common Rail (HPCR) fuel systems cannot have even small amounts of water in the injectors. The presence of water in diesel fuel systems may cause the following problems:

- Water causes rust and corrosion of iron components, forming loose particles of iron oxide which contribute to injector wear and component failure.
- At the interface of water and diesel fuel, microbiological growth rapidly occurs under proper conditions. The microbes form a sludge that can plug filters and hinder injector performance. Additionally, the acid excreted by these microbes causes the corrosion of storage tanks and vehicle tanks, which leads to an increase in particles found in fuel.
- Water can overwhelm standard on-engine fuel filtration. Water that makes it past the fuel filtration system to the injector system can cause premature wear and injector failure, since it doesn't have the same lubrication as diesel fuel oil.
- Water in fuel can also lead to premature wear of fuel pumps and other system components that rely upon the lubricating properties of diesel fuel oil.

Biodiesel and bio-oil fuels have become increasingly popular. However, these fuels have a greater affinity to water, and therefore it is more difficult to remove water from them. Additionally, these fuels contribute to the more aggressive growth of microbes. Both issues require the addition of secondary filtration systems to adequately protect modern HPCR systems.

Water is the worst contaminant that affects engine operation. Therefore, fuel control is part of maintenance operations to extend the life of the engine, optimizing performance, preventing breakdowns and reducing fuel consumption and harmful atmospheric emissions.
Their deterioration may be caused using poor-quality fuel. Water is the main contaminant affecting fuel quality, in automotive [2], [7]. Water causes the reduction of lubricating properties, the reduction of engine power and the growth of microorganisms; it influences the combustion process, the wear and the corrosion of the power system, including feed pumps, filters, injectors and pipelines. Water contamination can occur in different ways: during filling of the fuel tank; from vapor condensation; or from a source of contaminated fuel during the refueling process. In the automotive field, the EN 590 standard prescribes the characteristics that fuel must have to be sold in the European Union and in many other European countries. The maximum allowable water limit in fuel is within a range of 200 to about 500 ppm for the automotive field, e.g. 200 ppm according to [5]. Furthermore, the chemical-physical characteristics of fuel varies with the region of origin of the crude oil. Therefore, we must consider different limits in the rest of the world [8]. As prescribed by ISO 12937 [6], water concentration measurements in fuel are executed by the Karl Fischer titration. However, these techniques have the limitation of being performed in the laboratory and therefore cannot provide

online monitoring. In fact, EN ISO 12937 describes the method to be used in determining the water content of petroleum product with boiling points below 390°C, excluding fuel oils and compounds that contain ketones. The method covers water mass fraction concentrations (%(m/m)) between 0,003 % (m/m) to 0,100 % (m/m). The apparatus used for determining water content is comprised of automatic coulometric Karl Fischer titrator, non-aerating mixer, syringes, balance with capacity to weigh ± 0,1 mg, 100 ml volumetric flask, sealable bottles, ovens, cooling bath and thermometer.

Figures 1.2-1.4 show examples of damage caused by the presence of water, like rust, corrosion cavitation and even the broken shaft.

Figure 1.2. Rust and Corrosion [2].

Figure 1.3. Cavitation.

Figure 1.4. Broken Shaft.

Hence, water content is to be considered as an important parameter of diesel fuel, however it represents one of the most common contaminants found in all types of fuels, not only diesel. The main effects of water contamination are to be seen on the injection elements (fuel pipes, fuel pumps, injectors) that are exposed to corrosion and thus on lower combustion quality. Water corrosion will occur only if water is in free form. Fuel properties, like viscosity or density will change when mixed with dissolved water. In general, water causes reduction of lubricating properties, wear and corrosion of fuel system, motor power reduction and growth of bacteria. EN 590 standard allows a concentration of 200 mg/kg of water contamination, which has been proven to be the maximum possible level on most of the markets.

1.5 Metal Contamination

During the last year of research, Bosch has expressed interest in a further problem, the formation of solid particles, inside the feed pump, due to the passage of the diesel flow and metal contamination. These particles cause wear and damage to the pump. Although there is a filter at the pump inlet, we would like to identify these solid particles, to generate an intelligent system of sensors connected in series, to improve the quality of the fuel, on which the operation of the entire fuel system of the engine depends. Wear in one of the main reasons that cause mechanical equipment failures, and numerous wear particles are produced during the device operation.

The sources of metal contamination can be particles generated by wear inside the pump body due to the passage of fuel flow. The sources of contamination are numerous and not even the strictest controls manage to avoid occasional accidents.

Normally the contamination is attributable to four sources:

- Raw materials: Typical examples include metal plates, wheat filaments, sieve threads in powdered materials, tractor pieces in vegetables, fishhooks, staples from containers.
- Personal effects: Buttons, pens, jewels, coins, keys, hair clips, drawing pins, pins, clips, etc.
- Contaminants due to maintenance: screwdrivers and similar tools, swarf and welding scraps following repairs, pieces of copper wires following electrical repairs, various objects left after inaccurate cleaning, or due to carelessness and metal splinters following repairs of pipes.
- Workings inside the plant: The danger of contamination occurs whenever the product is handled or subjected to a process. Crushers, mixers, blenders, slicers, and conveyor systems:

they all do their part. Examples include pieces of broken objects, splinters from milling machines and metal sheets from the returned products.

The identification of the probable source of contamination is an important step in the development of a global metal detection program.

CHAPTER 2

Del giorno in cui mi cadde il mondo addosso
Ricordo tutto, pure l'ora e il posto
Il contraccolpo poi la stretta al collo
La stretta al collo, la stretta al collo
…
A me interessa poco il tuo pianeta bello e vandalo
Piuttosto mi do fuoco, sto più lieta dentro il Tartaro!"
Ed a quel punto sono io che non ci ho visto più

La Caduta di Atlante - Caparezza

"If you want to find something, there is nothing better than searching"

John Ronald Reuel Tolkien

STATE OF ART

2.1 Measurement Techniques for Water Detection

Important requirements of the intended measurement system are that it should work in-line, during engine operation, be of small size and low cost. It may complement other on-board diagnostic systems [9, 10, 11, 12]. A wide variety of measurement systems has been developed to ensure quality and reliability of components [13, 14, 15, 16, 17, 18].

There are two potential families of measurement methods which can be used for online fuel quality monitoring: optical techniques and microwave techniques. Other methods, based on capacitive and resistive sensors, are only able to detect water presence; in addition, corrosion of sensitive parts in contact with the fuel can occur, because it has a very aggressive chemical nature, which makes them unsuitable for in-line monitoring and poses difficulties to the use of electrochemical sensors [19, 20, 21, 22, 23, 24, 25]. For example, interdigitated capacitive sensing technology, show in figure 2.1, uses the fuel as the dielectric material of a capacitor and measures the impedance to output the dielectric constant between different capacitors, to characterize different fuels.

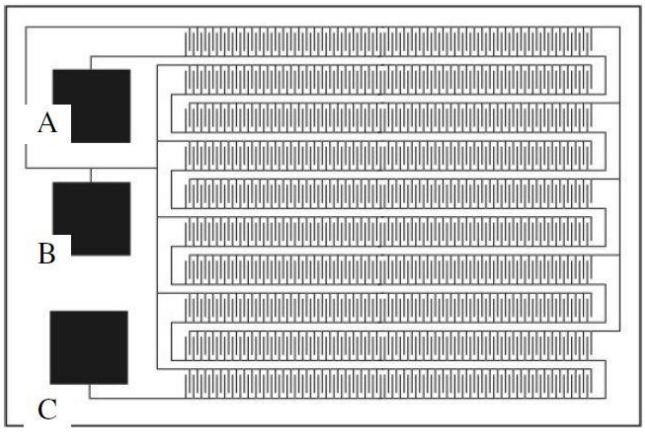

Figure 2.1. Interdigitated Capacitive Sensing Technology.

Methods based on neural networks have also proved useful for quantitative and qualitative evaluation of fluids [26, 27]. Optical measurements (e.g. spectrophotometry, fluorescence spectroscopy, etc.) present evident difficulties in the calibration of an extremely low detection threshold as the one required by previously described standards (examples show in figure 2.2, NIR, and in figure 2.3, Fluorescence). The physical principle of UV-VIS and NIR is based on the absorption of electromagnetic radiations that have wavelengths in the region of about 400-800 nm and 750-2500 nm, respectively. Therefore, it measures the absorption spectrum to describe the physical fluid properties and chemical properties. In fluorescence techniques, a species excited at a higher energy electronic level emits radiation to return to the ground state. The radiation emission is at a wavelength greater than that of excitation, called Stokes Shift. The measured parameters are excitation spectrum and emission spectrum. However, the literature on water absorption spectra is very large [28, 27, 29, 30].

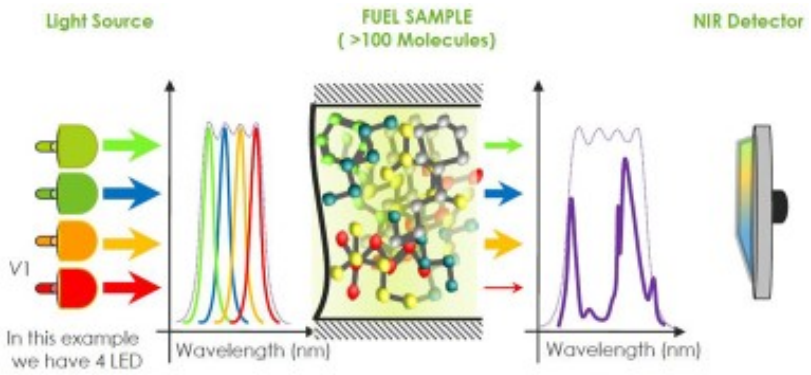

Figure 2.2. NIR Technique.

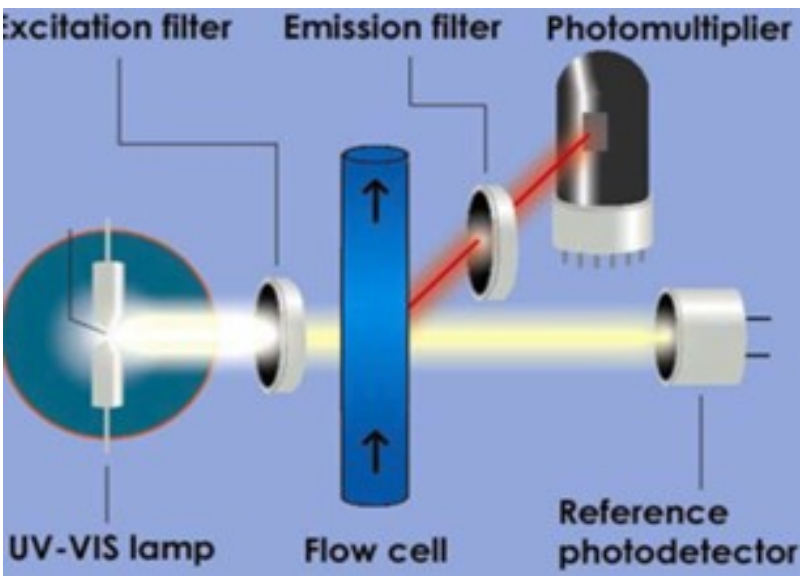

Figure 2.3. Fluorescence Technique.

More complex technologies like the tuning fork technology or the NIR spectroscopy can detect more fluid parameters, and the final algorithms are able to ensure good accuracy and repeatability of measurements. Most of the simpler technologies can be described in some way in terms of the above mentioned ones as regards the working principle or the acquired parameters (e.g. interdigitated capacitive sensing and thermal detection are related to tuning fork [31] (figure. 2.4), while UV-VIS are related to NIR). Considering the total number of measured parameters, the NIR spectroscopy is the technology that is able to read more fuel parameters than the tuning fork technology. Yet, there are NIR sensors on the market that are not able to read, for example, fuel viscosity, a characteristic that the tuning fork can measure, instead. Also, being still under development, there might be that other parameters are not in the required measurement range with the required accuracy.

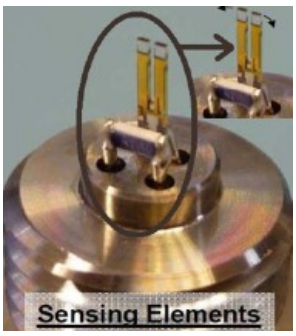

Figure 2.4. Tuning Fork.

In general, an optical system consists of a source and a detector which measures the absorption spectrum of the analyzed sample and extracts the information to be sent to the Engine Control Unit [32, 33].

2.2 Microwave Techniques

Microwaves are electromagnetic radiations with a wavelength between the upper ranges of radio waves and infrared radiation. The microwave spectrum is defined in the frequency range between 1 GHz and 1000 GHz, but other conditions foreseen by the lower frequencies. In most applications the range between 1 and 40 GHz is exploited. Electromagnetic (EM) waves are waves of energy that travel through a vacuum at the speed of light, approximately $c=3\times10^8$ m/s. EM waves consist of two primary components: an electric (E) field and a magnetic (H) field.

Microwave techniques permit to measure an important parameter associated with electromagnetic propagation, namely the complex permittivity of the propagation medium [7, 34, 35, 36]. Time

Domain Reflectometry (TDR) is a technique based on the analysis of the signal traveling along a transmission line and reflected by a generic load [37, 38].

The permittivity of the medium affects how the signal will be reflected, attenuated and transmitted between a source and a receiver. Many factors such as read-out rate, accuracy, convenience, and material shape and form are important in selecting the most appropriate measurement technique. The most used microwave measurement techniques are open-ended probe, transmission line, resonant cavity and free space, with applications that span radar, environmental monitoring and medical imaging [39, 40, 41, 42, 43, 44, 45, 46, 47]. These measurement techniques are different and each one has advantages and disadvantages compared to the others; moreover, it is often difficult to determine which measurement method may perform better for a given material sample, because this choice depends on several factors, such as the nature of the dielectric material to be measured, the frequency of interest and, also, the degree of precision required. Often, electromagnetic properties of media can be measured by means of waveguide transmission lines and coaxial lines [48, 49, 50, 51, 52].

The three most used techniques for the characterization of the permittivity are the coaxial probe, transmission line and resonant cavity.

2.2.1 Coaxial Probe

The open-ended coaxial probe is a cut off section of transmission line. The material is measured by immersing the probe into a liquid or touching it to the flat face of a solid (or powder) material. The fields at the probe end "fringe" into the material and change as they come into contact with the device under test (DUT), see figure 2.5. The reflected signal (S_{11}) can be measured and related to ε_r. A typical measurement system using a coaxial probe method consists of a network analyzer or impedance analyzer, software to calculate permittivity, and a coaxial probe, probe stand and cable [53]. It is the easiest method to use for liquids, or soft semi-solids, even if very flat hard solids can be measured.

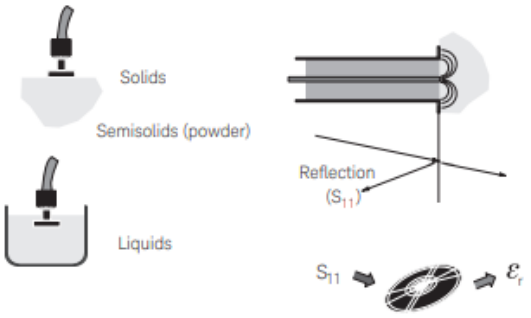

Figure 2.5. Coaxial Probe Method.

2.2.2 Transmission Line

Transmission line methods involve placing the material inside a portion of an enclosed transmission line. The line is usually a section of a rectangular waveguide or coaxial airline, see figure 10. ε_r and μ_r are computed from the measurement of the reflected signal (S_{11}) and transmitted signal (S_{21}).

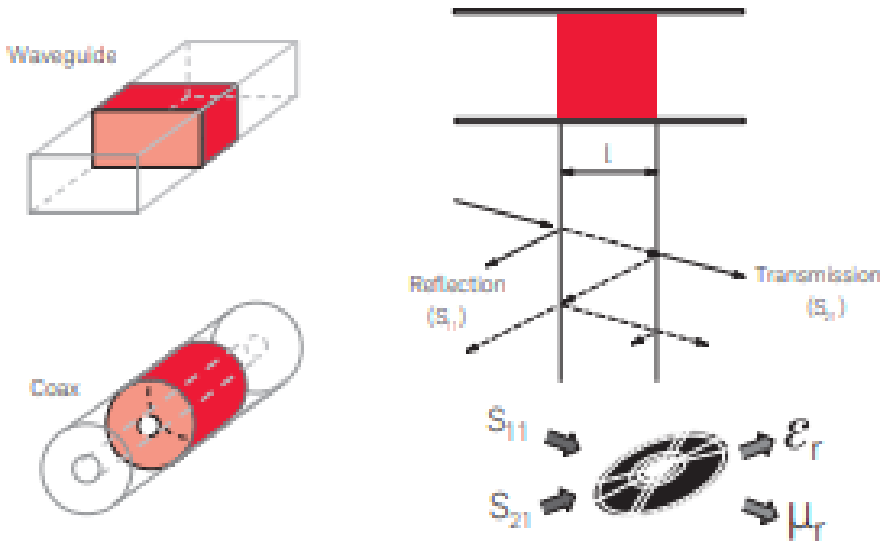

Figure 2.6. Transmission Line Method.

Coaxial transmission lines cover a broad frequency range. Waveguide fixtures extend to the mm-wave frequencies and the samples are simpler to machine, but their frequency coverage is banded. A typical measurement system using the transmission line method consists of a vector network analyzer, a coaxial or waveguide transmission line, and software to calculate permittivity and permeability. There are various transmission techniques for measuring the dielectric properties of dielectric samples. The main advantage of the transmission techniques is the swept frequency capability. The transmission techniques can be further divided into two categories too. The first is the distributed transmission method, in which the S_{11} and S_{21} parameters are measured for the calculations of dielectric properties. The other is the lumped impedance method in which the calculations of dielectric properties are based on the circuit theory and the electric field in the measured sample is assumed to be uniform, i.e., under low frequency condition.

A transverse loaded dielectric slab or disk can be bounded by a waveguide for the distributed transmission method. The measurement parameters are transmission signal (S_{21}) and reflection signal (S_{11}). The application of both S_{11} and S_{21} to calculate the dielectric properties is called S_{11} and S_{21} transmission and reflection technique. The limitation on the measurement of permittivity is based on the thickness of the sample. The thickness should be less than one half of the wavelength to avoid

resonance. However, the loss measurement is only valid for tanδ >10^{-2}. For material with loss tangent less than 10^{-2}, the decay for the S_{11} and S_{21} is too small to be precisely detected by the measurement instrument.

The parameter that will be evaluated is the attenuation of the transmission line. Each transmission has some losses, since the resistance of the conductors and of the power is consumed in the dielectric used to isolate the conductors. The power lost in a transmission line is not directly proportional to the length of the line but varies exponentially with the length. Line losses are usually presented in terms of decibels per unit of length. The losses in the transmission line are due to the following causes: radiation, dielectric losses, loss of the skin effect. The skin effect occurs in conductors carrying an alternating current. As the frequency increases, the current tends to be concentrated near the surface of the conductor, and the skin effect becomes more pronounced and the loss in the conductors increases dramatically. Hence, that loss is due to the non-homogeneous distribution of the current caused by the skin effect. For a perfect coaxial cable, the resistance of the skin is proportional to the square root of the frequency. Moreover, there is the dielectric loss which is due to the absorbent electrical energy since it is polarized in every direction. It occurs when the conductance is different from zero. Dielectrics have increasing losses when the voltage on the conductors is increased. Dielectric losses also increase with frequency as the shunt conductance increases approximately linearly with frequency.

In the preliminary design, the diameter of the inner cylinder has been determined from the condition that the characteristic impedance of the Kopecky coaxial line [54], Equation (2.1), should be equal to 50 Ω:

$$Z_0 = \frac{1}{2\pi}\sqrt{\frac{\mu}{\varepsilon}}\ln\left(\frac{D}{d}\right) \qquad (2.1)$$

where μ and ε are the permeability and permittivity of the medium inside the Kopecky coaxial line, respectively, while D is the internal diameter of the external conductor and d is the outer diameter of the inner conductor. The 50 Ω condition is necessary to obtain impedance matching with the measurement device, which has a standard 50 Ω SMA connector.

2.2.3 Resonant Cavity

This method uses a resonant cavity for sample support and a network analyzer to measure the resonance frequency and quality factor of the cavity, in two conditions: when it is empty and when

the sample is present. From this we can calculate permittivity (Figure 2.7). This method has the best loss factor resolution. Resonant cavities are high quality factor (Q) structures that resonate at specific frequencies. A piece of sample material inserted into the cavity affects the resonant frequency (f) and Q. From these parameters, the complex permittivity of the material can be calculated at a single frequency. A typical measurement system consists of a network analyzer, a resonant cavity fixture and software to make the calculations.

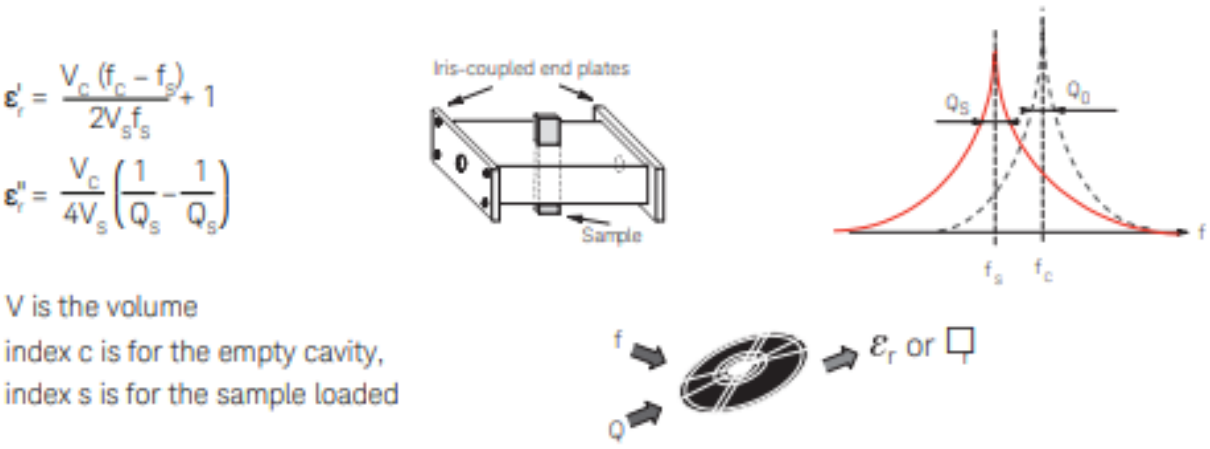

Figure 2.7. Resonant Cavity Measurement.

There are many parameters that affect results accuracy for dielectric materials measurements. Q-value is one of the most important factors for estimating the quality of the cavity resonator, as a high Q-value gives high accuracy and narrow bandwidth. The effects of the Q-value can be conditioned by many factors, e.g. the metallic material for building cavity resonator, the filled material inside cavity, the coupling device and the transverse modes. However, these conditions can be fixed by design. On the other hand, the effects of the coupled external circuit also needs to be taken into account: indeed, when the external circuit is connected to the cavity resonator, the measured Q-value will no longer be the original Q-value (Q_0), which will be hanged to the loaded Q-value (Q_L).

Therefore, the accuracy of the measured results for the dielectric samples depends on the accuracy of the Q-values. The dielectric sample also needs to be fabricated to a property size so that when the sample is fully placed in the cavity resonator the critical coupled occurring [55].
Generally, the cavity resonator can be constructed from a circular waveguide shorted at both ends or built by a cylindrical metal box, i.e. a cylindrical cavity resonator [56]. The basic concept of the circular waveguide and the cylindrical cavity resonator are similar. An illustration for the cylindrical cavity resonator is given in figure 2.8. Inside the cavity resonator, the electric and magnetic fields exist, the total energies of the electric and magnetic field are stored within the cavity, and the power

can be dissipated in the metal wall of the cavity resonator as well as the filled dielectric material. Besides, the filled dielectric material will affect the resonant frequency and Q-value. The transverse modes used in the cavity resonators are the TE and TM mode, which will provide the different dimensions, resonant frequencies and Q-values. For the use of the cavity resonator, it has to be excited via a coupling device. The energy is transmitted from the external equipment to the cavity via the coupling device.

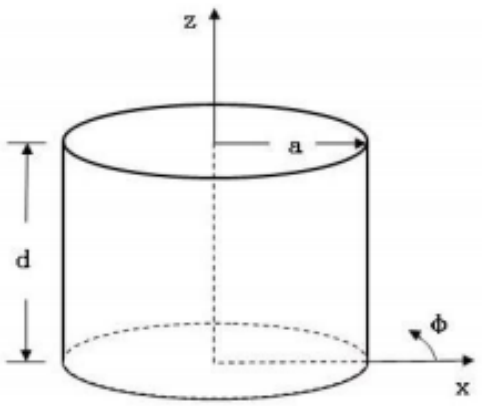

Figure 2.8. Cylindrical Cavity Resonator.

The resonant frequency operates in the cavity resonator and have to be higher than the cut off frequency when it is operating. Basically, the resonant frequency is related to the dimension of the cavity and the filling materials. Equation (2.2) gives the derivation of the resonant frequency [57]:

$$f_{mnl} = \frac{c}{2\pi\sqrt{\mu_r \varepsilon_r}} \sqrt{\left(\frac{p_{nm}}{a}\right)^2 + \left(\frac{l\pi}{d}\right)^2} \qquad (2.2)$$

where f_{mnl} is the operation frequency of the cylindrical cavity resonator, c is the speed of light, μ_r is the permittivity of the filled material inside the cylindrical cavity resonator, ε_r is the permeability of the filled material inside the cylindrical cavity resonator, d is the height of the cylindrical cavity resonator and a is the radius of the cylindrical cavity resonator.

The coupling devices are used for transferring the energy from the feed line to the resonator. If the method of the reflection coefficient is used, only one coupling device is needed, and two when the method of transmission coefficient is used. Coupling holes are designed in a waveguide which is used as the feeding transmission line. The coupling probe is formed by extending the feeding coaxial cable with a small distance into the cavity resonator. Finally, the coupling loop is formed by extending the

feeding coaxial cable, at a given distance, into the cavity resonator and bent and grounded on the cavity wall. The center of the loop is located midway between the top and the bottom walls of the cavity.

2.2.3.1 Cavity Perturbation Technique

In practical applications, cavity resonators are normally modified by making small changes to the cavity volume or introducing a small dielectric sample. To achieve that, the cavity resonators can be tuned with a small screw that enters the cavity volume, or by changing the size of the cavity resonator. The other way involves the measurement of the permittivity by determining the shift of the resonant frequency when a small dielectric sample is inserted into the cavity. The perturbation method assumes that the actual fields of a cavity with a small shape or material perturbation are not greatly different from those of the unperturbed cavity.

There is an equation 2.3 for the change in resonant frequency due to material perturbations. If we assume that $\Delta\epsilon$ and $\Delta\mu$ are small, then we can approximate the perturbed $\bar{E}$, $\bar{H}$ by the original fields $\bar{E}_0$, $\bar{H}_0$, to give the fractional change in resonant frequency as [58]:

$$\frac{f - f_0}{f_0} = \frac{-\int_{V_0} (\Delta\epsilon|\bar{E}_0|^2 + \Delta\mu|H_0|^2)dv}{\int_{V_0} (\epsilon|\bar{E}_0|^2 + \mu|H_0|^2)dv} \tag{2.3}$$

This result show that any increase in ϵ at any point in the cavity will decrease the resonant frequency.

2.2.4 Comparison of Methods

Many factors such as accuracy, convenience, and the material shape and form are important in selecting the most appropriate measurement technique. Some of the most significant factors to consider are summarized here:

- Frequency range
- Expected values of ε_r and μ_r
- Required measurement accuracy
- Material properties (i.e., homogeneous, isotropic)
- Form of material (i.e., liquid, powder, solid, sheet)
- Sample size restrictions

- Destructive or non-destructive
- Contacting or non-contacting
- Temperature
- Cost

Figure 2.9 provides a quick comparison between the measurement methods that have been discussed already.

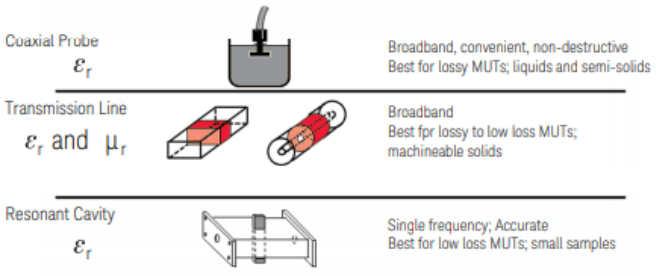

Figure 2.9. Summary of the Measurement Techniques.

Other noteworthy methods are explained in the following paragraphs.

2.2.5 Re-Entrant Cavity

The re-entrant microwave cavity (RMC) is a very attractive sensor for dielectric characterization of small (mL to µL) liquid volumes due to the high concentration of electric field in its gap region. The structure is also easy to manufacture and retains a high quality (Q) factor (~3000) even when machined from aluminum. Unlike the electric field, the associated magnetic field magnitude is small and spread over a much larger volume, leading to low surface loss on the exposed metal surfaces, hence the high Q. These desirable features (high Q, high concentration of electric field in the gap) contribute to a high-performance dielectric sensor, as will be demonstrated. A cross section of the RMC is shown in Figure 2.10, showing the electric field distribution.

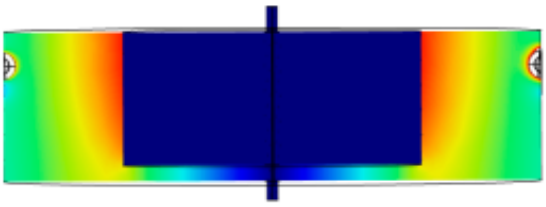

Figure 2.10. Cross Section of a Re-entrant Microwave Cavity.

Re-entrant cavities can be modeled using a lumped-element approximation in the limit when the gap dimension is small compared with the other dimensions of the cavity and with the resonant wavelength λo. The electric field concentrates in the gap between the center post and the cavity wall and its direction from the inner post points to the cavity wall, perpendicular to the two surfaces of the gap thus formed. If the gap region is small, then the electric field in the gap will be approximately uniform and the magnetic field will be infinitesimally small near the axis. This region acts like a parallel-plate capacitor, its capacitance being inversely proportional to the gap width [59].

2.2.6 Substrate Integrated Waveguide Re-Entrant Cavity

Substrate integrated waveguide (SIW) technology, realized through rows of metallic via-hole arrays or grooves embedded in a dielectric substrate whose upper and lower surfaces are covered by metal plates, has attracted increasing attention in the last few years. This technology makes it possible to design the re-entrant cavities in planar forms that can be readily fabricated using standard printed circuit board (PCB) or low-temperature co-fired ceramic (LTCC) technology. The SIW re-entrant cavities not only inherit the advantages of traditional cavities such as high Q-factor and high-power capacity, but also provide the merits of low cost, low profile and easy fabrication. More importantly, their planar configurations make them much easier to be monolithically integrated with other planar circuits and systems (without any other costly and sophisticated transition). The sensor consists (figure 2.11) of two parts, namely the SIW re-entrant cavity resonator design and the microfluidic subsystem design. The primary objective for the cavity design is to obtain a compact size as well as a high Q-factor, while for microfluidic subsystem, it is to achieve a high sensitivity [60].

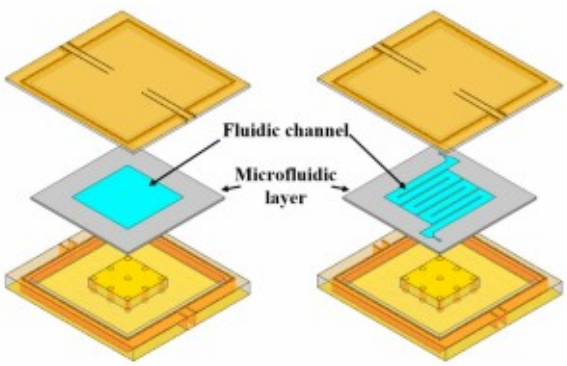

Figure 2.11. Substrate Integrated Waveguide Re-Entrant Cavity.

2.3 Measurement Techniques for Metal Detection

In the literature, there are several solutions used for monitoring solid particles in liquids. The most important techniques are briefly listed [95, 96, 97, 98, 99, 100].

2.3.1 Capillary Hydrodynamic Fractionation

The motion of particles near 1 μm and below in size follows a very distinct pattern when the liquid containing them is forced through capillary tubes. A combination of Brownian motion and liquid boundary effects, associated with the very fine capillaries used, causes the larger particles to flow faster than the smaller ones, and a definite pattern is detectable (Fig. 2.12).

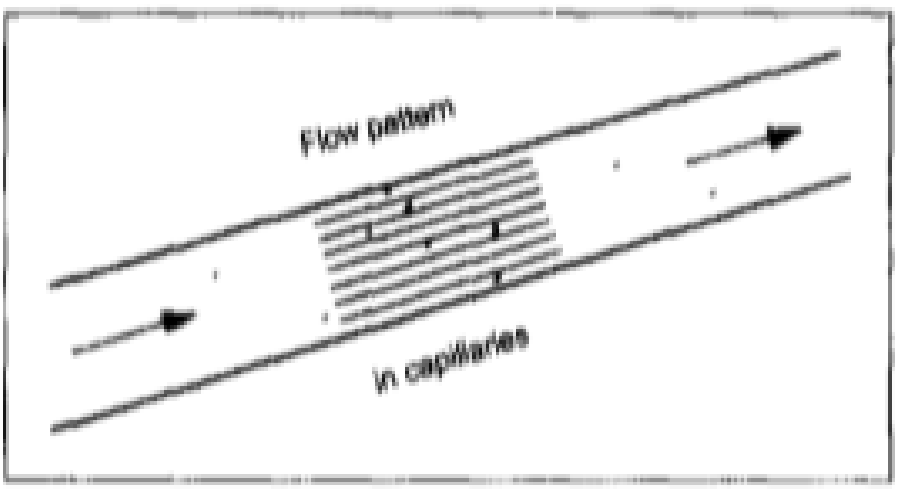

Figure 2.12. Capillary Hydrodynamic Fractionation.

2.3.2 Electrical Sensing Zone (Coulter)

This technique is unusual in that it can determine the particle 'size' in terms of the true volume of the particle. As each particle passes through a small orifice or tube, so the electrical resistance between the two ends of the liquid column in the tube is changed. The technique will only work for electrically conducting liquids, but most particle types can be detected. It is currently used only as a laboratory method (Fig. 2.13).

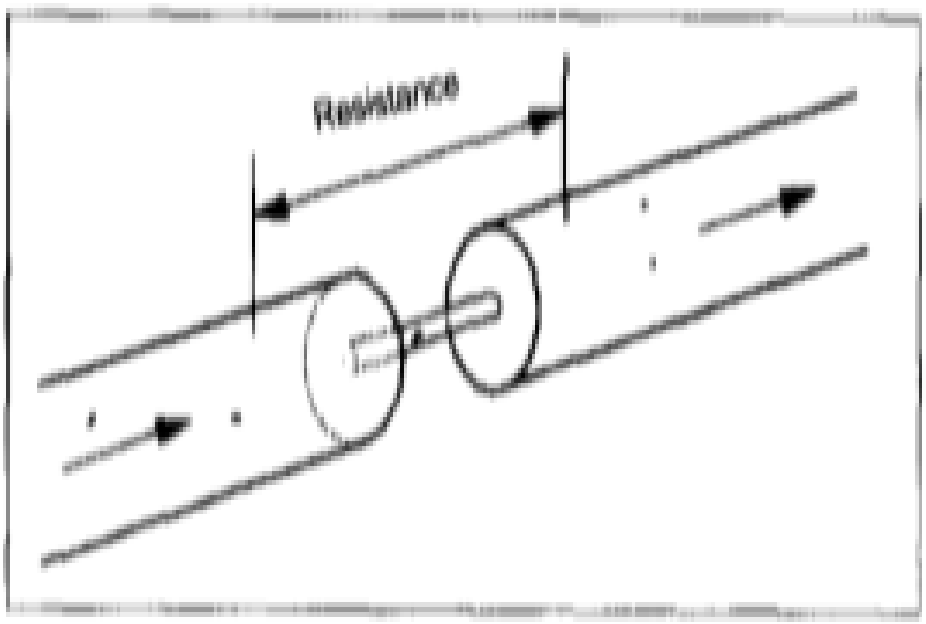

Figure 2.13. Electrical Sensing Zone (Coulter).

2.2.3 Electroacoustic

An alternating electric field, at varying frequency (in the megahertz band), is applied to the volume of liquid. By measuring the magnitude and phase angle of the sound wave produced by the particles, it is possible to determine both the particle size and the effective charge (zeta potential). A large range of particle concentrations is measurable, from 0.5% to above 40%, but the particles must have been charged (Fig. 2.14).

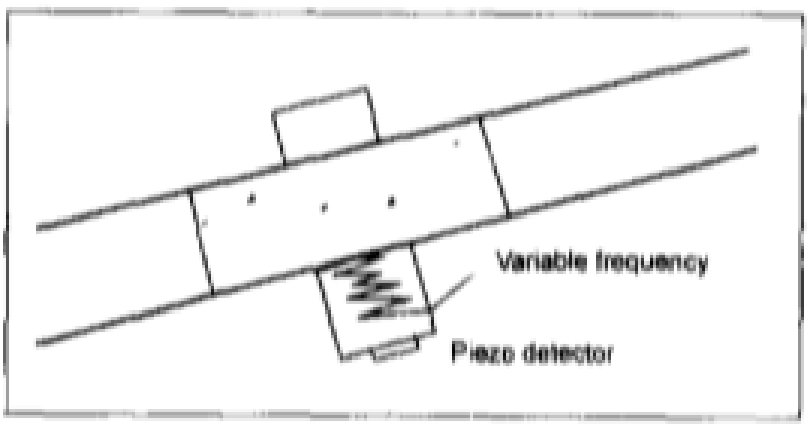

Figure 2.14. Electroacoustic.

2.2.4 Filter Blockage

This technique can be used both on-line and off-line with no restriction on fluid mixes or particle types. By merely sensing the change in flow characteristics (flow and pressure drop), the level of particle count associated with the pore size of the filter can be determined (continuous operation occurs when the flow is reversed and the filter backflushed). Several refined filters can be fitted, and a particle distribution obtained (Fig. 2.15).

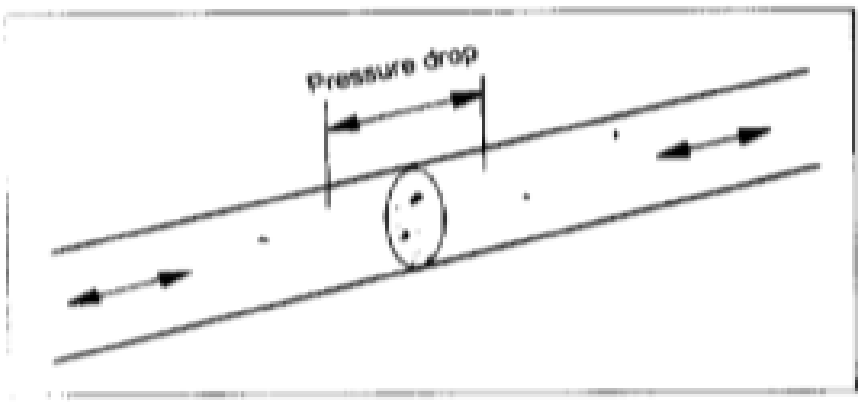

Figure 2.15. Filter Blockage (Mesh Obscuration).

2.2.5 Magnetic Attraction

There are numerous devices which may either trap particles, magnetically or otherwise, or sense them either statically or as they pass, by detecting a change in the magnetic flux. Only the presence of ferromagnetic particles can be accurately determined. These devices do not normally give a particle count, but rather provide an overall view of the 'large' and 'small' particulates present (Fig. 2.16).

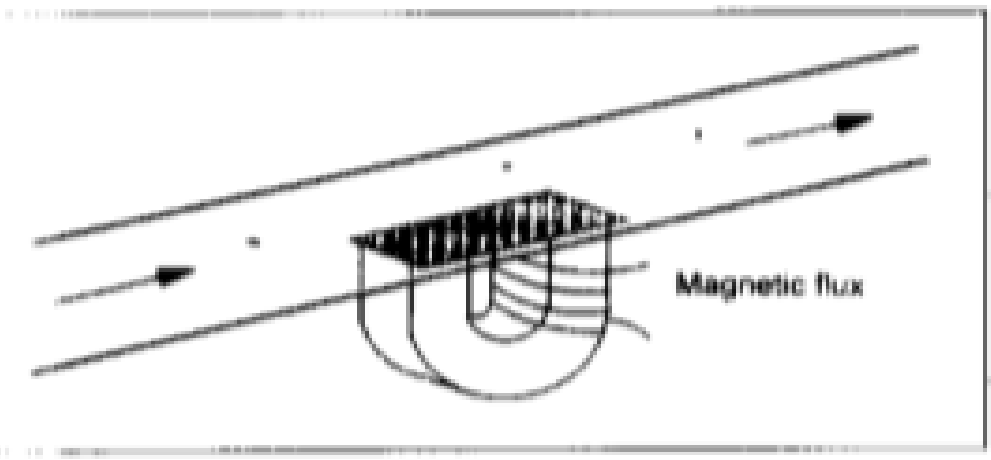

Figure 2.16. Magnetic Attraction.

2.2.6 Optical Method

The optical method includes a pair of light transmitter and receiver, operating with the light passing through the fluid. Since the light could be blocked by debris particles, the change of light intensity may reflect the size of the debris particle (Fig. 2.17).

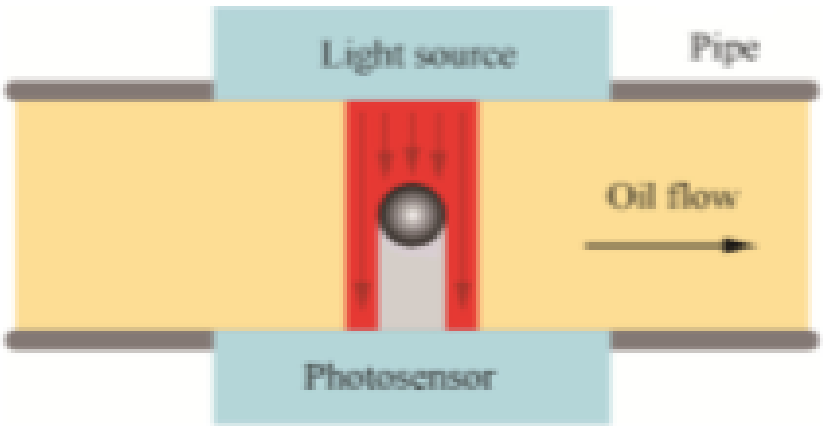

Figure 2.17. Optical Method.

There are many instruments based on the Fraunhofer detection method. They are designed to obtain a very accurate assessment of the particle distribution from 0.1 μm upwards, and some instruments can detect even smaller particles. An array of detectors receives the light rays, diffracted forwards according to the size of the particles, the smaller the particle, the greater the diffraction (Fig. 2.18).

Light obscuration is the simplest type of light-based instrument, looking solely at the shadows cast when particles pass through the light beam. Much work has been undertaken to reduce the probability of more than one particle being counted at any one time (Fig. 2.19).

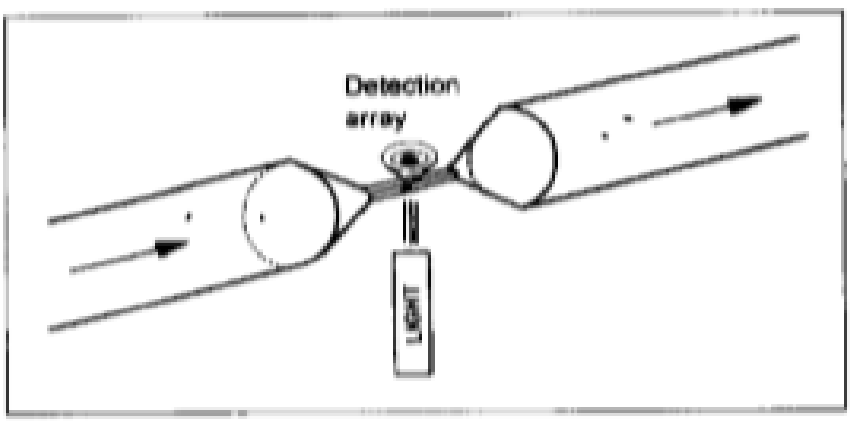

Figure 2.18. Fraunhofer Detection Method.

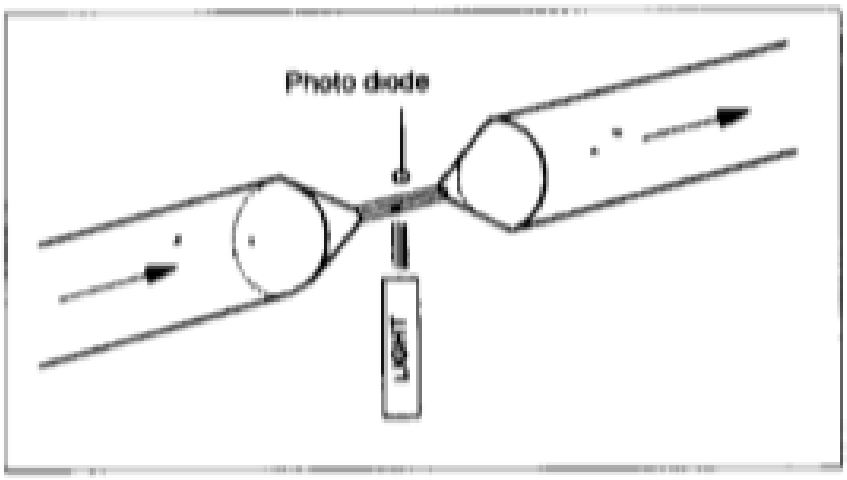

Figure 2.19. Light Obscuration.

2.2.7 Acoustic Sensors

The acoustic method (Fig. 2.20) is composed of an acoustic transmitter and an acoustic receiver, which are placed in oil so that the acoustic wave can penetrate through the flow. A debris particle would distort a part of the wave transmitted into the sensor. Therefore, the strengths of both transmitted waves and reflected waves could be detected in a channel of 6.5 mm by 6.5 mm, and bubbles could be distinguished from solid debris by the phase of a received wave. However, this method is difficult to be applied in the real system because viscosity, flow speed, and mechanical vibration all may affect its performance.

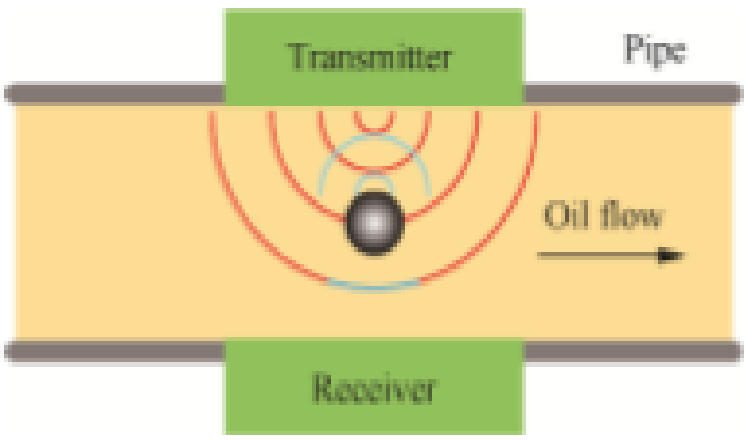

Figure 2.20. Acoustic Sensor.

2.2.8 Ultrasonic Sensors

Ultrasonic monitoring devices are also based on the principle of the Doppler Effect. A source in the sensor emits a high-frequency ultrasonic signal through the flow. The signal is reflected to the receiver from the contaminants, debris particles and turbulence in the flow. Scattering and absorption mechanisms are the primary causes of the attenuation of an ultrasonic wave as it propagates through a medium. The frequency is proportional to the flow velocity and can be converted into voltage or current. The technique is very sensitive to the positioning of the transducer as it will be influenced by the acoustic emissions from background sources and the signal attenuation varies with the temperature of the flow. However, they can measure particle sizes as small as 3 μm and are simple, cost-effective, and robust in use (Fig.2.21).

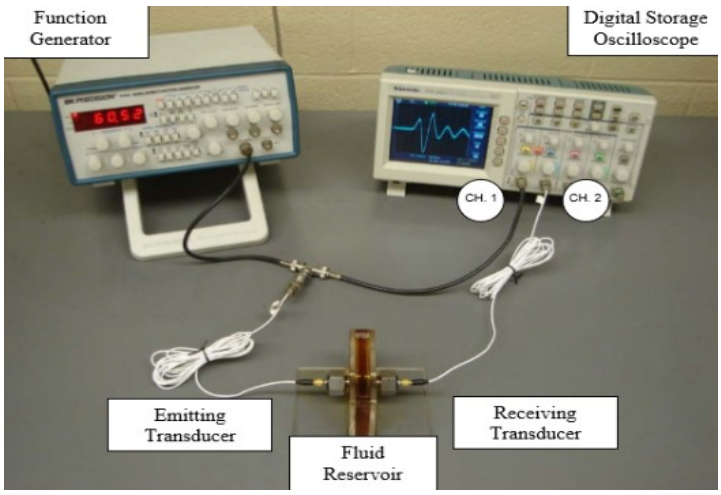

Figure 2.21. Ultrasonic Sensor.

2.2.9 Comparison of Methods

The way to decide which instrument is best for a particular application will depend on the user's priorities. On the other hand, because of the high costs involved, one would expect much more care in the choice. The following is a suggested order of decision-making, which will vary slightly with the application:

1. What size of particle is expected (or particle size range)?
2. What liquid is the particle immersed in (or mixed liquids)?
3. Decide where the instrument is to be used, and by whom.
4. What special hazards may be present (such as air, vibration, shock, etc.)?

Following that guidelines, the sensor that we decided to design for our purposes is based on the physical principle of inductance.

CHAPTER 3

Passo alla meditazione ma dura per poco
Io di natura nervoso
Il tipo di uomo che recita il Sutra del loto
Poi dopo si butta nel vuoto
Vorrei raggiungere il Nirvana
Come loro, idem
Raggiungere i Nirvana
Non il loro leader
Infedele quanto vuoi
Ma giuro sono mite
Anche se sembro roccia
Con il cuore Dolomite

Confusianesimo – Caparezza

"I was looking for a new image of the world that would give meaning to our grayness and be worth all the beauty that was lost, saving it. A new face in the world."

Italo Calvino

MEASUREMENT PARAMETERS

3.1 Sensor Characterizations

A sensor can perform multiple energy conversions before producing a signal at its output that is easy to process, transmit and represent. The analysis of the characteristics of a sensor requires only the study of the relationships between the stimuli and the responses of the device without the need to examine the energy transformation processes taking place inside it. Therefore, we will look at the sensor as a "black-box" examining just the input-output relationships of the device. For each sensor, there is an ideal input-output relationship that allows obtaining the "true" value of the stimulus at the output. It is obvious that this never occurs in the real case. This ideal function is expressed in the form of a mathematical equation, a table or a graph: it can be linear or non-linear. In real operation, the sensor describes a characteristic that differs from the ideal function. To consider the inaccuracy of the device, it is necessary to measure the deviations existing between the real values and the ideal values.

A complete characterization of the sensor requires the description of the following characteristics:

1. Static: describe the performance of the sensor in normal conditions with slow variations of the input and in the absence of external stresses.
2. Dynamics: describe the behavior of the sensor to changes in the input with the time.
3. Environmental: refer to the performance of the sensor after exposure or during exposure to specific external stresses.
4. Reliability: relate to the useful life of the sensor.

In this thesis, the parameter to be measured will be the permittivity.

3.2 Permittivity (Water Detection)

Permittivity is a physical quantity that describes how an electric field affects and is influenced by a dielectric medium and is determined by the ability of a material to polarize in response to an applied electric field, and therefore to partially erase the field inside of the material. Permittivity, therefore, refers to the ability of a material to transmit (or "allow") an electric field. The permittivity of a material is usually provided with respect to that of the vacuum, as a relative permittivity, (also called a dielectric constant in some cases).

The most used techniques for measuring dielectric properties at microwave frequencies include open probe methods, transmission methods, resonant cavity methods and free space methods that use horn waveguides. Each of these measurement techniques can be designed to operate in a specific microwave frequency range. The appropriate measurement techniques for each application depend on the dielectric properties of the materials to be measured, the physical state of the materials (solid, semi-solid or liquid), the frequency range and the degree of precision required. The microwave electromagnetic radiation spectrum lies within a frequency range of 108 to 1011 Hz with wavelengths of 0.3-300 cm. More specifically, the frequency range of microwaves is generally considered to be in the range of 1 GHz to 30 GHz. An important parameter associated with electromagnetic propagation is the complex permittivity of the propagation medium. The permittivity of the medium influences how the signal will be reflected, attenuated and transmitted between a source and a receiver. An electromagnetic field can interact with matter by transforming part of its energy into thermal energy. The origin and extent of the energy transformation are linked to the response to the applied field of the microscopic charges present in the matter. Dielectric losses of the material at the origin of which there are polarization phenomena that take place under the action of the field contribute mainly to the generation of heat in the microwave band.

The behavior of a material towards electromagnetic waves depends on the complex (relative) scalar permittivity ε, (eq. 3.1):

$$\varepsilon = \varepsilon' - j\varepsilon'' \tag{3.1}$$

with ε' relative dielectric constant and ε'' loss factor which takes into account dielectric losses. Furthermore, we define a loss tangent, in equation 3.2:

$$\tan\delta = \frac{\varepsilon''}{\varepsilon'} \tag{3.2}$$

The complex permittivity depends on the frequency, on the temperature (generally with increasing temperature ε′ increases while ε′′ can increase or decrease), density of the material and composition and structure of the material. At macroscopic level the complex permittivity,ε, can be expressed in the following way, equation 3.3:

$$\varepsilon = \varepsilon' - j\varepsilon'' = \varepsilon_0(\varepsilon_r' - j\varepsilon_r'') \qquad (3.3)$$

For the realization of the method described in the model section it is important to analyze the above equation. The electric field interacts with the material in two ways: storing energy and dissipating energy. The ability of a material to store electric energy from the electric field is described by the real part of the permittivity ε_r'. The ability of a material to dissipate electric energy from the electric field is described by the imaginary part of the permittivity ε_r''. Both ε_r' and ε_r'' are dimensionless parameters. An analogous demonstration can be made for the permeability [70].

Dielectric constant (k) is equivalent to relative permittivity (ε_r) or the absolute permittivity (ε) relative to the permittivity of free space (ε_0). The real part of permittivity (ε_r') is a measure of how much energy from an external electric field is stored in a material. The imaginary part of permittivity (ε_r'') is called the loss factor and is a measure of how dissipative or lossy a material is to an external electric field. The imaginary part of permittivity (ε_r'') is always greater than zero and is usually much smaller than (ε_r'). The loss factor (Fig. 24) includes the effects of both dielectric loss and conductivity. When complex permittivity is drawn as a simple vector diagram, the real and imaginary components are 90° out of phase. The vector sum forms an angle δ with the real axis (ε_r'). The relative loss of a material is the ratio of the energy lost to the energy stored. The loss tangent or tan δ is defined as the ratio of the imaginary part of the dielectric constant to the real part. D denotes dissipation factor and Q is quality factor. The loss tangent tan δ is called tangent loss or dissipation factor (Fig. 3.1). Sometimes the term “quality factor or Q-factor” is used with respect to an electronic microwave material, which is the reciprocal of the loss tangent. For very low loss materials, since tan δ ≈ δ, the loss tangent can be expressed in angle units, milliradians or microradians [71, 72].

$$\tan\delta = \frac{\varepsilon_r''}{\varepsilon_r} = D = \frac{1}{Q} = \frac{\text{Energy lost per cycle}}{\text{Energy stored per cycle}}$$

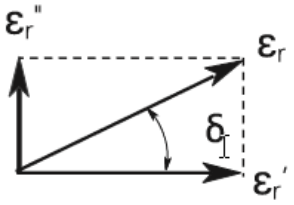

Figure 3.1. Loss Tangent Vector Diagram.

3.2.1 Dielectric Theory

A wide variety of industries need a better understanding of the materials they are working with to shorten design cycles, improve incoming inspection, process monitoring, and quality assurance. Every material has a unique set of electrical characteristics that are dependent on its dielectric properties. Accurate measurements of these properties can provide scientists and engineers with valuable information to properly incorporate the material into its intended application for more solid designs or to monitor a manufacturing process for improved quality control. A dielectric materials measurement can provide critical design parameter information for many electronics applications.

The material properties that will be discussed here are permittivity and permeability. It is important to note that permittivity and permeability are not constant. They can change with frequency, temperature, orientation, mixture, pressure, and molecular structure of the material. A material is classified as “dielectric” if it can store energy when an external electric field is applied.

If a DC voltage source (Fig. 3.2) is placed across a parallel plate capacitor, more charge is stored when a dielectric material is between the plates than if no material (a vacuum) is between the plates. The dielectric material increases the storage capacity of the capacitor by neutralizing charges at the electrodes, which ordinarily would contribute to the external field. The capacitance with the dielectric material is related to dielectric constant. Where C and C_0 are capacitance with and without dielectric, $k' = \varepsilon_r'$ is the real dielectric constant or permittivity, and A and t are the area of the capacitor plates and the distance between them.

$$C_0 = \frac{A}{t}$$

$$C = C_0 \kappa'$$

$$\kappa' = \varepsilon_r' = \frac{C}{C_0}$$

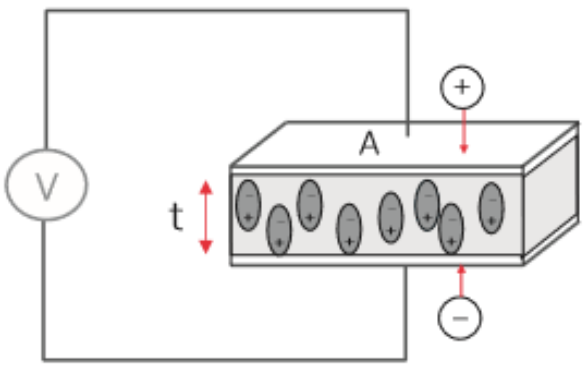

Figure 3.2. Parallel Plate Capacitor, DC case.

If an AC sinusoidal (Fig. 3.3) voltage source V is placed across the same capacitor, the resulting current will be made up of a charging current I_c and a loss current Il that is related to the dielectric

constant. The losses in the material can be represented as a conductance (G) in parallel with a capacitor (C).

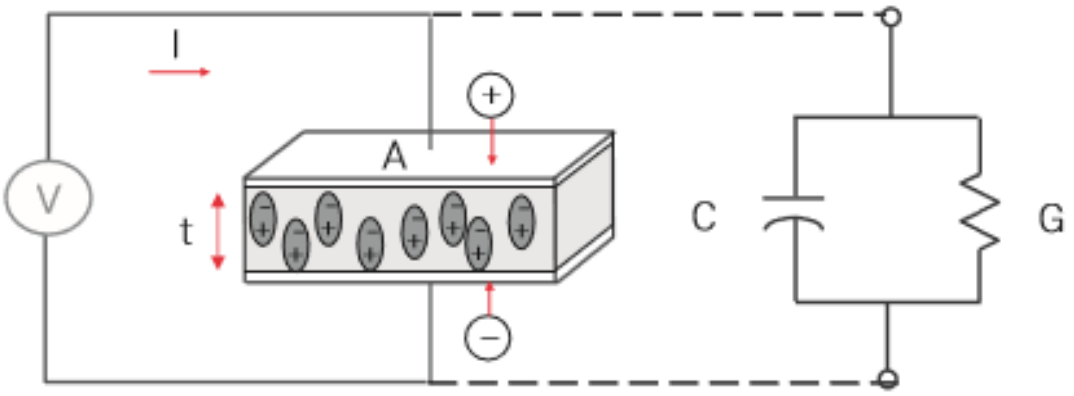

Figure 3.3. Parallel Plate Capacitor, AC case.

The complex dielectric constant k consists of a real part ε_r' which represents the storage and an imaginary part ε_r'' which represents the loss. From the point of view of electromagnetic theory, the definition of electric displacement (electric flux density) D_f is (eq. 4.4):

$$D_f = \varepsilon E \qquad (3.4)$$

where $\varepsilon = \varepsilon_0 \varepsilon_r$ is the absolute permittivity (or permittivity), ε_r is the relative permittivity, $\varepsilon_0 = \frac{1}{36}\pi 10^{-9}$ [F/m] is the free space permittivity and E is the electric field.

3.2.2 Electromagnetic Wave Propagation

In the time-varying case, electric fields and magnetic fields appear together. This electromagnetic wave can propagate through free space (at the speed of light, c = 3 x 10^8 m/s) or through materials at slower speed. Electromagnetic waves of various wavelengths exist. The wavelength l of a signal is inversely proportional to its frequency f ($\lambda = c/f$), such that as the frequency increases, the wavelength decreases.

Many aspects of wave propagation are dependent on the permittivity and permeability of a material. Let's use the "optical view" of dielectric behavior. Consider a flat slab of material (MUT) in space, with a TEM wave incident on its surface. There will be incident, reflected and transmitted waves. Since the impedance of the wave in the material Z is different (lower) from the free space impedance η (or Z_0) there will be impedance mismatch, and this will create the reflected wave. Part of the energy

will penetrate the sample (Fig. 3.4). Once in the slab, the wave velocity v is slower than the speed of light c. The wavelength λ_d is shorter than the wavelength λ_0 in free space according to the equations below. Since the material will always have some loss, there will be attenuation or insertion loss.

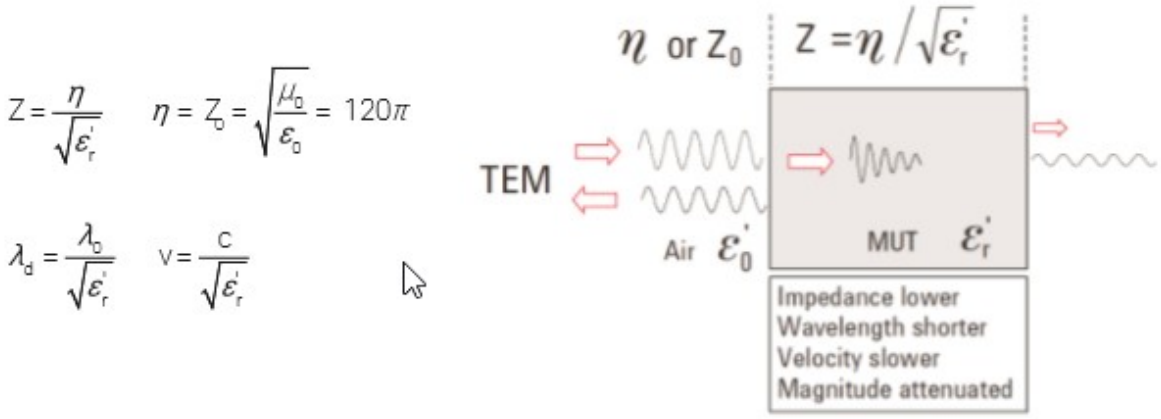

Figure 3.4. Wave Propagation.

Before the dielectric properties of a material can be measured with network analyzer, impedance analyzer, or LCR meter, a measurement fixture (or sample holder) is required to apply the electromagnetic fields in a predictable way and to allow connection to the measurement instrument. The type of fixture required will depend on the chosen measurement technique and the physical properties of the material (solid, liquid, powder, gas) [72].

3.2.3 Dielectric Mechanism

A material may have several dielectric mechanisms or polarization effects that contribute to its overall permittivity. A dielectric material has an arrangement of electric charge carriers that can be displaced by an electric field. The charges become polarized to compensate for the electric field such that the positive and negative charges move in opposite directions, like showed in figure 3.5.

At the microscopic level, several dielectric mechanisms can contribute to dielectric behavior. Dipole orientation and ionic conduction interact strongly at microwave frequencies. Water molecules, for example, are permanent dipoles, which rotate to follow an alternating electric field. These mechanisms are quite lossy which explains why food heats in a microwave oven. Atomic and electronic mechanisms are relatively weak, and usually constant over the microwave region. Each dielectric mechanism has a characteristic cutoff frequency. As frequency increases, the slow mechanisms drop out in turn, leaving the faster ones to contribute to ε_r'. The loss factor (ε_r'') will

correspondingly peak at each critical frequency. The magnitude and cut-off frequency of each mechanism is unique for different materials.

A resonant effect is usually associated with electronic or atomic polarization. A relaxation effect is usually associated with orientation polarization [72].

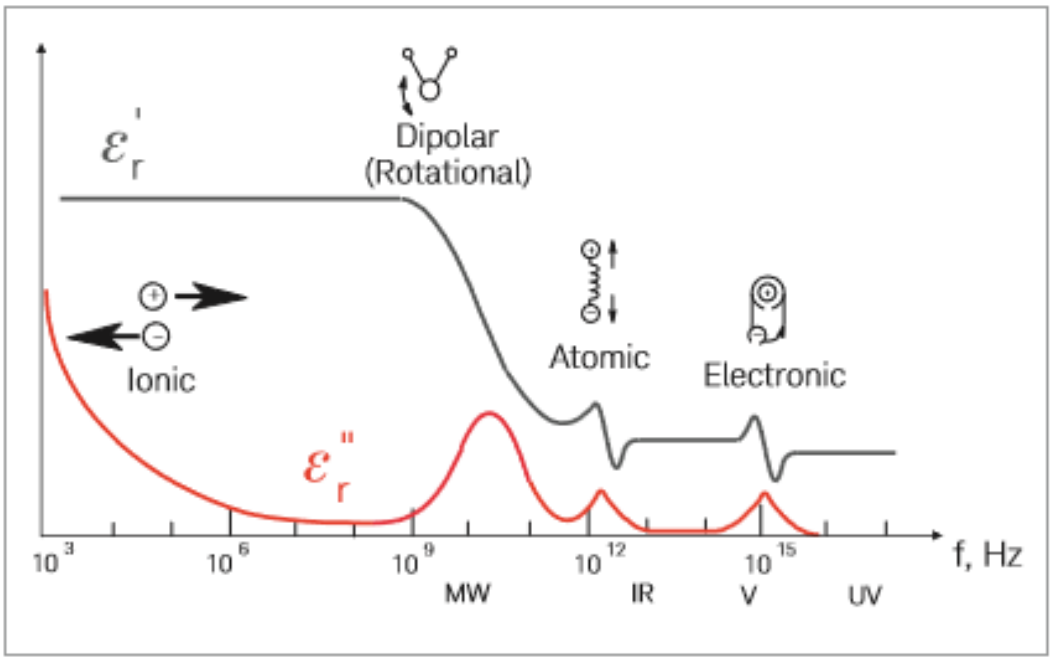

Figure 3.5. Frequency Response of Dielectric Mechanism.

3.2.4 Variation of Properties with Fuel Composition

The versatility of diesel engines with respect to the fuel they may combust places a requirement on any reliable fuel sensing system that it be able to detect and distinguish between a wide range of fuels. Consequently, a review of research related to how the chemical composition of fuel affects its bulk properties was necessitated Although the process of refining and distributing fuel is highly regulated in the United States fuels occasionally become contaminated through unintended consequences of transport and storage. The presence of contaminants could have significant impacts on the fuel pumping and injection systems, combustion, or exhaust gas after-treatment within a diesel engine. Consequently, there is a critical need for a fuel sensor to detect contaminants and extend the lifetime of a diesel engine [7, 73].

Dielectric permittivity is an important parameter for indirect determination of water content diesel fuel using electromagnetic methods. Among the approaches used for determination of the relationship

between the relative permittivity and volumetric water content, the use of purely empirical models and mixing models are often found on the literature. Mixing models are a class of models that relate the composite dielectric number of a multiphase mixture to the dielectric numbers and volume fractions of its constituents based on their geometrical arrangement. Thus, they offer an advantage over purely empirical models in that at least some of the mathematical coefficients involved have a physical meaning.

The effective or bulk relative permittivity (ε_b) of a porous material can be modelled using a class of models known as mixing models, which predict ε_b based on the individual relative permittivity values for each phase (ε_i). One of the simplest forms of mixing models is given by:

$$\varepsilon_b^{\alpha} = \sum_{i=1}^{n} \Phi_i \varepsilon_i^{\alpha} \tag{3.5}$$

here Φ_i is the volume fraction of each phase (cm^3*cm^{-3}), and α is a dimensionless fitting parameter.

3.2.5 Single-Phase Dielectric Mixing Model

For land surface remote sensing, two mixing theories have been proposed, namely the 'dielectric average' originally proposed by Brown [74, 75]:

$$\varepsilon_{eff} = \sum_{j=1}^{m} v_j \varepsilon_j \tag{3.6}$$

A further refinement proposed by Ansoult et al. [76] and by Dobson et al. [77] is the empirical modification of Equation (3.5) with an exponent α, the so-called 'shape factor', according to:

$$\varepsilon_{eff}^{\alpha} = \sum_{j=1}^{m} v_j \varepsilon_j^{\alpha} \tag{3.7}$$

3.2.6 The Mixing Formula

Many mixing formulas have been reported in the literature [78, 79, 80, 81, 75, 82, 83, 84, 85, 86] since the early work of Rayleigh [87]. Some of these formulas were examined with the measured data on the mixtures of conducting particles in a pure dielectric host [88]. Poe, Stogryn, and Edgerton [89] also tested a few of these formulas with some measured data of soil permittivity moisture variations. However, the data used by Poe et al. were measured only at a few moisture values. As a result, it was difficult to assess whether any of the mixing formulas they examined had provided an adequate description on the dielectric behavior of soil-water mixtures. Table II gives a list of the mixing formulas considered to be adequate for a comparison with the experimental data acquired in recent years. Most of these formulas dealt only with a mixture of two constituents. They basically implied a direct dependence of the mixture dielectric constant ε on the dielectric constants (ε_1 and ε_2) and the volume fractions (f_1 and f_2) of the constituents.

The study of dielectric constant and conductivity of binary mixtures of liquids is important, both from the point of view of dielectric theory and practical applications. Several formulas are available for the calculation of dielectric constant of mixture of liquids, but these appertain essentially to the dielectric constant at Dc or low frequency alternating voltage. Further, the formulas available are independent of temperature and therefore they are presumably applicable at room temperature or at a given constant temperature. If one wishes to calculate the dielectric constant of the mixture at any other temperature measurements on the individual components have to be carried out at the appropriate temperature and the mixtures formulas applied. In this paper, experimental results on the dielectric properties of silicone fluid and water free methanol are reported. The results are compared with the results obtained by calculations using the formulas quoted above. A new formula for the calculation of the dielectric constant based on the fundamental properties of the individual components has been suggested.

In macroscopic approach, many formulas are available for calculating the dielectric constant of the mixtures if the dielectric constants of the individual components at the same temperature are known. Denoting the two components by subscripts 1 and 2, we summarize some formulas as below (eq.3.8 – 3.13):

1. Lichtenecker Formula:

$$\varepsilon_m = \exp\left(V_1 \log \varepsilon_1 + V_2 \log \varepsilon_2\right) \qquad (3.8)$$

2. Raleighs Formula:

$$\varepsilon_m = \varepsilon_1 \frac{\frac{2\varepsilon_1+\varepsilon_2}{\varepsilon_2-\varepsilon_1} + 2V_2 - \frac{1.575(\varepsilon_2-\varepsilon_1)}{4\varepsilon_1+3\varepsilon_2} V_2^{10/3}}{\frac{2\varepsilon_1+\varepsilon_2}{\varepsilon_2-\varepsilon_1} - V_2 - \frac{1.575(\varepsilon_2-\varepsilon_1)}{4\varepsilon_1+3\varepsilon_2} V_2^{10/3}} \tag{3.9}$$

3. Formula of Meredith and Tobias:

$$\varepsilon_m = \varepsilon_1 \frac{\frac{2\varepsilon_1+\varepsilon_2}{\varepsilon_2-\varepsilon_1} + 2V_2 - \frac{1.277(\varepsilon_2+2\varepsilon_1)}{4\varepsilon_1+3\varepsilon_2} V_2^{7/3} - \frac{6.399(\varepsilon_2-\varepsilon_1)}{4\varepsilon_1+3\varepsilon_2} V_2^{10/3}}{\frac{2\varepsilon_1+\varepsilon_2}{\varepsilon_2-\varepsilon_1} - V_2 - \frac{1.277(\varepsilon_2+2\varepsilon_1)}{4\varepsilon_1+3\varepsilon_2} V_2^{7/3} - \frac{2.718(\varepsilon_2-\varepsilon_1)}{4\varepsilon_1+3\varepsilon_2} V_2^{10/3}} \tag{3.10}$$

4. Bruggeman's Formula

$$\frac{\varepsilon_2-\varepsilon_m}{\varepsilon_2-\varepsilon_1}\left(\frac{\varepsilon_1}{\varepsilon_m}\right)^{1/3} = 1 - V_2 \tag{3.11}$$

5. Looyenga's Formula

$$\varepsilon_m = \left[\varepsilon_1^{1/3} + V_2(\varepsilon_2^{1/3} - \varepsilon_1^{1/3})\right]^3 \tag{3.12}$$

6. Bottcher Formula

$$\varepsilon_m = \varepsilon_1 + \frac{3V_2\varepsilon_m(\varepsilon_2-\varepsilon_1)}{2\varepsilon_m+\varepsilon_2} \tag{3.13}$$

3.2.7 Theoretical Model – Initial Approach

Dielectric constant must be as close as possible to that of pure fuel because we want o not significantly to disturb the propagation of the stimulus signal.

$$\varepsilon_{blend} = \varepsilon_{B0} + \frac{\varepsilon_{B100} - \varepsilon_{B0}}{100} * B\% \quad (3.14)$$

For the preliminary simulations, a very simple mathematical model was chosen to express the dielectric constant of the analyte as a function of the water concentration (B%). Remembering that the dielectric constant varies with the amount of water and therefore the impedance of the cable also varies. There is an impedance mismatch in the interface with source and meter. Therefore, the noise increases. One last trick regards the electromagnetic field which must exhibit a limit of 1 MV/m because there might be a risk of ionization, i.e. the dielectric might lead.

3.3 Inductance (Metal Detection)

The inductive method is based on electromagnetic induction, in which debris particles will cause a corresponding inductive voltage and an inductance change in coils when the particles go through the sensor. In this method, the inductive voltage and inductance change are proportional to the debris size, and different materials such as ferromagnetic and diamagnetic ones will cause different signature phases. Consequently, the inductive method can provide information about debris sizes and materials. Inductive sensors have the advantage of detecting both ferrous metal and nonferrous metal particles. It also has the advantage of an on-line monitoring capability with an inductive coil as the sensing element. The debris may also be removed from the carrier fluid and placed between the sensing areas of the inductive coils causing an imbalance in the measurement. The electronics along with a microprocessor are a part of the on-line sensing. The disadvantage of this method is that if a ferrous and a non-ferrous particle appear at the same time, the effect nullifies each other, and no particle is detected. The changes in inductance monitored are small and hence the measurement circuitry must be extremely sensitive to very small variations.

This principle can be explained by looking at two coils a transmission coil (Tx), with an alternating current applied to it, and a receiving coil (Rx), in which a current will be induced, described in figure

3.6. The voltage signal in the Rx coil is proportional to the relative areas, geometry and displacement of both coils. However, as seen in capacitive techniques, other factors can also influence the behavior of the coils. One of them is temperature, but its effect can be neutralized by using multiple Rx coils and calculating the position from the ratio of the received signals (similar to a differential transformer). Therefore, if a temperature change occurs, the effect is canceled because the signal ratio is not changed for a given position. Unlike capacitive techniques, inductive methods are less influenced by foreign material such as dirt or water. The coils can be positioned at relatively large distances, installation accuracy is not a major problem and the main components of the sensors can be mounted with relatively relaxed tolerances. In their construction, a series of wound conductors or coils are used and must be carefully wrapped to obtain an accurate position measurement. To obtain strong electrical signals, a considerable number of coils must be wound. This wound coil structure makes traditional inductive position sensors heavy, bulky, and expensive.

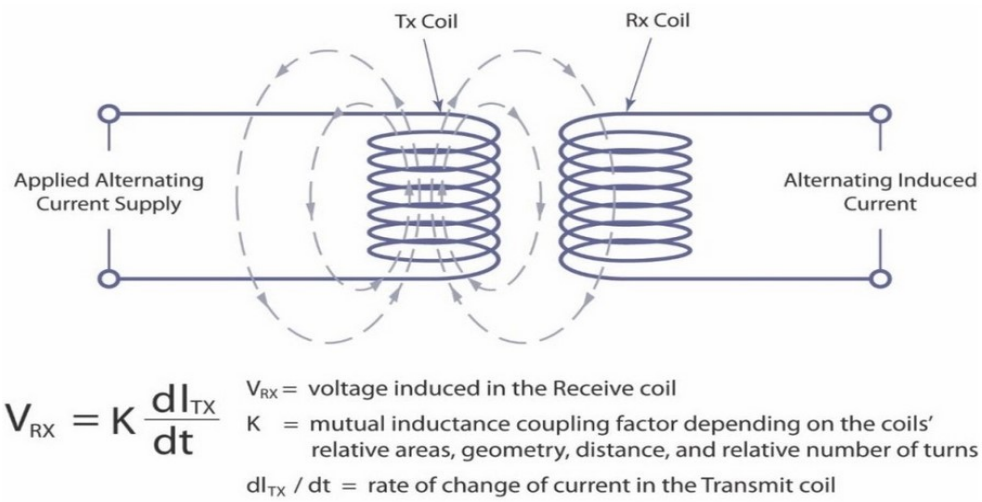

Figure 3.6. Physical Principle of Inductance.

3.3.1 Principle of Operation

The operating principle is based on a balanced coil system [95, 98, 96, 97, 99, 100]. Three coils are wound on a non-metallic or former frame, each exactly parallel to the others. The central coil (transmitter) is powered by a high-frequency electric current which generates a magnetic field. The two coils on each side of the central coil act as receivers (Fig. 3.7). Since these two coils are identical and at the same distance from the transmitter, the same voltage is induced in each of them. When the coils are connected in opposition, these voltages cancel each other resulting in a "zero output power". When a metal particle passes through the coil structure, the high-frequency magnetic field is disturbed

first near a receiving coil and then next to the other. This action alters the voltage generated in each receiver (in nano-volts). This variation of balance originates a signal that can be processed, amplified, and subsequently used to detect the presence of the unwanted metal. The control electronics divide the received signal into two separate components, magnetic and conductive, which are perpendicular to each other. The resulting vector, called the "product signal", has a phase size and an angle. Most metal detectors have a means of accomplishing this, which is often referred to as "phase control". To prevent electrical signals present in the environment generated by nearby systems from disturbing the detector, the complete structure of the coil is mounted inside a metal casing with an opening in the center to allow the passage of the product. This casing is normally made of aluminum (for applications in the absence of humidity) or stainless steel (for applications in contact with liquids). The metal casing constitutes a protection, as well as adding strength and rigidity to the structure, a fundamental factor for effective detector operation. The structure of a typical electromagnetic wear particle detection sensor is shown in Fig. 3.8.

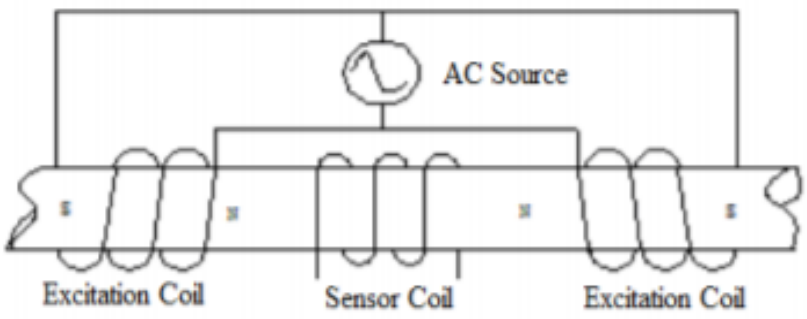

Figure 3.7. Balanced Coil System.

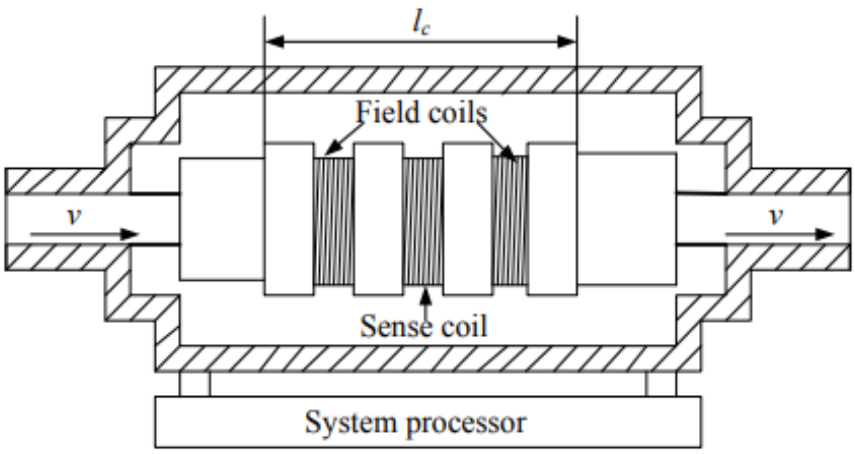

Figure 3.8. Wear Inductive Sensor.

The background electric noise is unavoidable for all-electric sensors. As for the vibration interferences, the following brief analysis can explain its generation mechanism. When the ambient vibration drives the sense coil to cut through the magnetic field of the eddy currents, an electromotive force E(t) following Faraday's law is generated as:

$$E(t) = Bl_c \frac{dx(t)}{dt} \tag{3.15}$$

where B denotes the magnetic field, x(t) is the vibration displacement of the sense coil and l_c is the length of the sensor

We assume that the exciting coil and the induction coil are wound on the plastic skeleton, and the skeleton is put into the metal shielding shell. The diameter of the inner pipe is the same as that of the detecting oil pipeline. The sensor is connected to the oil line through the thread of the screw and sealed by a gasket. Supposing that the excitation coil is a multilayer winding, based on the Biot-Savart law we could calculate the magnetic field intensity in the single-layer excitation coil. The formula is:

$$B = \frac{\mu_0 IN}{4L}\left(\frac{x+L}{\sqrt{R^2+(x+L)^2}} - \frac{x-L}{\sqrt{R^2+(x-L)^2}}\right) \tag{3.16}$$

Where B is the magnetic field intensity, μ_0 is the air permeability, I is the exciting current, N is the number of turns of the exciting coil, L is half of the coil length, R is the radius of the coil, and x is the distance from coil center in longitudinal direction. According to Faraday law of electromagnetic induction, the induced electromotive force E was calculated as:

$$E = j4\pi^3 f \frac{IR^4 N N_0 R_a^3}{3(R^2+x^2)^{3/2}}(\mu_r - \mu_0) \tag{3.17}$$

Where j is the imaginary unit, f is the exciting frequency, R, N, μ_0 and x are the same as above formula (8.2), N_0 is the number of turns of the detection coil, R_a is the radius of the particle, and μ_r is the particle permeability.

So, the output voltage of the vibration interference is approximately proportional to the vibration velocity. Hence the output signal of the oil debris sensor manifests the combined effect of particle signature, electric noise, and vibration velocity characteristics.

The signal phase of the non-ferromagnetic particles is opposite to the ferromagnetic particles which can be used to distinguish the types of wear particles. Therefore, the sensor can monitor the quantity, size, and distribution of ferromagnetic and non-ferromagnetic particles (Fig. 3.9).

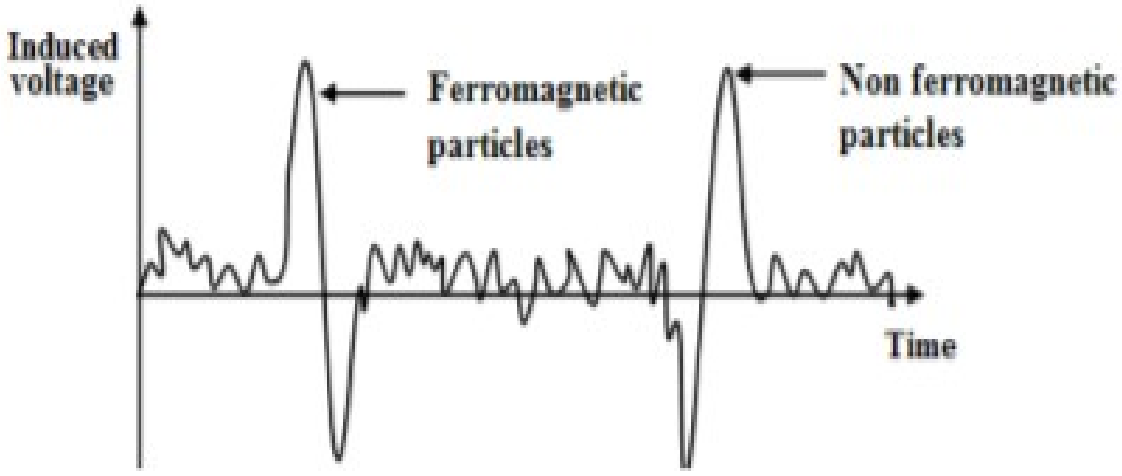

Figure 3.9. Signal Phase of the Particles.

CHAPTER 4

Scrivo tanto soddisfatto mai
Sono il vanto per i cartolai
E vado come un treno
Perché non mi sento arrivato
Non ascolto il giudizio del popolo intero
Perché non mi sento Pilato
E sì gente, sono esigente
No, non mi interessa chi scazza me
Sono alla ricerca come la tua offerta
Per le azalee, quindi ándale, ándale

Il Testo che Avrei Voluto Scrivere - Caparezza

"It is dreams that make man live. Fate is largely in our hands, if we know clearly what we want and are determined to get it"

Enzo Ferrari

CHARACTERIZATION OF CONTAMINANTS

In this chapter it describes the procedure to achieve some diesel samples of known quantities of water. These samples will first be characterized through laboratory techniques (off-line), to define an empirical relationship that quantifies the change in the dielectric constant of diesel as the water concentration changes.

4.1 Quality Analysis of Diesel

The first step is to qualify a certain quantity of EN590 diesel to know the starting chemical data of the diesel analyzed. This procedure was carried out in the QMM sector at CVIT in Bosch through the titration technique and the Karl Fischer method.

4.1.1 Titration Technique

Titration is defined as a technique to determine the concentration of a substance in solution by adding to it a standard reagent of known concentration in carefully measured amounts until a reaction of definite and known proportion is completed, as shown by a color change or by electrical measurement, and then calculating the unknown concentration. In figure 4.1 is showed the used instrument.

Titration is the most widespread technique to determine the number of acidities in petroleum products. The procedures for the measurement of this parameter vary depending on sample solubility in materials such as toluene or propanol, the dissociation constants of the acids in water, or the nature of the test sample. Therefore, the methodology used for lubricants maybe be different from the

methodology used for biodiesel. In new and used oils the constituents that may be considered to have acidic characteristics include organic acids, inorganic acids, esters, phenolic compounds, lactones, resins, salts of heavy metals, acid salts of polybasic acids, and additives such as inhibitors and detergents.

The test method is used to indicate relative changes that occur in oil during use under oxidizing conditions regardless of the color or other properties of the oil. The method is also used as a guide in the quality control of lubricating oil formulations or as a measure of lubricant degradation. It is not intended to measure an absolute acidic property that can be used to predict performance of oil under working conditions. There is no known relationship between corrosion of bearings and acid number. The methodology of performing the test involves dissolving the sample in a titration solvent and titrating potentiometrically as an acid/base titration with alcoholic potassium hydroxide.

A high concentration of acidic compounds in a lubricant can lead to corrosion of machine parts and clogged oil filters due to the formation of varnish and sludge. When a lubricant breaks down, acidic by-products will be formed from the chemical decomposition of the base stock and additives in the presence of air and heat. Total Acid Number (TAN) is a measure of acid concentration present in a lubricant. The acid concentration of a lubricant depends on the presence of additive package, acidic contamination, and oxidation by-products. Occasionally, the depletion of an additive package may cause an initial decrease in TAN of fresh oil. However, the accumulation of oxidation by-products and acidic contaminants in an oil over time will always lead to an increase in TAN.

Figure 4.1. Titrator Titrando 809.

4.1.2 Karl Fischer Method

Karl Fischer is an analytical technique used to measure the moisture (water) content in solids, liquids or gases. In figure 4.2 is showed the instrument. Karl Fischer's method uses a reagent that reacts (eq. 4.1) quantitatively and selectively with water to measure the moisture content. Karl Fischer's reagent consists of iodine, sulfur dioxide, a base and a solvent (usually an alcohol).

$$I2 + SO2 + 3base + CH3OH + H2O \rightarrow 2base\bullet HI + Base\bullet HSO4CH3 \qquad (4.1)$$

In general, K-F titration can be summarized into a series of steps:

- Add reagent ("titrant") to a burette

The reagents include alcohol, SO2, a base and I2

1. Add sample solvent to the titration vessel
2. Begin stirring the vessel
3. Zero the instrument by titrating unwanted moisture in the system
4. Add the weighed sample to the titration vessel
5. Begin adding reagent from the burette while stirring
6. When the endpoint is reached, the electrode will detect no change in current upon addition of more reagent
7. By knowing how much titrant was added, the water content can be calculated
8. Normally, the K-F instrument does the calculations and reports the results as "% water" or "ppm water."

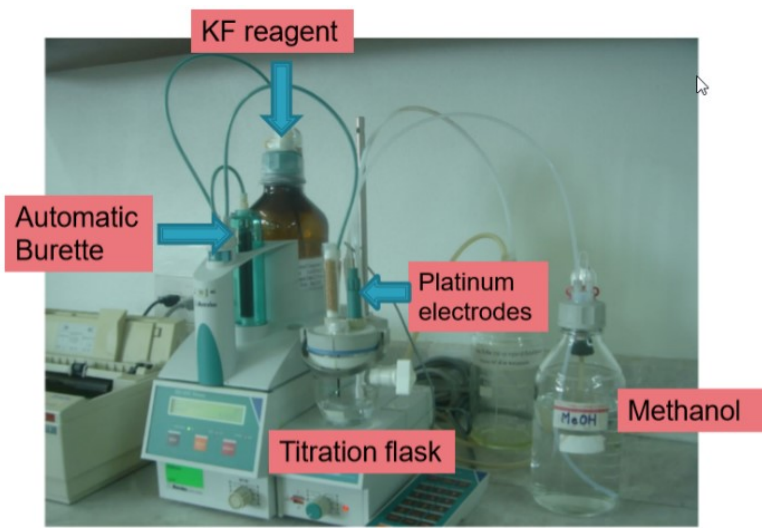

Figure 4.2 Titrator 831 KF Coulometer.

4.1.3 Water Determination

The titrimetric determination of water is based upon the quantitative reaction of water with an any solution of sulfur dioxide and iodine in the presence of a buffer that reacts with hydrogen ions. In the volumetric titration method, iodine required for reaction with water is previously dissolved in water determination and water content is determined by measuring the amount of iodine consumed as a result of reaction with water in a sample. This is a specific method. Only water will be determined. The method is rapid about a few minutes. With KF titration both free and bound water can be determined, e.g. surface water on crystals or the water contained inside them. Thanks to the quality analysis department, an amount of EN590 has been qualified which will be used for the preparation of the mixtures. The quality analysis document is shown in the figure 4.3.

Extra Analysis Report

Dettagli analisi:

Particolare:	Liquido	Richiesta:	124_QMM72-LAB
Nr campioni:	1	Motivo richiesta:	Progetto di ricerca: sensore per il monitor di acqua nel gasolio
Materiale:	Mezzo di prova (olio,gasol.)	Tipo di test:	Test Speciale – Progetto interno
Descrizione:	Gasolio (fornitore EVL)	Richiedente:	Pappalardi P. (CVIT/EHP1-CV)

1 **Analisi richieste:**
Analisi TAN e contenuto di acqua.

2 **Lista strumenti**
Titolatore Titrando 809; Titolatore 831 KF Coulometer;

3 **Istruzioni di lavoro:**
F01MD13311_AFK; F01MD12624_AFK;

4 **Norme:**
N28 BS101

5 **Temperatura:**
22,1 °C

6 **Conclusioni:**
Il contenuto di acqua è conforme, mentre il TAN è fuori rispetto al valore richiesto dalla norma N28 BS101

Analisi	Metodo	Unità di misura	Valore Riscontrato	Valore richiesto	Risultato
Contenuto di acqua	ISO 12937	ppm	43,5	Max.100	O.K.
TAN	EN 12634	mgKOH/g	0.0912	≤ 0.04	N.O.K.

Figure 4.3. Diesel Quality Analysis Report.

4.2 Mixture EN590-Water Preparation

One of the most properties of diesel fuels is its readiness to auto ignite at the temperatures and pressures present in the cylinder when the fuel is injected. First, we blended all the ingredients not less than 15 minutes. The longer for blending the fuel, the results will become better. And the results, diesel fuel is mixed perfectly by water. The key benchmark for a stable EN590-water emulsion is the existence in single phase. Then the mixing speed will be varying from 1000-5000 rpm. The ready samples of EN590-water emulsion were refilled into 50 ml glass vessels. Through emulsification, the interfacial area among two liquids will grow. Liquids need to reduce this surface area and mixing energy is needed for emulsification. More stable emulsion was produced with higher mixing speed. The stability of EN590-water emulsion fuel increase with the increasing of mixing time up to 5 minutes.

In the Chemistry Laboratory at CVIT have been prepared some samples at different concentrations of water (Fig. 4.4)

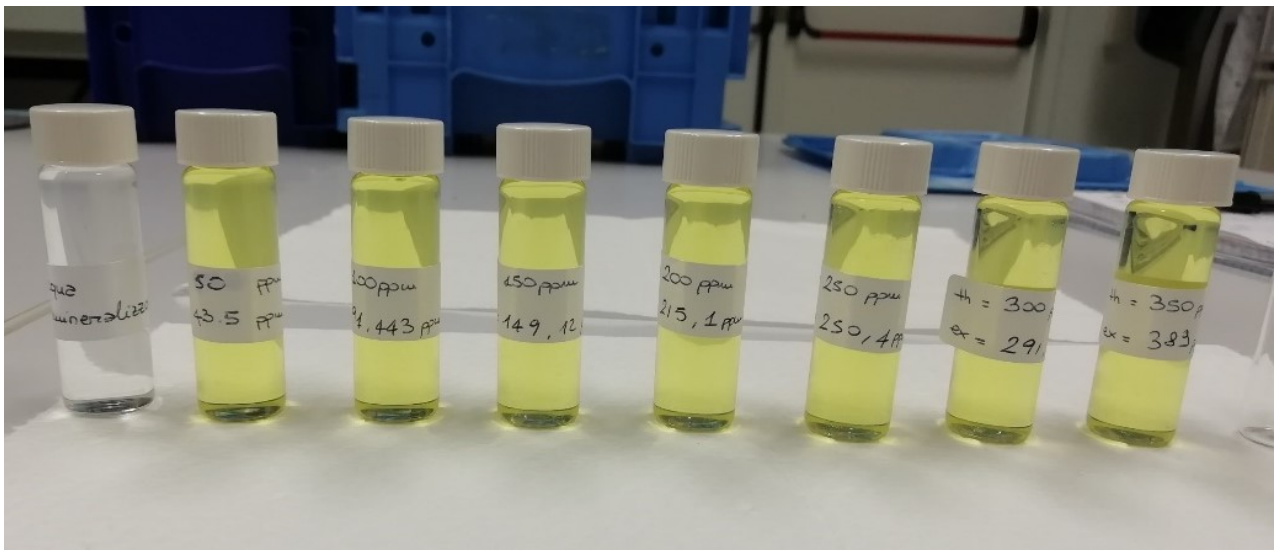

Figure 4.4. Sample of Water – Diesel (EN590).

The following instruments were used for the preparation:

- Analytical Balances
  - KERN ABT 320-4M (Fig. 4.5)
  - ETERNITY GIBERTINI (Fig. 4.6)
- Homogenizer
  - Unidrive X1000D (Fig. 4.7)

Figure 4.5. KERN ABT 320-4M.

Figure 4.6. ETERNITY GIBERTINI.

Figure 4.7. Unidrive X1000D.

The homogenizer was used to standardize the mixtures and avoid the formation of layers while the balances, having different capacities, were useful for defining two techniques for preparing the mixtures, the weighing and dilution techniques.

The weighing technique starts a starting quantity of EN590 and adds, for each container, the quantity of water in ppm, which is suitably weighed. The weight measured on the balance is compared by a balancing equation 4.2 to quantify the correct amount of ppm of water with which to contaminate the diesel, considering the tare weight of the empty containers.

$$1\ ppm = \frac{1\ mg}{kg} \rightarrow (i.e.)\ 50\frac{mg}{kg} \rightarrow 50{:}\ 1000 = x{:}\ 100{,}456 \rightarrow x \\ = 5.0228\ mg \tag{4.2}$$

Table 4.1 lists the measurements made for each specimen, applying equation 4.2 and subtracting the tare of the containers.

Net Weight [g]	**Proportion [mg] (theoretical)**	**Proportion [mg] (experimental)**	**Real ppm [ppm]**	**Blend [g] (Net)**
77,7276	3,88638	***3,3811506***	***44***	77,7276
74,3633	7,343633	***6,8***	***93***	73,7543
79,8213	11,973207	***11,9***	***149***	79,1367
77,4301	15,48602	***14,4***	***186***	76,6037
80,5227	20,130675	***20,1***	***250***	79,6413
76,407	22,9221	***23,6***	***309***	75,6287
82,3323	28,816305	***25,8***	***313***	81,2453
77,0366	30,81464	***29,9***	***388***	76,2101
72,5457	32,645565	***31,6***	***436***	71,6528
75,1353	37,56765	***39,5***	***526***	74,416

Table 4.1. Weighing Technique Procedure.

While the dilution method is divided as follows:

1. Weighing of the solute (standard of the maximum quantity to be analyzed)
2. Weigh the initial volume of solvent with the solute, weighed at the point
3. Progressive addition of solvent to obtain the other standards in smaller quantities, by dilution.

No further solutes are added after the one in step 1. The mixture is weighed every time we change the mixing container for measuring operations with the spectrophotometer and for progressive dilution, evaluating the error induced during the preparation. For each measurement, the volume of the mixture is divided into two parts. One part will be used for measuring the spectrophotometer, while the other half will be used to prepare the other standards, by dilution, taking into account that the weight has changed. The difference is that in this technique, diesel oil is periodically added, to reduce the maximum ppm of water, in order to reach the desired quantities.

4.3 Characterization of Contaminants

After preparing the samples with the following ppm values of water, 50, 100, 150, 200, 250, 300, 350, 400, 450, 500, a calibration curve is characterized to evaluate the validity of the laboratory methods subsequently described. We need this to define an empirical relationship to be used in sensor modeling in the next chapter.

4.3.1 UV-Vis Spectrophotometry

Optical characterization of the water in diesel was conducted in UV-Vis Spectrophotometry Laboratory at CVIT.

Light absorption can be used in analytical chemistry for characterization and quantitative determination of substances. UV/VIS spectroscopy is a technique based on the absorption of light by an unknown substance or by an unknown sample. Here, the sample is illuminated with electromagnetic rays of various wavelengths in the visible (VIS, i.e. the different colors) and adjacent ranges i.e. ultraviolet (UV) and part of the lower infrared region (near IR) of the spectrum. Depending on the substance, light is partially absorbed. The remaining light, i.e. the transmitted light, is recorded as a function of wavelength by a suitable detector, providing the sample's UV/VIS spectrum. As a result, because each substance absorbs light in a different way, a unique and specific relationship exists between the substance and its UV/VIS spectrum. The spectrum can then be used to identify or

quantify a substance. The obtained UV/VIS spectra are very useful for quantitative measurements of a specific compound. In fact, the concentration of an analyte in solution can be determined by measuring the absorbance at a specific wavelength. From the absorbance value of the sample, its concentration can be calculated. UV/VIS spectroscopy is a measurement technique in which the recording of the absorption spectra of different samples using ultraviolet (UV) and visible (VIS) light is achieved by a spectrophotometer, i.e. an instrument able to measure the spectrum of a sample in the UV/VIS range. A UV/VIS spectrophotometer measures the intensity of light passing through a sample solution in a cuvette and compares it to the intensity of the light before it passes through the sample. The main components of a UV/VIS spectrophotometer are a light source, a sample holder, a dispersive device to separate the different wavelengths of the light (monochromator), and a suitable detector.

The working principle of a spectrophotometer is based on the following steps:

1. Blank (measure of the intensity of light transmitted through the solvent):

    a. The solvent (e.g. water or alcohol) is added into a suitable, transparent and not absorbing container, called cuvette.

    b. A light beam emitted by the light source passes through the cuvette with the solvent.

    c. The intensity of the transmitted light at different wavelengths is then measured by a detector positioned after the cuvette with the solvent and recorded.

This is known as the blank, which is needed for the sample measurement.

Sample determination:

1. A sample is dissolved in the solvent and added into the cuvette.
2. A light beam emitted by the light source passes through the cuvette with the sample.
3. When passing through the cuvette, the light is partially absorbed by the sample molecules in the solution.
4. The transmitted light is then measured by the detector.
5. The light intensity change at different wavelengths is calculated by dividing the transmitted intensity of the sample solution by the corresponding values of the blank. This ratio is finally stored by a recorder.

The detector measures the intensity of light after passing through the sample solution. This fraction of light collected by the detector is called the transmitted intensity I. The intensity of the transmitted

light is attenuated by the sample solution. Therefore, its value is lower than the original intensity I_0 at the light source.

The ratio between the two intensities I/I_0 is defined as Transmittance T, and its unit is %, written in equation 5.3:

$$T = \frac{I}{I_0} \tag{4.3}$$

The transmittance is the main value determined by UV/VIS spectroscopy, but it is not the only one. In fact, the absorbance A represents an additional result widely used when recording UV/VIS spectra. It is defined as the negative logarithm of the transmittance and it has a great advantage, like written in equation 5.4.

$$A = -\log(T) \tag{4.4}$$

Note that the absorbance A does not have any unit of measurement. In other words, it is a dimensionless value. However, it is often represented using the letter "A" or as AU for absorbance units. The transmittance spectrum of a sample is recorded as a function of the wavelength. When passing through a transparent cuvette filled with sample solution, the light intensity is attenuated proportionally to the sample concentration. In other words, a higher concentrated sample solution will absorb more light. In addition, the attenuation is also proportional to the length of the cuvette; a longer cuvette will lead to a higher absorption of light.

There are several reasons to measure UV/VIS spectra:

- UV/VIS spectra allow components present in the sample solution to be identified.
- Absorption peaks can be used to quantify the investigated sample.
- Based on the relationship between absorbance and sample concentration, UV/VIS spectroscopy is applied as a quantitative analytical technique.
- The position of the peaks in the spectrum reveals information about the molecular structure of the sample.

The applications of UV-Vis spectroscopy are mainly focused on qualitative and quantitative analysis. In qualitative analysis, UV/VIS spectroscopy can be used as a tool to identify if the analyte is pure and did not undergo decomposition. Qualitative analysis is based on the specificity of UV/VIS

spectroscopy. In fact, samples absorb light of one or more distinct wavelengths, with specific maximum absorbance values. For this reason, each sample has a characteristic and unique UV/VIS spectrum that can be used for its identification. In particular, this is achieved by comparing the spectrum of the sample with spectra of known, pure compounds. Quantitively analysis is based on the Lambert-Beer Law, the concentration of a compound in a solution can be determined quantitatively by UV/VIS spectroscopy. To perform that, a calibration line is first determined by measuring the absorption of several standard solutions of known concentration. The linear relationship between absorbance and concentration of a sample opens the door for a variety of quantitative analyses.

To determine an unknown concentration of a sample solution by UV/VIS spectroscopy, a calibration line must first be created. This is done by measuring the light absorption of several standard solutions of different, known concentrations at a predefined, fixed wavelength.

The total absorbance of a solution at any given wavelength is equal to the sum of the absorbance of the individual components in the solution. This relationship makes it possible in principle to determine the concentrations of the individual components of a mixture even if total overlap in their spectra exists. To analyze the mixture, the molar extinction coefficients for the individual components have first to be determined at specific wavelengths, optimally wavelengths are selected so that the coefficients of the components differ significantly.

The tools used are:

- Cary 60 UV-Vis spectrophotometer (Fig.4.8)
  - Scan Rate = 250 nm/min
  - Wavelenght range = 190 – 1100 nm
  - T = 42,5°

- Single Cell Peltier Accessory (Fig.4.9)
  - The Peltier 1 x 1 Cell Holder enables you to perform temperature-controlled measurements for a single sample and reference. The temperature of each cell holder is independently regulated, allowing you to utilize both the sample and reference cell holders or just the sample cell holder. The cell holders are mounted onto the standard Cary cell holder base (supplied with the Agilent Cary). The pump supplied can be used for a water circulating system or alternatively you can use a water bath.

- Cuvettes with capacity of 3mL (Fig.4.10)

- Wash with soap and water and then alcohol three times after each measurement.

Figure 4.8. Cary 60 UV-Vis Spectrophotometer.

Figure 4.9. Single Cell Peltier Accessory.

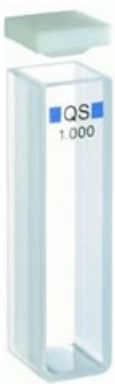

Figure 4.10. Cuvette.

Before scanning the absorption spectrum, a preliminary operation, called Kinetic Stability of Measurement, is required to calculate the reaction rates from the absorbance versus the time data, as shown in figure 4.11. Furthermore, the measurements are repeated several times, in order to evaluate their stability and reliability.

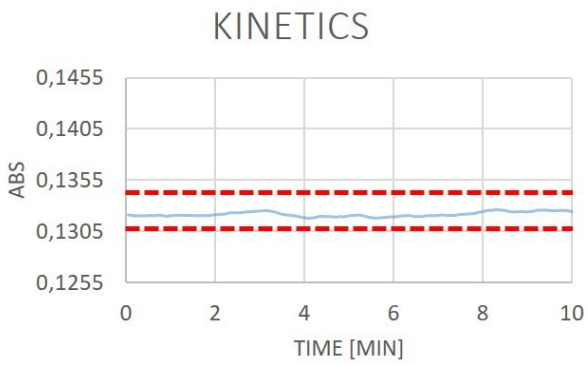

Figure 4.11. Kinetics Stability of the Measure.

The absorption spectrum of the EN590 diesel is shown in figure 4.12, while the absorption spectrum of the EN590 diesel is shown in figure 4.13 together with the demineralized water used as contaminant.

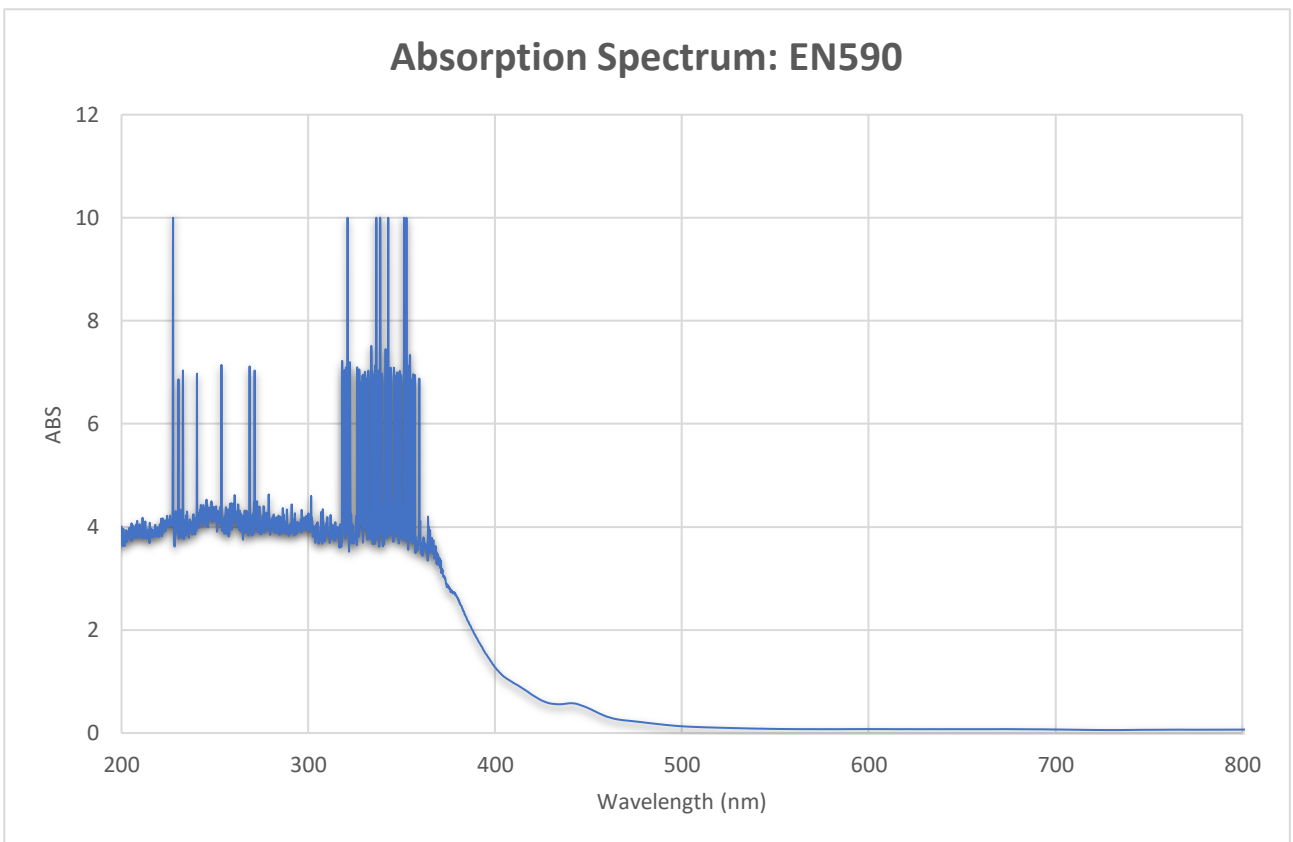

Figure 4.12. Absorption Spectrum of the EN590 Diesel.

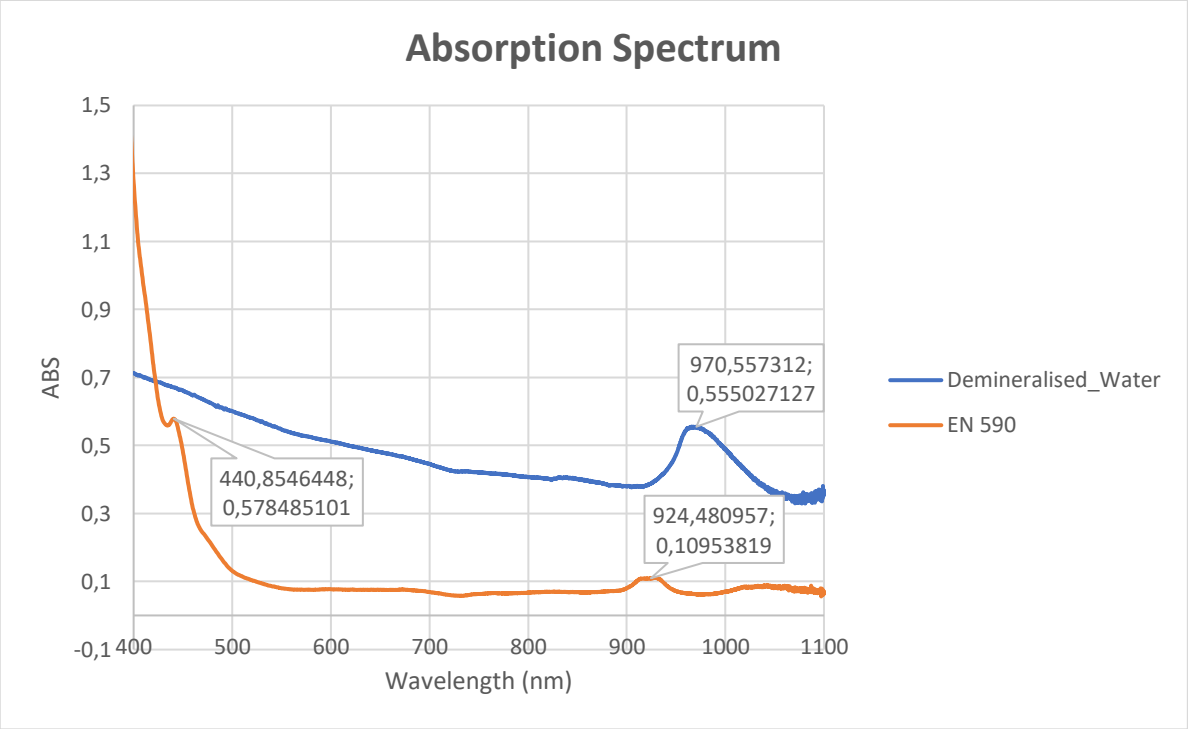

Figure 4.13. Absorption Spectrum of the EN590 Diesel and of the Water.

The peaks are at wavelengths of about 440 nm and 924 nm for diesel and about 970 nm for water are highlighted.

Figure 4.14 and 4.15 show the various spectra of the diesel when water concentration changes. In particular, it is noted that between 180-380 nm, the noise is high due to the window effect. Therefore, we will focus on the wavelength in the range between 400-1000 nm.

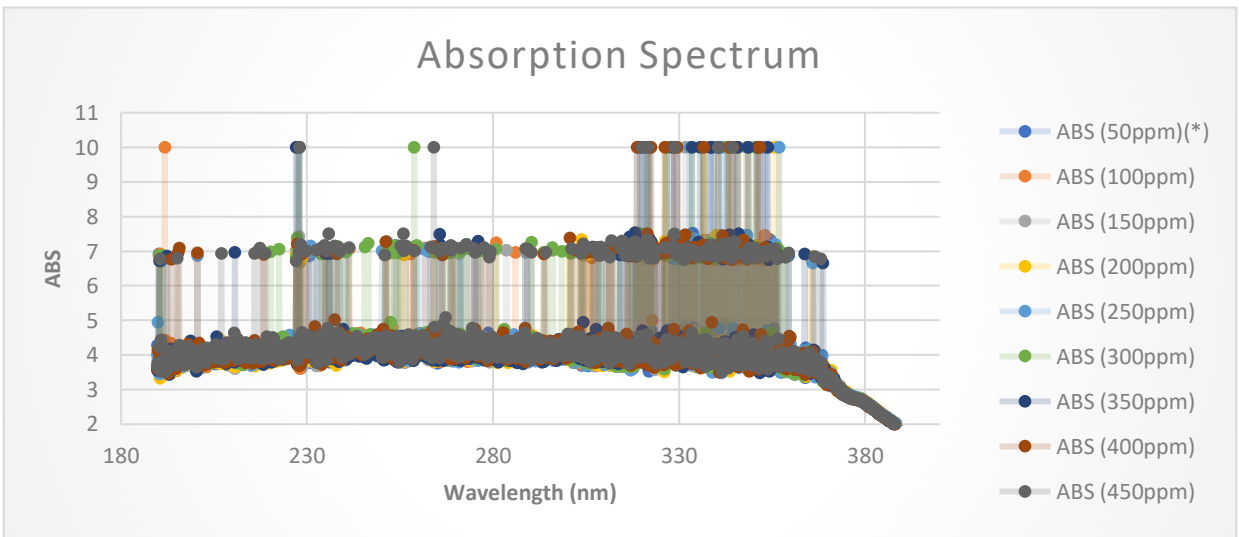

Figure 4.14. Absorption Spectrum of the Diesel-Water at 180-380 nm.

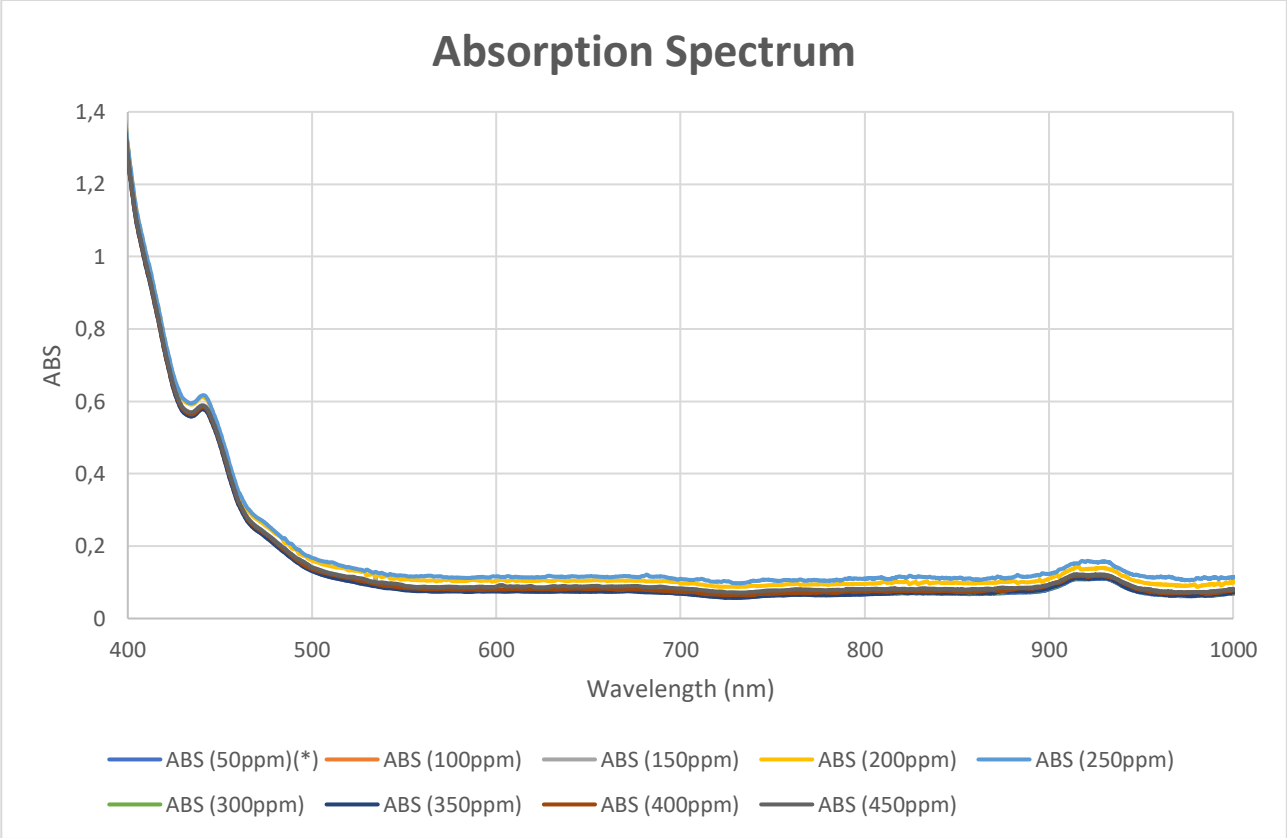

Figure 4.15. Absorption Spectrum of the Diesel-Water at 400-1000 nm.

Focusing the spectrum on the wavelength range in the 915-935 nm range (Fig. 4.16), we identify several peaks that will be used to calculate the regression line and the determination coefficient.

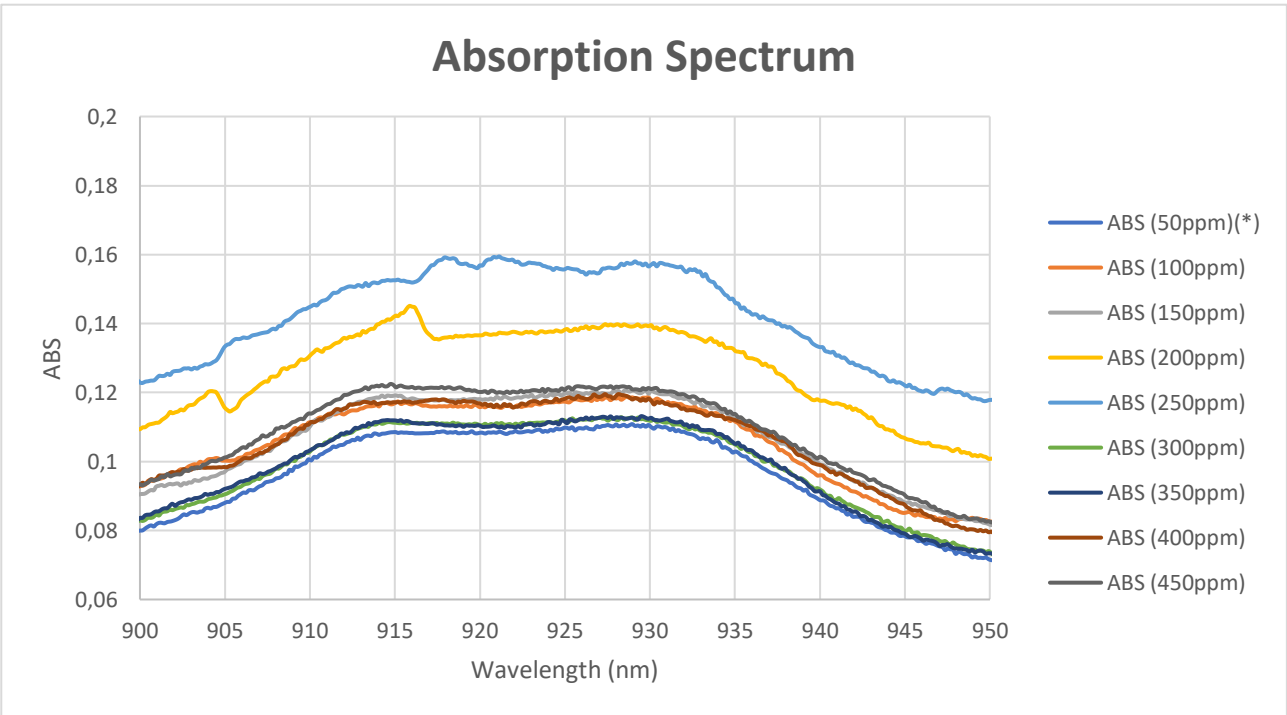

Figure 4.16. *Absorption Spectrum of the Diesel-Water at 915-935 nm.*

The most evident peaks occur at:

- *λ = 918,0823 nm*
- *λ = 921, 2678 nm*
- *λ = 930,0748 nm*

At the different concentrations, like showed in table 4.2, the calibration curves are obtained (Figures 4.17-4.19). Besides the linear equations that describe them and the coefficient R^2 are reported.

λ[nm] / c [ppm]	**50**	**100**	**150**	**200**	**250**	**300**	**350**	**400**	**450**	**500**
930,0748	0,109976	0,117741	0,120597	0,139546	0,157073	0,111807	0,112671	0,117625	0,121006	0,260519
921,2678	0,108487	0,115553	0,118259	0,137241	0,159005	0,111162	0,110216	0,115936	0,11999	0,261075
918,0823	0,10832	0,115943	0,117497	0,135966	0,158985	0,111017	0,110488	0,117667	0,121466	0,263975

Table 4.2. Data for Construction of Calibration Curve.

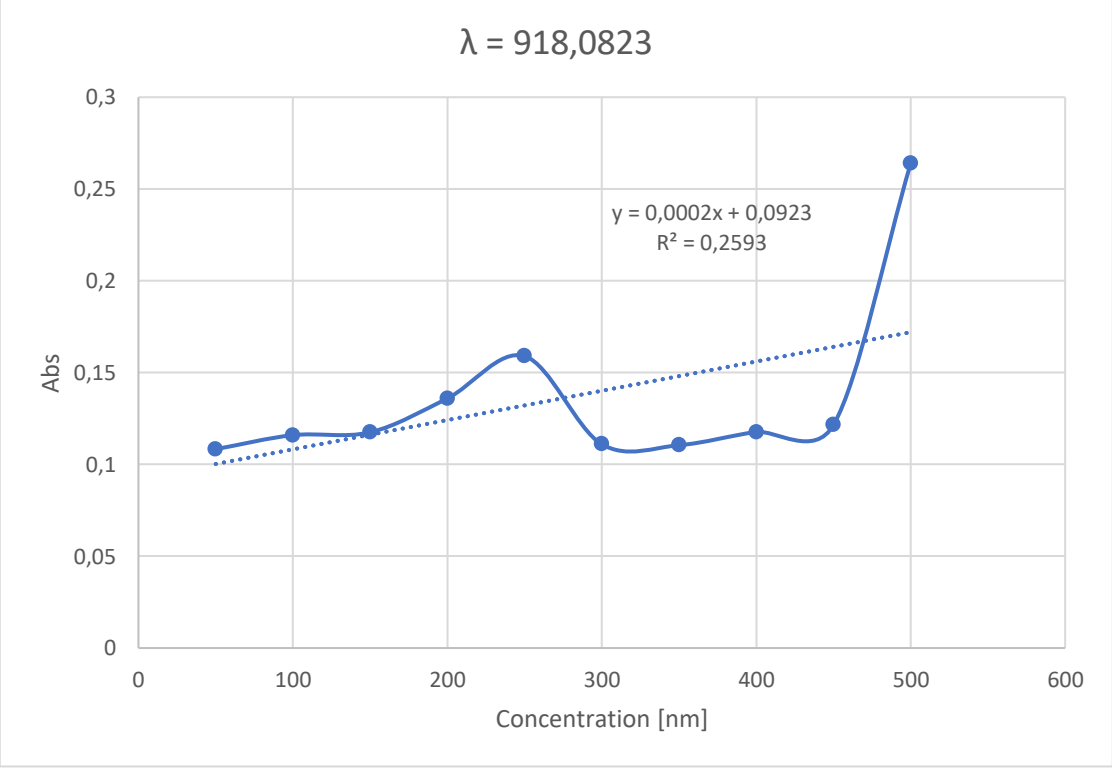

Figure. 4.17. Calibration Curve at λ = 918,0823 nm.

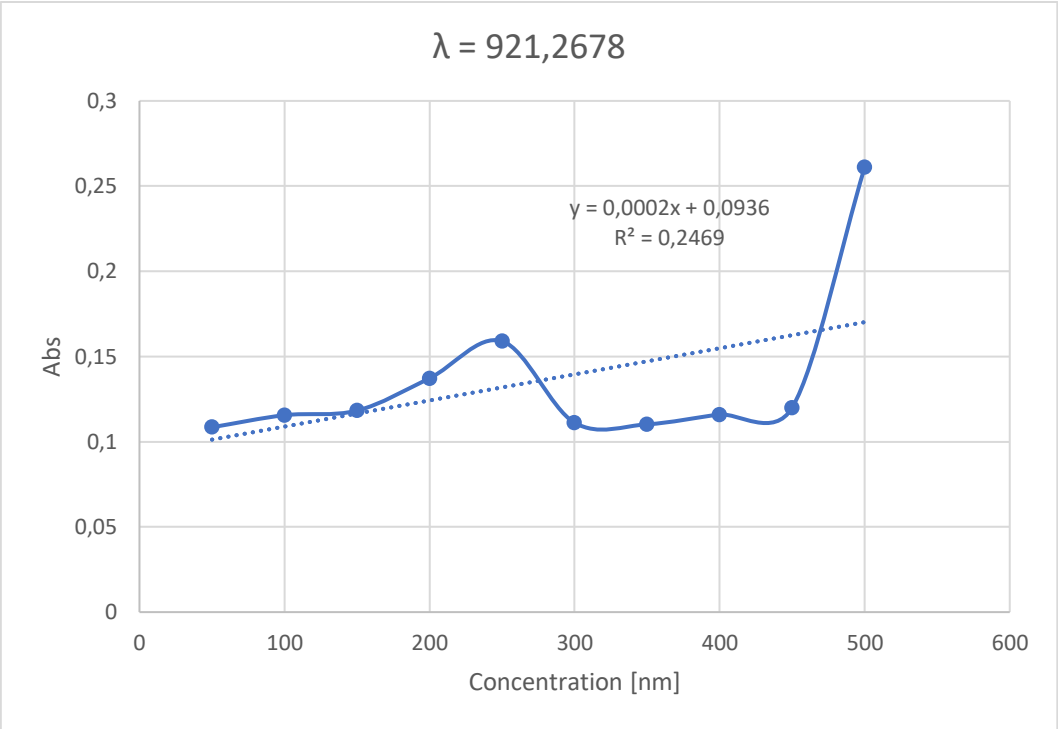

Figure. 4.18. Calibration Curve at λ = 921, 2678 nm.

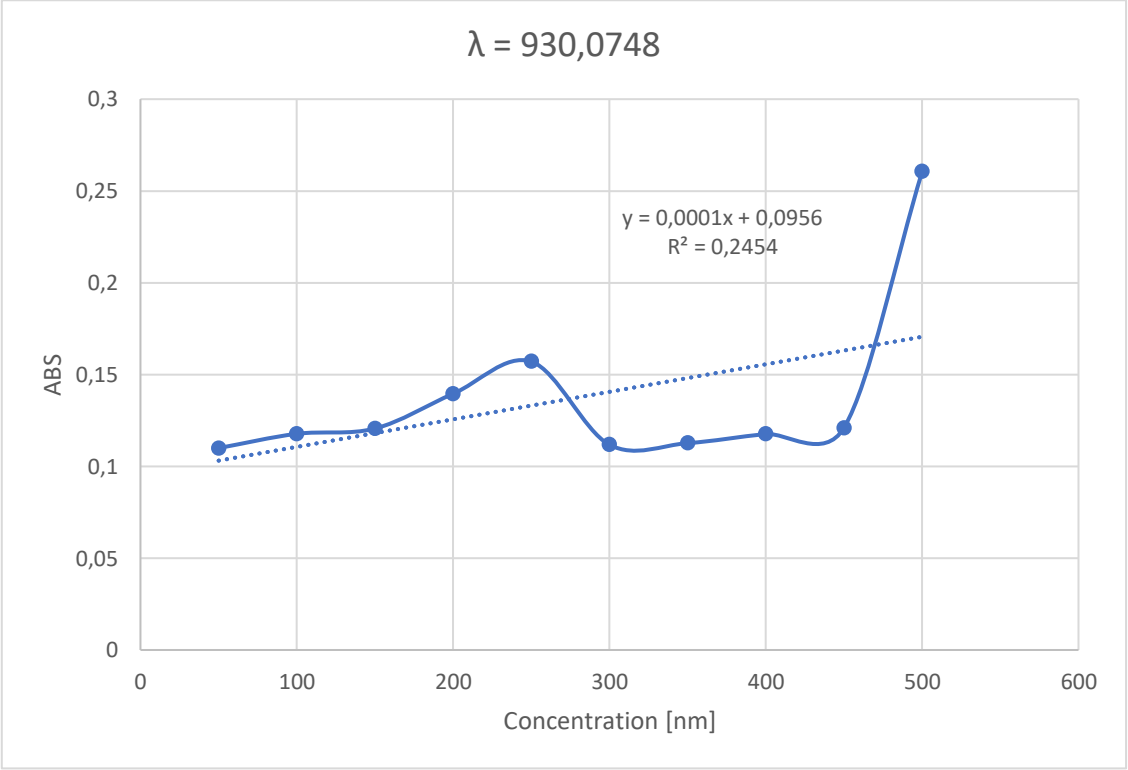

Figure. 4.19. Calibration Curve at λ = 930,0748 nm.

4.3.2 Characterization with a Microwave System

In the Microwave Laboratory at Polytechnic of Bari, the same samples were characterized with a microwave system, consisting of a VNA, described in chapter 3, and a DAK, the dielectric assessment kit that allows material characterization of samples with limited size or volume. DAK is used for dielectric measurements of liquids, solids and semi-solids. It is designed for fast, precise, non-destructive and easy-to-use measurements in the 10 MHz to 67 GHz frequency range. An example of experimental set-up is described in figure 4.20.

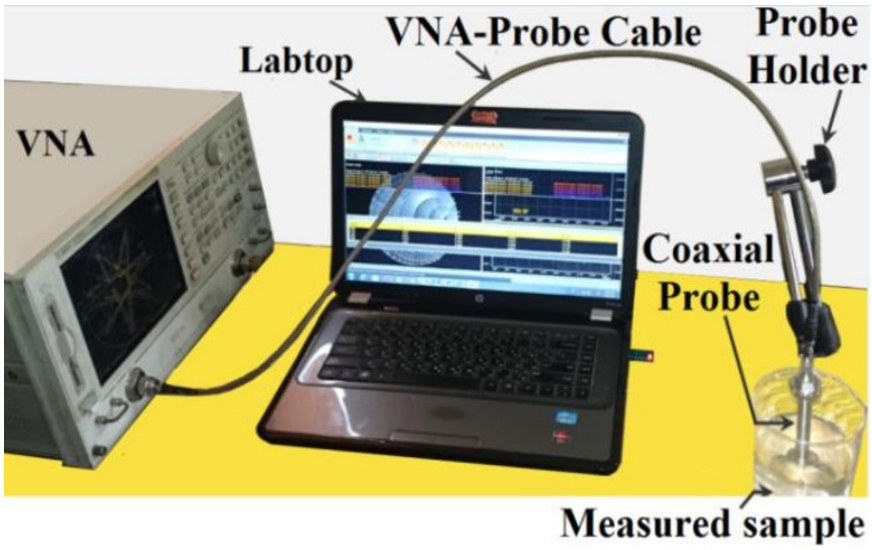

Figure 4.20. Microwave System (DAK and VNA).

Table 4.3 lists the measurements made on the various mixtures, through which the real and imaginary part of the dielectric constant have been calculated.

Folder Name	EN590_1	EN590_2	EN590_3	EN590_4	EN590_5	EN590_6	EN590_7	EN590_8	EN590_9	EN590_10
Date	17/04/2019	17/05/2019	17/05/2019	24/05/2019	29/05/2019	02/08/2019	02/08/2019	23/10/2019	24/10/2019	24/10/2019
Temperature	20°C	22.9°C	22.9°C	22°C	22°C	29°C	29°C	25.5°C	25.5°C	25.5°C
Probe	DAK_3.5	DAK_3.5	DAK_3.5	DAK_3.5	DAK_3.5	DAK_3.5	DAK_3.5	DAK_12	DAK_3.5	DAK_3.5
Frequency start	200 MHz	1 GHz	1 GHz	8.5 GHz	15 GHz	10 GHz	12 GHz	1 GHz	1 GHz	3 GHz
Frequency stop	18 GHz	3 GHz	3 GHz	10.5 GHz	17 GHz	12 GHz	14 GHz	3 GHz	3 GHz	6 GHz
Frequency step	10 MHz	10 MHz	50 MHz	50 MHz	50 MHz	50 MHz	50 MHz	50 MHz	50 MHz	50 MHz
Nr. measurements for each sample	3	10	10	10	20	20	20	10	10	10
Samples:										
water	x	x		x				x	x	x
50 ppm	x	x	x	x	x	x	x	x	x	x
100 ppm	x							x	x	x
200 ppm	x							x	x	x
500 ppm	x							x	x	x
1000 ppm	x	x	x	x	x	x	x	x	x	x

Table 4.3. List of Measurements on EN590-Water Samples.

The following experimental model was compared with other models present in the literature, in particular with the Lichtenecker, Looyenga, Brown and Birchak models. For the different mixtures, the results were compared to evaluate the coherence of the empirical mathematical model, as shown in table 4.4.

Water contaminant in the EN590 [ppm]	***EXPERIMENTAL*** $\varepsilon_r^{mixture}$	***LICHTENECKER*** $\varepsilon_r^{mixture}$	***LOOYENGA*** $\varepsilon_r^{mixture}$	***BROWN*** $\varepsilon_r^{mixture}$	***BIRCHAK*** $\varepsilon_r^{mixture}$
0	210,1733684	210,1733684	210,1733684	210,1733684	210,1733684
50	210,2476842	210,2108566	210,2203676	210,2507655	210,2263045
100	210,322	210,3040458	210,3371936	210,4431019	210,3578826
150	210,3963158	210,4071819	210,4664796	210,6558685	210,5034851
200	210,4706316	210,6683402	210,7938072	211,1941643	210,8720819
250	210,5449474	210,8640964	211,0391179	211,5972167	211,1482821
300	210,6192632	210,9842497	211,1896687	211,8444212	211,3177737
500	210,9165263	211,4470143	211,769375	212,7952039	211,9702955

Table. 4.4. Comparisons between Experimental Data and Mathematical Models.

It can be seen that the experimental model obtained from the characterization differs slightly from the mathematical models described in chapter 3.

Finally, the calibration curve was calculated for f = 2.45 GHz (Table 4.5). The calibration curve of the real part of the dielectric constant and the calibration curve of the tangent loss are shown in figures 4.21-4.22.

ppm	*0*	*50*	*100*	*150*	*200*	*250*	*300*	*350*	*400*	*450*	*500*
ε_r	2,0591	2,06103	2,0628	2,0644	2,0659	2,0672	2,0684	2,0694	2,0703	2,07103	2,0716
tan_δ	0,0284	0,02503	0,021353	0,0195	0,018219	0,0173	0,0166	0,016	0,015545	0,01513	0,014771

Table. 4.5. Data for Calibration Curve at f=2,45 GHz.

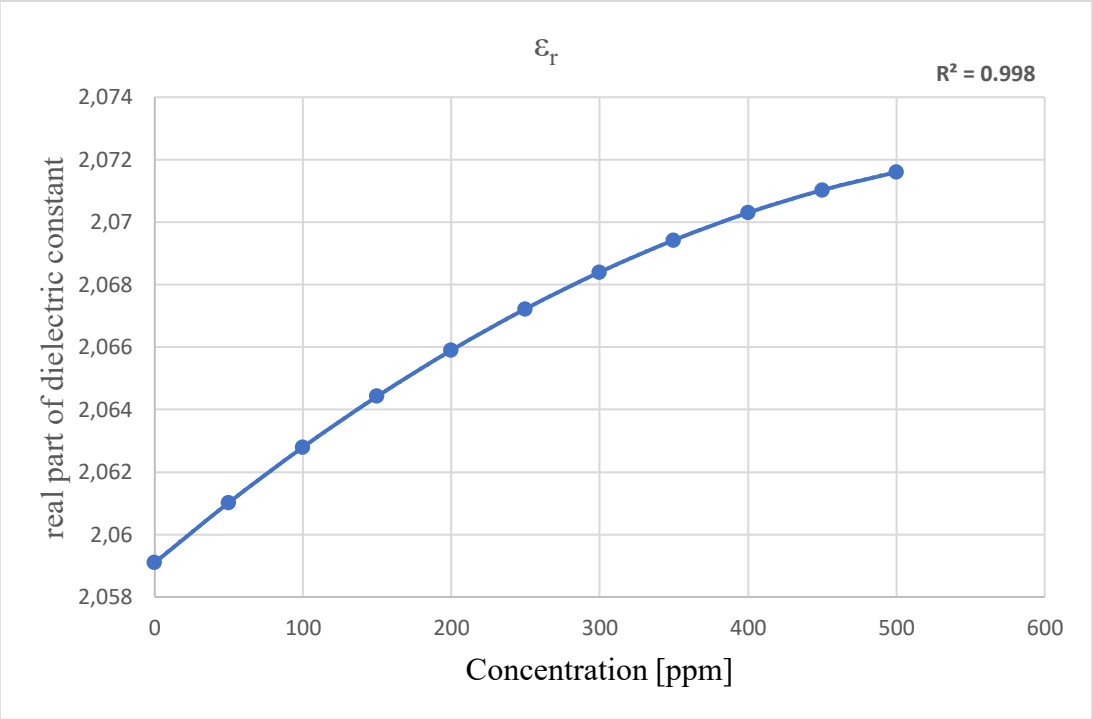

Figure 4.21. Calibration Curve at f=2,45 GHz of ε_r.

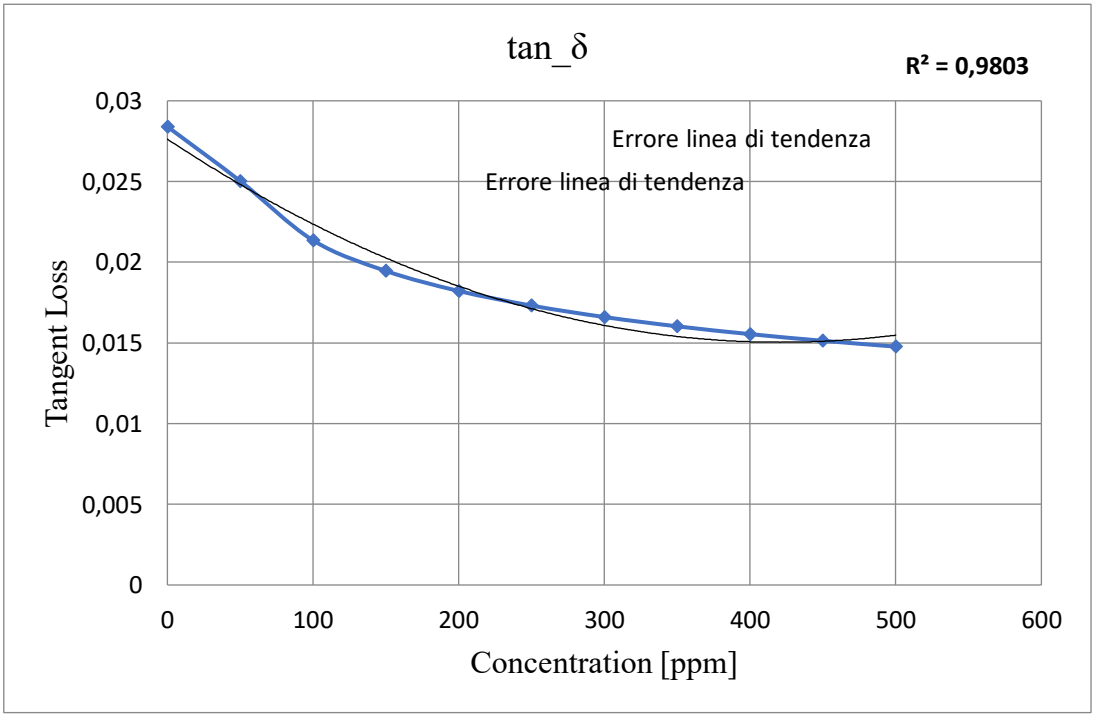

Figure 4.22. Calibration Curve at f=2,45 GHz of Tangent Loss.

The empirical formula of the dielectric constant, which will be used in the following chapter, for modeling the sensor, is extrapolated from these curves. Respectively, the real part of the dielectric constant and the loss tangent are reported in the empirical formulas, (equations 4.4-4.5):

$$\varepsilon_r = -3E^{-08}ppm^2 + -3E^{-05}ppm + 2,0591 \quad (4.4)$$

$$tan\delta = 7E^{-08}ppm^2 + -6E^{-05}ppm + 0,0276 \quad (4.5)$$

4.4 Conclusion

In this chapter immediately highlights how optical techniques are not useful for the characterization of water-diesel mixtures. First of all, for the small quantities of contaminant, which make the preparation and cleaning of the samples difficult. Despite the repetition of the measurement, from the calibration curves it can be seen that the determination coefficient does not exceed a value of 0.3, however they have been highlighted by the characteristic peaks. However, the small quantities of water are confused with each other, without the possibility of distinguishing them progressively. Despite the repetition of the measurement, from the calibration curves, it can be seen that the determination coefficient does not exceed a value of 0.3. Besides the ABS of 50 ppm is similar to ABS of 300 ppm

Instead, the characterization through the probe and the VNA provided encouraging data which were confirmed by comparison with the mathematical models present in the literature. The determination coefficient is major of 0.9.

The modeling of the sensor will be studied through the use of the empirical relationships obtained.

CHAPTER 5

La vita è un cinema tanto che taci
Le tue bottiglie non hanno messaggi
Chi dice che il mondo è meraviglioso
Non ha visto quello che ti stai creando per restarci
Rimani zitto, niente pareri
Il tuo soffitto: stelle e pianeti
A capofitto nel tuo limbo in preda ai pensieri
Procedi nel tuo labirinto senza pareti
No! Non è vero!
Che non sei capace, che non c'è una chiave

Una Chiave - Caparezza

"In each branch of knowledge, progress is proportional to the quantity of elements on which it is possible to build, and therefore to the ease of obtaining data"

James Clerk Maxwell

SENSOR MODELING AND SIMULATION

The following chapter will describe the design, sizing and modelling of the prototypes that will be realized for the experimental tests presented in the next chapter. The focus is essentially on two families: transmission lines and resonant cavities.

5.1 Sensor Parameters and Constraints

The initial constraints are imposed by the electromagnetic formulas described in chapter 2 and by the geometric constraints imposed by Bosch, showed in the table 5.1. These data will be useful to define the fluid dynamics of the diesel flow that will pass through the sensor. This is an important aspect because of the innovativeness of the sensor that you want to make and the possibility of using the fluid to be measured as part of the sensor to create a prototype that works online. From a geometric point of view, since the sensor must be installed upstream of the pre-feed pump, it must exhibit a maximum size of 100 mm.

Flow rate [l/h]	T [°C]	Delta p [bar] Rel	P [bar] Abs	eGP speed [rpm]	Flow speed [m/s]
100	40	4	0,925	1474	0,3539
200	40	4	0,912	2653	0,7077
300	40	4	0,893	3846	1,0616
400	40	4	0,866	5038	1,4154

Table 5.1. Data Provided by Bosch.

Therefore, after a preliminary analysis, the geometry that maximizes the detection capacity of the water concentration in the diesel will be chosen.

The COMSOL Multiphysics software will be used in which the permittivity models obtained in the previous chapter will be implemented. In particular, the more generic model, written in equation 5.1 based on the relationship 3.15, which we will name *theoretical model*, will be compared with the empirical one obtained from the characterization through laboratory techniques in the fifth chapter (equations 4.4-4.5), which we will name *experimental model*, in the equation 5.2.

$$\varepsilon_{mixture} = (\varepsilon_{water} - \varepsilon_{diesel})\, ppm[\%] + \varepsilon_{diesel} \tag{5.1}$$

$$\varepsilon_{mixture} = \varepsilon_r(1 - jtan\delta) \tag{5.2}$$

For the simulation, the RF Module of COMSOL Multiphysics is used. Finite element discretization is used by COMSOL for solving the governing equations. Under the assumption that material response is linear with field strength, COMSOL formulates Maxwell's equations in the frequency domain given as (eq. 5.3):

$$\nabla \text{ x } (\mu_r^{-1} \nabla \text{ x E}) - \frac{\omega^2}{c_0^2}\left(\varepsilon_r - \frac{j\sigma}{\omega\varepsilon_r}\right) E = 0 \tag{5.3}$$

where μ_r is the permeability, ε_r the permittivity and the electric conductivity of the material; ε_0 is the permittivity of the vacuum, ω the wave angular frequency and E the electric field. Fields are computed in the dielectric and air medium inside waveguide and waveguide wall.

5.2 Sensor Concept – Transmission Line

Electromagnetic waves are waves of energy that travel through a vacuum at the speed of light, approximately c=3×108 m/s. EM waves consist of two primary components: an electric (E) field and a magnetic (H) field. The multi-parameter nature of wideband microwave analysis can provide unique signal spectrum signatures. Typically, these would be in the form of a reflected signal S11 or/and a transmitted signal S21, which are influenced by parameters such as conductivity and permittivity.

The sensor is designed for the automotive field, with the aim of monitoring the quality of the diesel in real time. The sensor is expected to be housed in the pipes of the power supply system. The innovative aspect of this sensor is the ability to exploit the diesel as an element that flows inside the sensor itself and, during its passage, measure microwave attenuation. In this way, the presence of water can be detected and, if the system is appropriately sized, conditioned and calibrated, water content can be measured. A transmission measurement method has been chosen as it appears the simplest and most economic technique, because of the availability of very low-cost integrated circuits for the generation of the stimulus signal, and the use of a simple sensor with an envelope threshold detector for the measurement of the attenuated signal, which can be part of a small and low power embedded system. The signal attenuation can be evaluated through the scattering parameter S_{21} (forward voltage gain, or transmission coefficient), which is the ratio between outgoing wave amplitude at output port 2 and ingoing wave amplitude at input port 1, assuming load impedance matching at port 2. A threshold detector may be useful, in particular, to provide an alert around a programmable level of the signal output. The most suitable guiding structure is certainly the coaxial one that guarantees the maximum fringing of the EM field in the analyte and, consequently, the maximum sensitivity [90, 91, 92].

5.2.1 Validation of the Physical Principle

Currently, the proposed methodology has been simulated with diesel fuel in the following conditions: a signal frequency range from 2 GHz to 8 GHz, the variation of the water concentration in the diesel according to the limits imposed by the EN590 standard and the variation of the radius of the core of the coaxial structure. Sensor geometry is shown in figure 6.1. Preliminary sizing was defined by imposing a characteristic impedance Z_0 of the transmission line equal to 50 Ω, using the following equation:

$$Z_0 = \frac{138}{\sqrt{\varepsilon_r}} \; log_{10}\frac{D}{d} \; \Omega \tag{5.4}$$

where ε_r is the relative dielectric constant of diesel equal to 2.1, D is the inner diameter of the shield equal to 4.5 mm and d is the diameter of the core. The diameter of the shield is imposed by the size of the power supply system piping. From this equation we have obtained an initial value of the core

diameter, according to which we have designed spacers that support the core within the shield, as shown in figure 5.1.

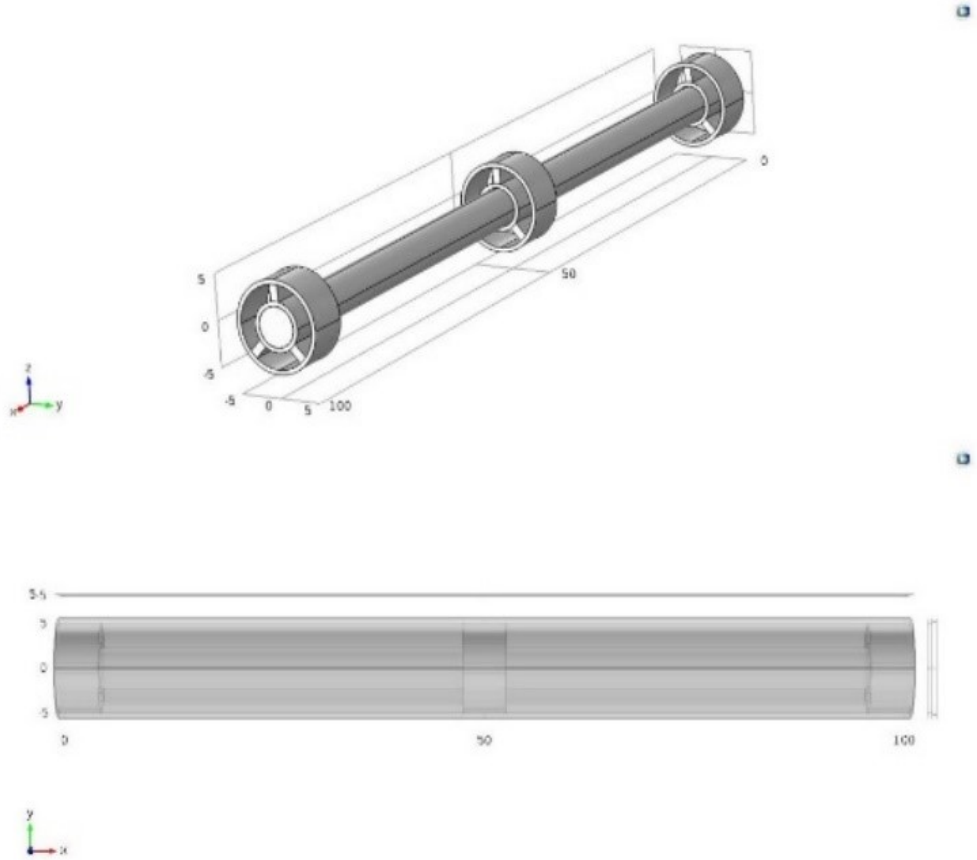

Figure 5.1. Preliminary Geometry of the Coaxial Structure.

The operating environment has specific characteristics such as temperature range, presence of vibrations, shocks and corrosive elements. These environmental and working aspects play an important role when choosing a material for this application.

Hence, one of the critical steps in the design process is the selection of materials. Materials must have good or excellent electrical, mechanical and environmental performance, especially good electrical conductivity, machinability and ductility, good stability and tensile strength to withstand mechanical influences, good stress relieving, hardness and reasonable price [93, 94].

Regarding the conductive part of the guiding structure, common materials on the market are copper, stainless steel and aluminum. Copper is one of the most commonly used metals for conducting electrical signals and is preferred to stainless steel which is more difficult to process than the former. Copper and aluminum offer good corrosion resistance and good breaking strength. The final choice,

however, relies on copper, due to its versatility and its ability to be used in copper-copper welding without the use of a filler material.

To minimize the housing space and get an electric length such as to observe the attenuation of the signal, the axial length of the sensor has been fixed at 100 mm.

As for the spacers, they must guarantee good corrosion resistance, good mechanical resistance and minimum signal attenuation. As seen in the preliminary design, they will not have to occupy much free volume. The spacer will be stuck to the core and glued to the shield. The separation between core and shield is ensured by three equidistant fins and arranged radially around the core to minimize the space occupied by the spacer, as shown in figure 5.2.

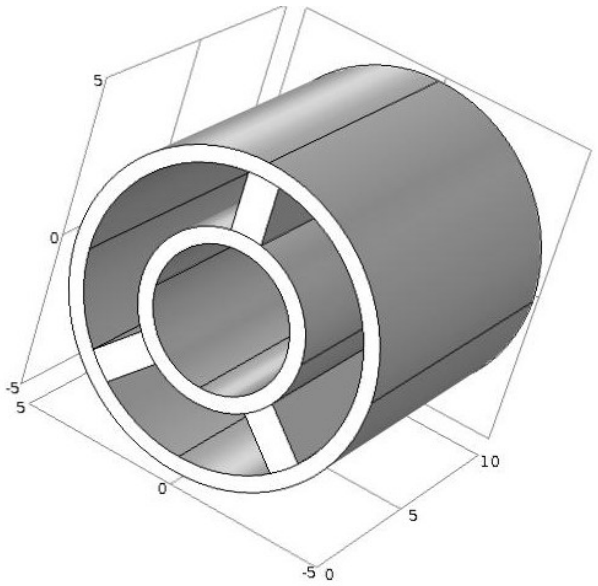

Figure 5.2. Spacer Geometry.

The following materials are commercially available: polyethylene (PE), polytetrafluoroethylene (PTFE), PEEK (or polyether-ether-ketone), polyphenylene oxide (PPO) and silicone rubber. The final choice will be between PE and PTFE, because in addition to their good workability and discrete mechanical properties, they have a dielectric constant very similar to that of diesel. The latter is a necessary condition to avoid significantly disturbing the propagation of the stimulus signal.

We have modeled the sensor by studying the mechanical resistance, the stiffness, the fluid dynamic load and we have performed the electromagnetic validation of the physical measurement principle. The sensor must evaluate the attenuation of the signal, in terms of power, due to the different permittivity of the water with respect to the diesel. It was decided to evaluate the permittivity because it is an important indicator of the quality of diesel oil. When this differs from the standard value it can indicate the presence of contaminants, such as water.

In the multi-physics simulation, the sensor was modeled considering the core suspended in the shield, thanks to three spacers, two at the ends and one at the centerline. The spacers were constrained at the spacer-core and spacer-shield interfaces while the shield was externally constrained. The acting loads are the weight of the same physical structure and the fluid dynamic load of the diesel fuel flow, in terms of pressure. The simulations were conducted by comparing the materials listed in the previous section and it was verified that under static conditions, the maximum deflection that the core undergoes is negligible, of the order of nanometers, as shown in the figure 5.3. In the same way, the velocity profile that is generated inside the structure does not cause excessive local pressure peaks, particularly in the areas of connection between spacers and cores. Also, in this case, the deformations of the spacers have orders of the nanometers, as shown in figure 5.4. When varying the radius among feasible values, we obtained, in general, increasing deflections of the core that remain, however, of the same order of magnitude, as shown in table 5.2.

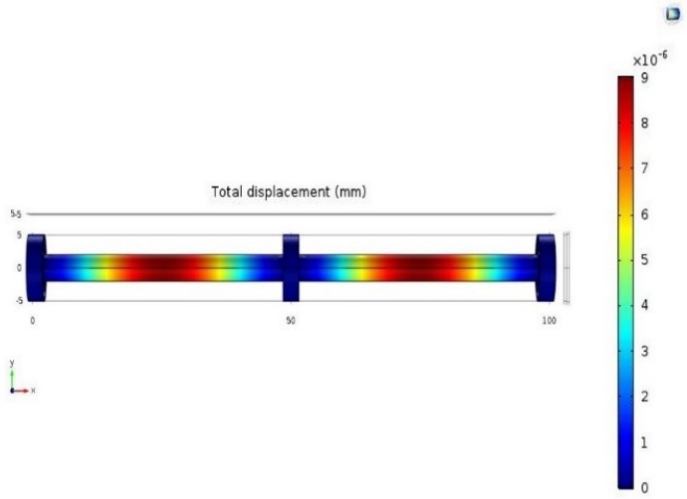

Figure 5.3. Displacement Field of the Core.

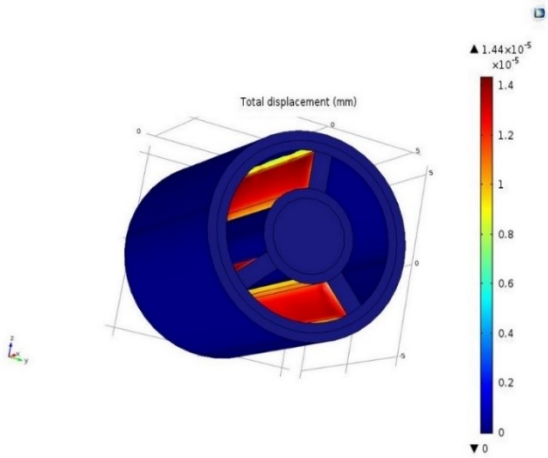

Figure 5.4. Displacement Field of the Spacer.

RADIUS OF CORE [mm]	MAXIMUM CORE DEFORMATION [nm]
1.00	0.79
1.35	1.35
1.70	1.92
2.05	2.29
2.40	2.43
2.75	2.28
3.10	1.90
3.45	2.33
3.80	2.82
4.15	3.36
4.50	3.94

Tab. 5.2. Maximum Core Deformation depending on its Radius.

After comparing the static strength of the critical elements of the guiding structure, core and spacer, we have identified in the copper and polyethylene, respectively, the materials suitable for the development of the sensor, as shown in tables 5.3 and 5.4. For the compared materials, the maximum deflection arrow of the core is always very low. Copper is also chosen because of its greater electrical conductivity and the lower price. The same considerations apply to spacers. The thinning of the material, the dielectric constant and the price are evaluated. Polyethylene is the best choice.

	COPPER	ALUMINUM	STAINLESS STEEL
POISSON COEFFICIENT	0.34	0.35	0.27
DENSITY [kg/m^3]	8960	2700	8000
YOUNG MODULE [GPa]	117	70	2000
ELECTRIC CONDUCIBILITY [S/m]	59.6×10^6	37.7×10^6	$1{,}45\times10^6$
PRICE	LOW	HIGH	HIGH
MAXIMUM DEFLECTION OF THE CORE [nm]	86.6	44.7	46.5

Tab. 5.3. Comparison of Materials for the Core.

	PE	PTFE	PEEK	PPO	SILICONE RUBBER
POISSON COEFFICIENT	0.42	0.45	0.38	0.38	0.48
DENSITY [kg/m^3]	930	2200	1320	1060	1100
YOUNG MODULE [MPa]	1000	400	360	250	50
DIELECTRIC CONSTANT	2.3	2.1	3.3	2.7	2.9 ÷ 4
PRICE	LOW	VERY HIGH	VERY HIGH	HIGH	LOW
MAXIMUM THINNING OF THE SPACER [nm]	0.4	0.11	938	0.17	0.79

Tab. 5.4. Comparison of Materials for the Spacer.

Subsequently, the electromagnetic analysis of the sensor has been refined. In figure 5.5 it is highlighted that the structural characteristics of the system under test invite decidedly to use coaxial structures, since they ensure the maximum fringing field EM near the core and, consequently, the maximum sensitivity. The electromagnetic simulation was conducted by fixing a power to the input port equal to 1 W.

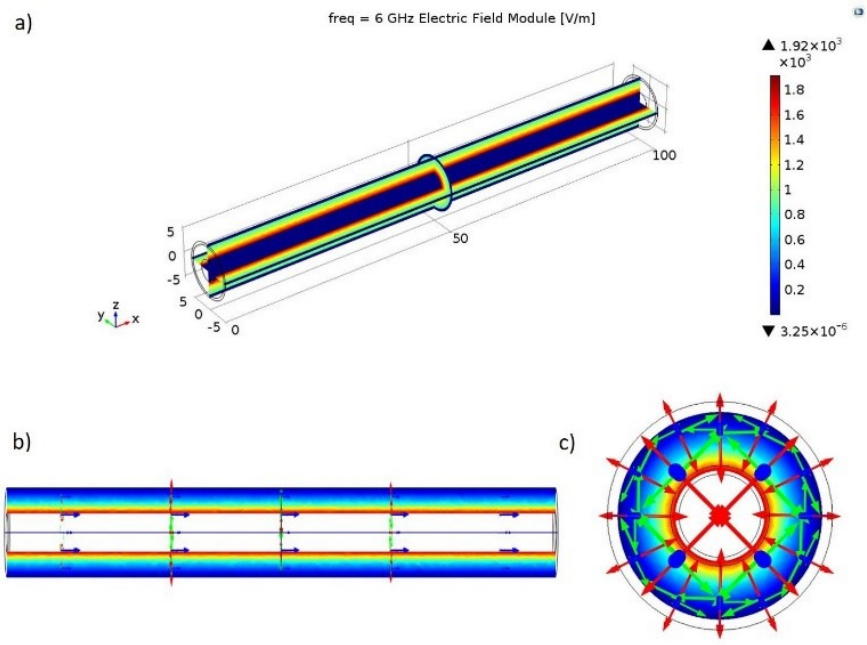

Figure 5.5. The Electric Field in the Coaxial Structure with Pure Diesel Dielectric, at f= 6 GHz: a) module of electric field, b) detail of the electrical field (in red), the magnetic field (in green) and the propagation of the electromagnetic wave (in blue) in xz plane and c) detail in yz.

Simulations were performed by using COMSOL Multiphysics software in order to find the relation between critical sensor parameters and sensitivity. For the preliminary simulations, it was decided to

adopt a very simple mathematical model to express the relative permittivity of the analyte as a function of the water concentration:

$$\varepsilon_{eff} = (\varepsilon_W - \varepsilon_D)\rho + \varepsilon_D \quad (5.4)$$

where ε_D = 2.1 is the relative permittivity of pure diesel, ε_W = 80.4 is the relative permittivity of water and ρ is the concentration of water in the analyte. Unfortunately, there are not many data on dielectric loss tangent which, therefore, has been neglected to the first approximation. This approximation should not invalidate the simulations given that, in practice, extremely small water concentrations will be measured which affect negligibly tan δ. It is expected, in any case, that tan δ grows with ρ, therefore, the sensitivity of the system should at least improve considering dielectric losses.

Multiparametric simulations were performed, essentially by varying three parameters: the frequency of the stimulus signal, f, the thickness of the core, r_i, and the concentration of water in the fuel, ρ. The first two are operational parameters, while concentration is the independent variable of the problem under analysis. The geometric constraints are the diameter of the shield, of the same diameter of the conduct in which the sensor will be housed, of about 5 mm and the length of the coaxial transmission, of 100 mm. Figure 5.6 shows the results of the simulations performed at f = 6 GHz, for different values of the radius of the core r_i. From these results, it is clear that attenuation increases for larger radii.

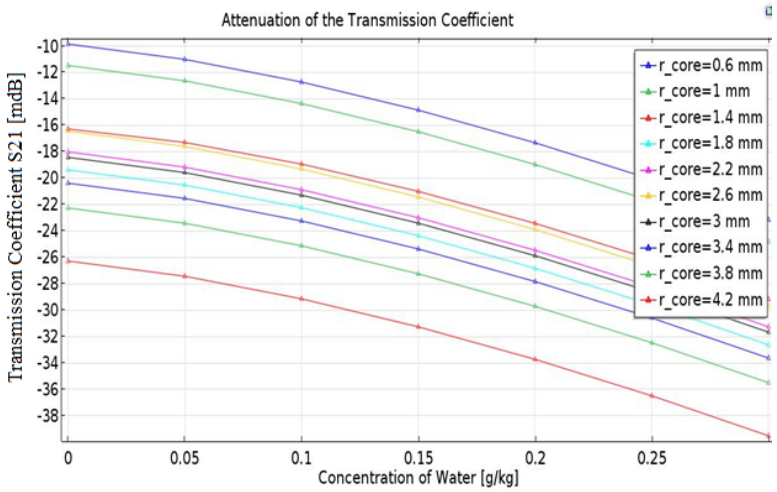

Figure 5.6. Transmission Coefficient for Different Values of Core Radius r_i.

Moreover, we have verified that with the increase of the frequency of the stimulus signal, with the same radius, sensitivity increases, hence sensor detectivity may be tuned. This can be useful because,

although the standards set a maximum limit of water, this limit will vary according to the geographical area of origin of the diesel, as shown in figure 5.7.

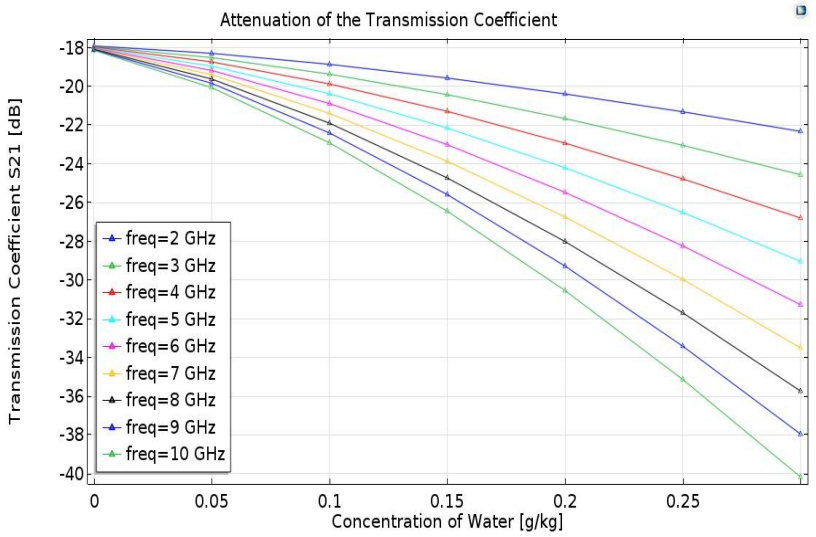

Figure 5.7. Transmission Coefficient for Different Values of Frequency of the Stimulus Signal.

Considering both the electromagnetic modeling and the fluid-dynamic modeling, we conclude that a small core radius is advantageous. This choice is strengthened by the fact that the size of the core determines the weight and bulk of the line. Obviously to minimize the weight and mass of the coaxial transmission line and decrease attenuation, we should reduce the radius as much as possible. However, there are lower limits on core radius as regards manufacturability, power carrying capabilities, and safety. Indeed, for lower radii the electromagnetic field increases within the coaxial line, which can lead to breakdown of the dielectric due to ionization, a dangerous condition. For these reasons, we have chosen, for the dimension of the core, a radius equal to 2.2 mm, which gives a maximum field of about 3 kV/m.

With that value, high fringing on the core and good sensitivity are achieved, as shown in the figure 5.7. In the graph, the linearity of the transmission coefficient is appreciated up to the maximum permissible concentration of water in diesel according to standards, i.e. not exceeding 0.25 g/kg, namely 250 ppm, as prescribed by EN590. Mechanically, the stiffness of the structure is guaranteed by the arrangement and the geometry of the spacers that, thanks to the core size, occupy only a small portion of space between shield and core.

For in-line integration, the sensor needs stimulus, conditioning and read-out devices to be installed directly on it. The maximum sensitivity configuration, at f = 6 GHz, shows a discrete linearity of the

transmission coefficient ΔS_{21} with respect to the water concentration Δρ in ppm, with sensitivity, in eq 5.5:

$$\frac{\Delta S_{21}}{\Delta \rho} = 0.043 \frac{\text{dB}}{\text{ppm}} \tag{5.5}$$

A Δρ of 50 ppm produces a variation of S_{21} equal to 0.03 dB, which is appreciable if the sensor is appropriately conditioned and calibrated.

So, this study to optimize the geometry of sensor is carried out in order to verify the rigidity and strength of the guiding structure and the corrosion resistance of the system. This is achieved by choosing copper and polyethylene, respectively for the core and spacers. The material of the core has excellent electrical conductivity and good mechanical strength. The material of the spacers avoids signal reflection and permits to support the core in the shield, minimizing the core deflection and taking up less volume with a suitable geometry. It has been verified by simulations that introducing into the sensor fuel with a different water contents, i.e. a different permittivity, microwave attenuation changes with a sensitivity of 0.6 mdB/ppm at 6 GHz. It is expected a total change of the scattering parameter S_{21} from -24 dB for pure fuel, to -32 dB for fuel contaminated by water at the limit of 200 ppm prescribed by EN590. The results show that the sensitivity increases with frequency, while core size is a compromise between electromagnetic performance and manufacturability. Tuning of sensitivity may be useful in order to work in different geographical area, since the chemical nature of the fuel changes with respect to production place. In figure 5.8, it is represented in CAD how the sensor should be.

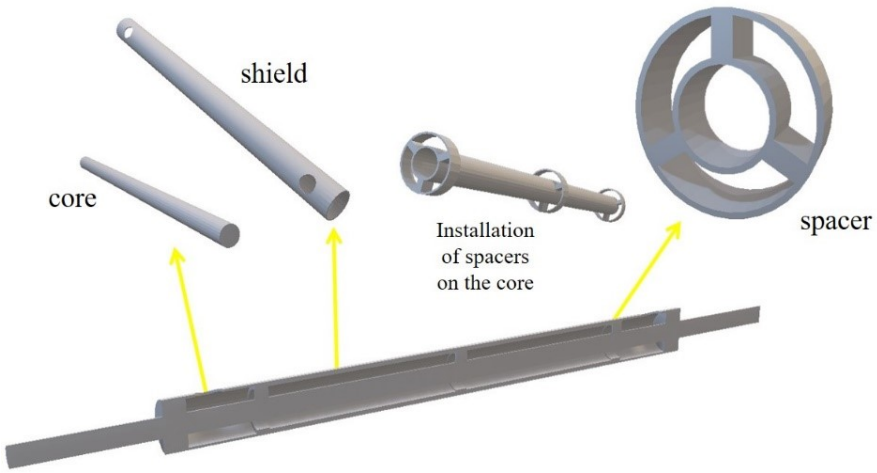

Figure 5.8. CAD of Transmission Line.

5.2.2 Fluid Dynamic and Mechanical Sizing of the Complete Structure

The shield will have two holes along its wall, for the entry and exit of the diesel flow. It is preferred to change the direction of the flow by tapping and not to deform the core, as the implications on electromagnetic fringing would not be optimal (Fig. 5.9). To divert the flow rather than the electromagnetic waves, because otherwise the behavior of the new bended core geometry could affect the extent of the attenuation. Also, the bending processing to be applied to the core could affect the stiffness of the guiding structure.

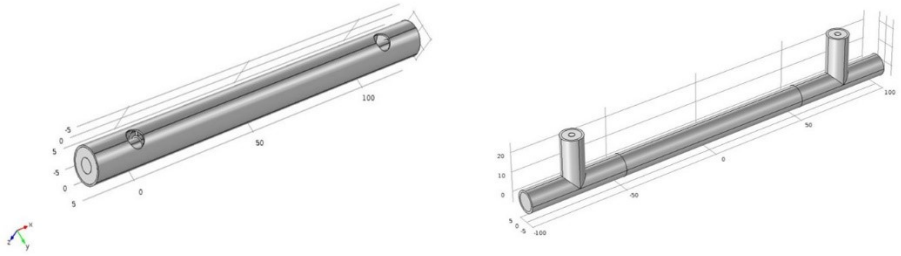

Figure 5.9. Solutions for the Passage of Diesel.

As the sensor length changes, the core undergoes deformations along the maximum arrow of the order of micrometers. If the length is 250 mm, the maximum deformation will be about 200 while if the length is 200 mm, the maximum deformation is about 902 micrometers (Fig. 5.10).

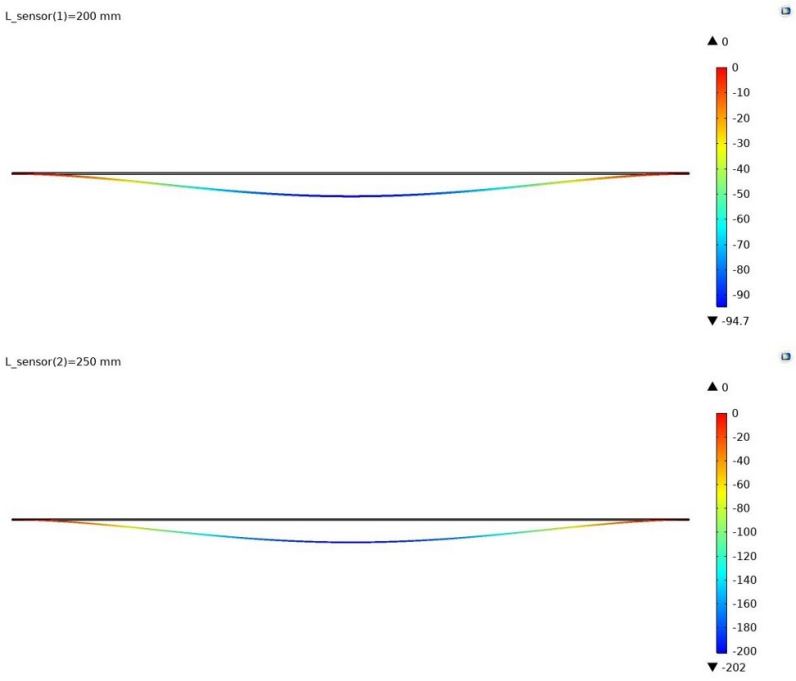

Figure 5.10. Maximum Deformation [μm] with varying Sensor Length.

On a fluid dynamic level, assuming an input speed of the flow in the sensor of 2 m/s it occurs that if the radius of the internal diameter of the shield increases, the output velocity of the flow decreases, thus reducing the stress of the flow on the core (Fig. 5.11). This would maximize the solidity and rigidity of the core of the transmission line. It is evident that the maximum pressure decreases when radius increases. However, its value is in the order of magnitude of millibars, therefore very low (Fig. 5.12).

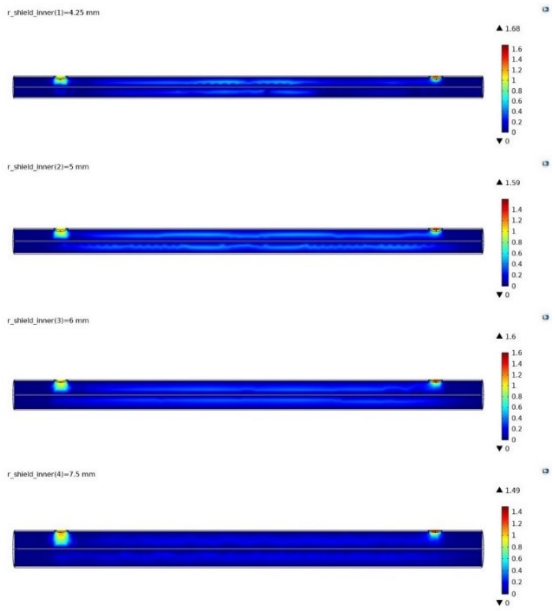

Figure 5.11. Output Flow Speed.

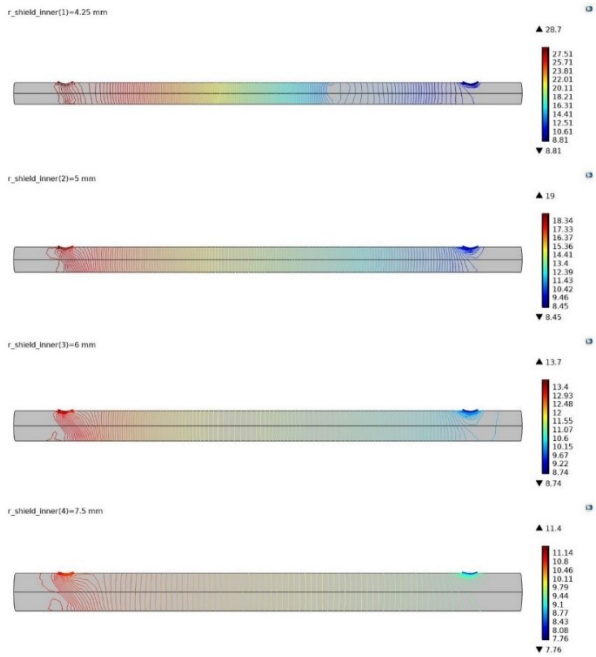

Figure 5.12. Maximum Outlet Pressure [mbar].

In addition, the maximum fringing that occurs on the core was evaluated, calculating the modulus of the electric field (V m) as the core radius changes, in two conditions: when the mixture has 0 ppm and 200 ppm of water, the latter being the limit prescribed by EN590, like showed in figure 5.13.

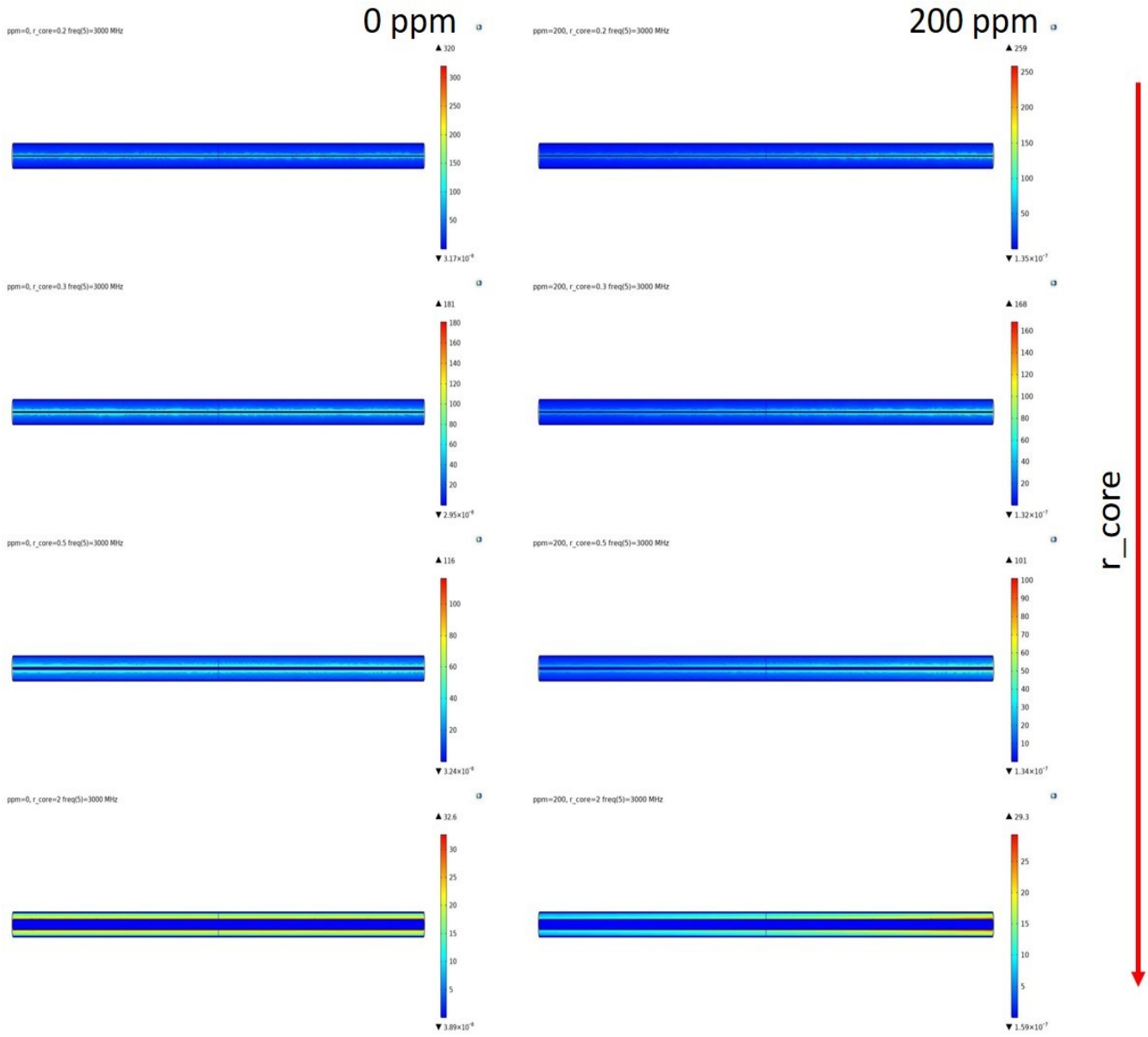

Figure 5.13. Maximum Fringing when the Radius of Core Increase.

Note that for a fixed frequency value, the variation of parameter S21 measured for the two mixture values, 0 and 200 ppm, is greater for smaller diameters, varying from 5.93 dB (0.2 mm diameter) to 5.89 dB (2 mm diameter) at 1 GHz (Fig. 5.14). The difference is minimal because the variation of water we are measuring is very small., however it is evident that a smaller diameter will increase the sensor sensitivity.

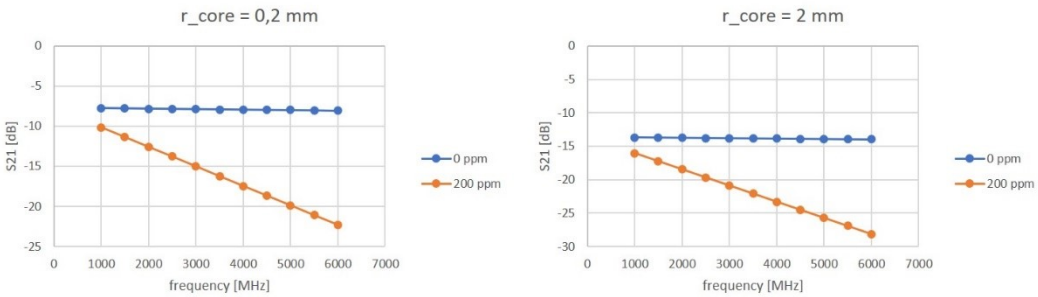

Figure 5.14. Attenuation when the Radius of the Core Changes.

However, as the variation is very small, a diameter of 1.2 mm was chosen to reach a compromise between stiffness and ease of sensor manufacturing.

5.2.2 Final Design

To obtain the final design, simulations were conducted with a parametric sweep (0 50 100 150 200 250 300 500 ppm) in the frequency domain in a range between 1 GHz - 6 GHz with a step of 100 MHz. The results refer to the empirical mathematical model explained in the chapter 5. Two designs were selected for the prototypes.

5.2.2.1 Prototype 1

Prototype 1 has a length of 200 mm. The external diameter of the shield is 9.5 mm with a thickness of 1 mm while the core diameter is 1.2 mm (Fig. 5.15). The power at input port is 1 W. The electric field is shown in figure 5.16.

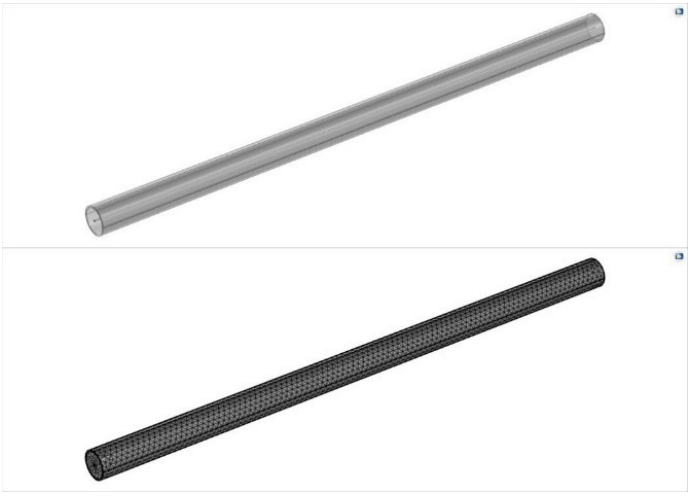

Figure 5.15. Model of the Prototype 1.

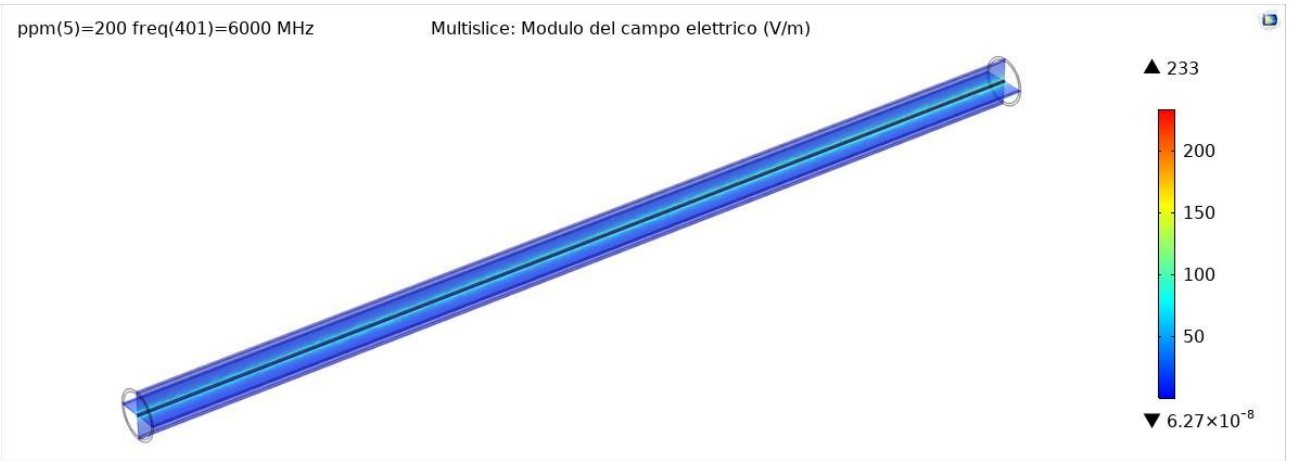

Figure 5.16. Electric field of the Prototype 1.

Figure 5.17 shows the graph of the transmission coefficient S_{21}, the attenuation, for different frequencies and water concentrations. In figure 5.18 there is the sensor calibration curve for a frequency value equal to 2.54 GHz which highlights an R^2 equal to 0.8261 when interpolated linearly.

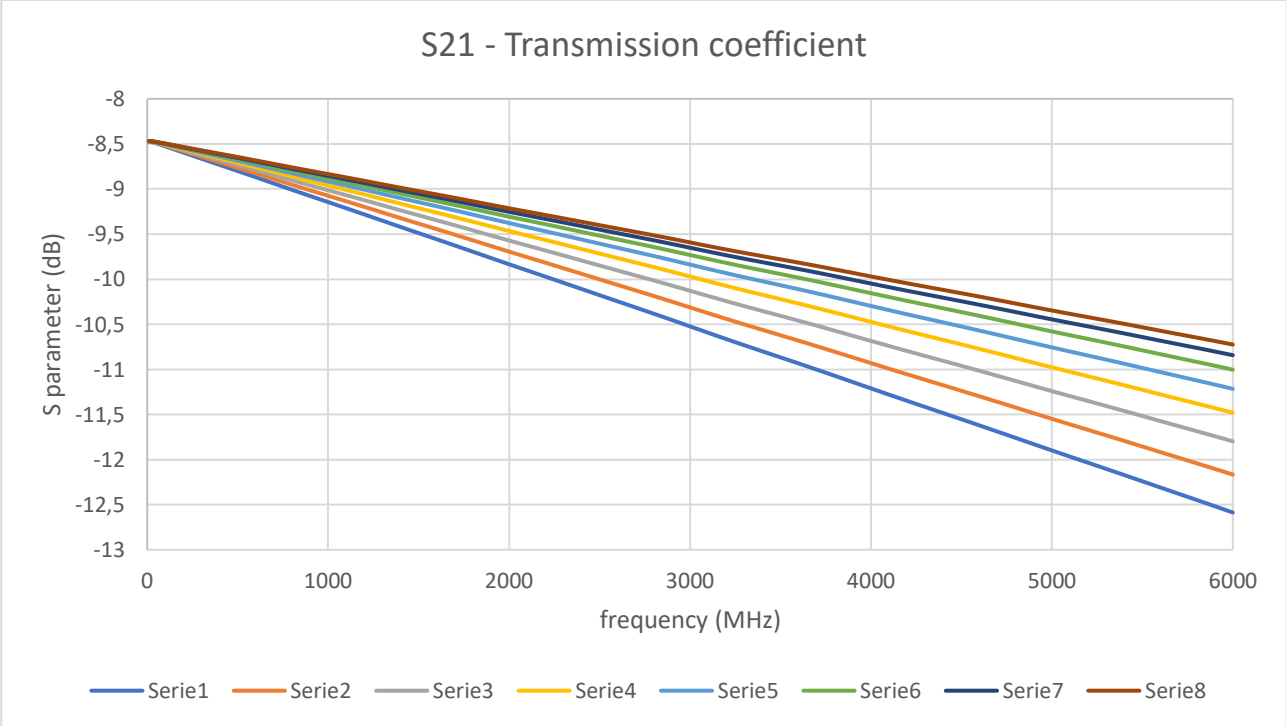

Figure 5.17. S_{21} of Prototype 1.

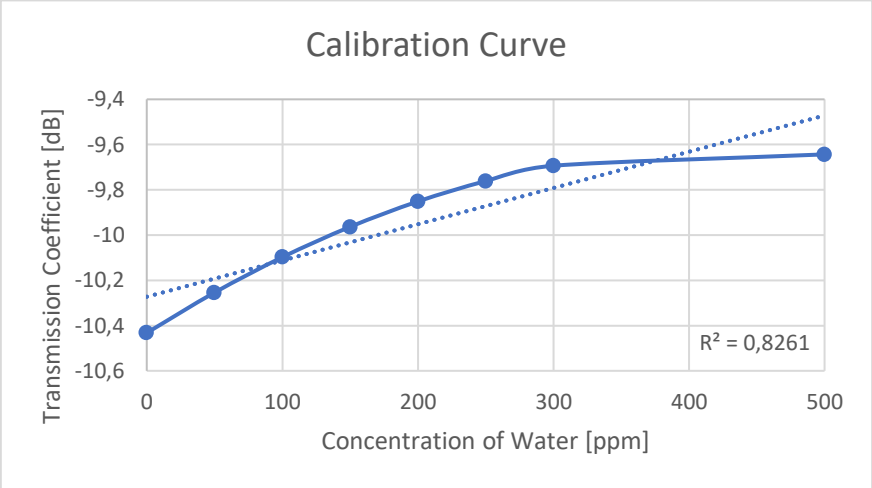

Figure 5.18. Calibration Curve of the Prototype 1.

5.2.2.2 Prototype 2

Prototype 2 has a length of 250 mm. The external diameter of the shield is 16 mm with a thickness of 1 mm while the core diameter is 1.2 mm (Fig. 5.19). The power at input port is 1 W. The electric field is shown in figure 5.20.

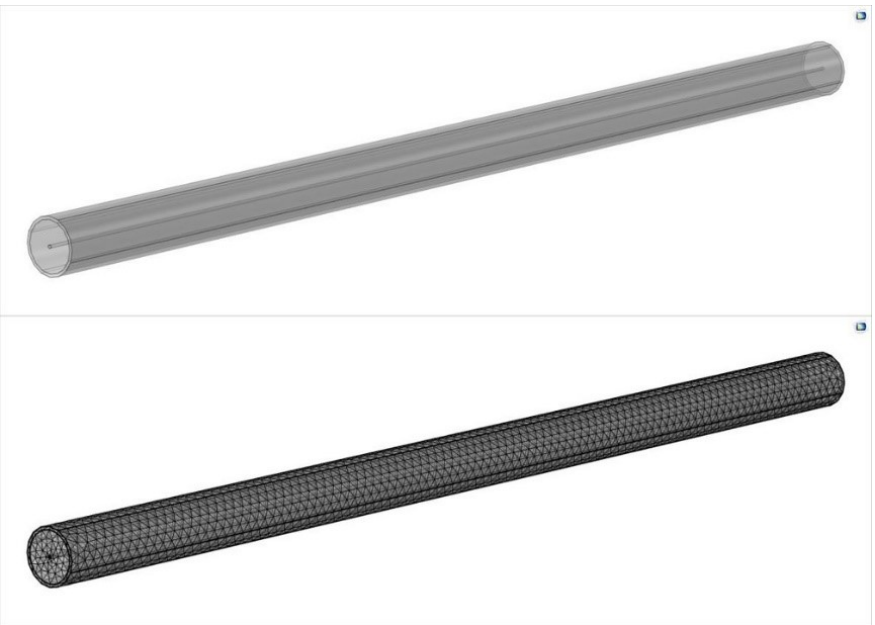

Figure 5.19. Model of the Prototype 2.

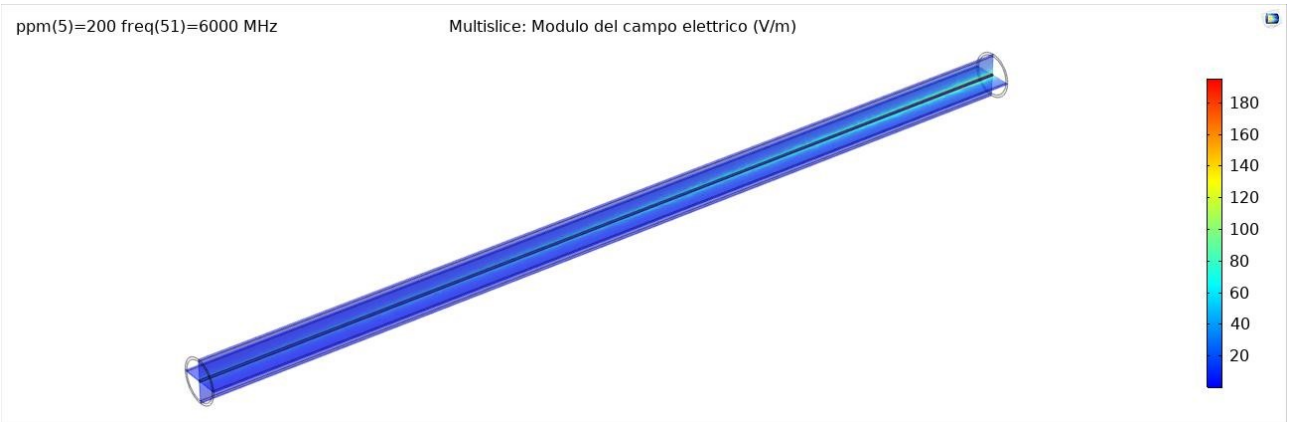

Figure 5.20. Electric field of Prototype 2.

Figure 5.21 shows the graph of the transmission coefficient S21, the attenuation, for different frequencies and water concentrations. In figure 5.22 there is the sensor calibration curve for a frequency value equal to 2.54 GHz which highlights an R2 equal to 0.8261.

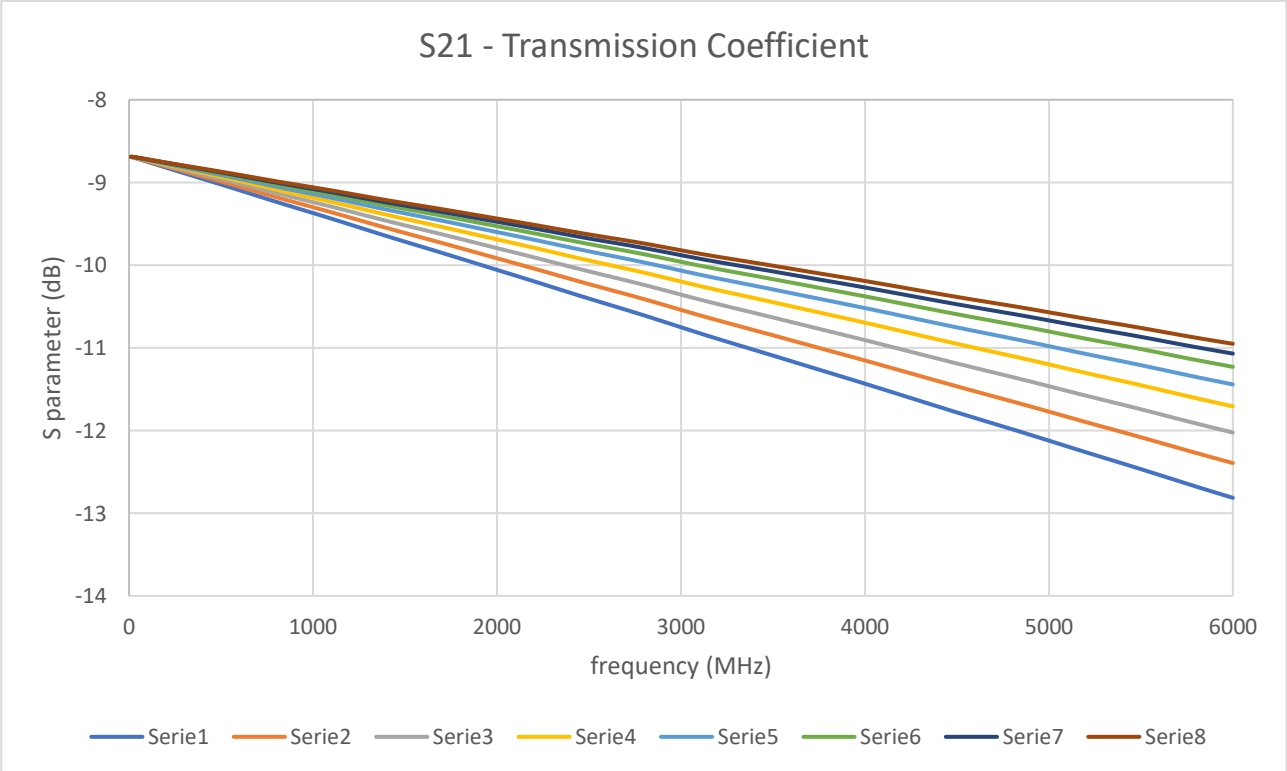

Figure 5.21. S21 of the Prototype 2.

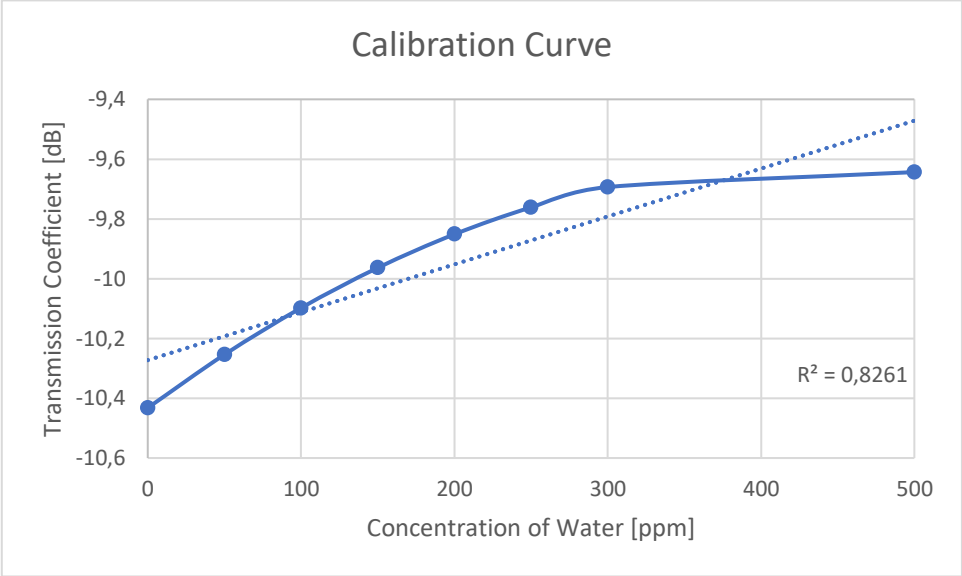

Figure 5.22. Calibration Curve of the Prototype 2

5.3 Resonant Cavity

Microwave cavities are widely used for characterizing the properties of materials. A cavity is usually made by shortening the two ends of a waveguide segment. The electrical power is transported through the waveguide through electromagnetic waves, which can take several different configurations (modes), depending on the frequency, the dimensions and the material properties inside. The different configurations of an electric and magnetic field which can exist in a waveguide are known as transverse electromagnetic (TEM) modes. The transverse electric (TE) and transverse magnetic (TM) are the two types of modes which usually exist in the waveguide. A cavity will resonate when it is excited at an appropriate frequency. In this section we verify that variation of dielectric constant can give a significant frequency shift in properly designed resonant cavity. The resonant modes occur when the electric and magnetic fields form standing waves, which depend on the internal dimensions of the cavity and the dielectric properties of the water in diesel. Therefore, its relative permittivity (ε_r) will change. The resonant frequency for TE_{nml} and TM_{nml} modes in a circular waveguide can be calculated using equations 5.5 and 5.6:

$$f_{mnl}{}^{TM} = \frac{c}{2\pi\sqrt{\mu_r\varepsilon_r}}\sqrt{\left(\frac{p_{nm}}{r}\right)^2 + \left(\frac{l\pi}{h}\right)^2} \qquad (5.5)$$

$$f_{mnl}{}^{TE} = \frac{c}{2\pi\sqrt{\mu_r \varepsilon_r}} \sqrt{\left(\frac{p_{nm}{}'}{r}\right)^2 + \left(\frac{l\pi}{h}\right)^2} \tag{5.6}$$

where: c is the speed of light, μ_r is the relative permeability, ε_r is the relative permittivity, p_{nm} is the value of the Bessel function for the TE or TM modes of a circular waveguide, r is the radius of the cavity and h is the height of the cavity. Therefore, all TE and TM modes are dependent on $\sqrt{\varepsilon_r}$, so when the waveguide is excited by a range of frequencies, the magnitude signal spectrum is captured and resonant peaks corresponding to these particular modes will shift to lower frequencies as the permittivity is increased. Moreover, we must remember that quality factor (Q-value) is an essential parameter for estimating the quality of the cavity resonators. The perturbation method assumes that the actual fields of a cavity with a small shape or material perturbation are not greatly different from those of the unperturbed cavity. Generally, the calculation of the dielectric parameters is performed by measuring the S-parameters of the network under examination. Through the resonance frequency formula, we define two models of cavities, so that we have the propagation of the TE and TM modes. To obtain propagation of the TE mode, the height of the cavity must be greater than twice the radius, while to obtain propagation of the TM mode, the height of the cavity must be less than twice the radius. A circular cross-sectional cavity is formed by closing both ends of a circular waveguide with plates. Coupling in and out the cavity can be done using irises or probes. Equating both above equations, an identical frequency is found when h/a = 2.03. When h/a < 2.03, the dominant or fundamental mode is the TM010 whereas for h/a > 2.03, the dominant mode is the TE111 mode. . The dimensions of the cavity to be studied in this project are fixed such that to have a dominant mode resonant frequency at 4.206 GHz that is a TE111 mode. In this case, the length h and the radius a of the cavity are fixed to have the ratio of h/a which is bigger than 2.03. The mode to be analyzed is then the TE111 one. As mentioned earlier, an infinity of modes would coexist in the cavity, and Table I shows a few of the lowest modes and their resonant frequencies.

In this section, we verify that dielectric constant can give a significant frequency shift in a properly designed resonant cavity. COMSOL simulation package was used to analyze the eigenfrequency inside the cavity resonator and its associated mode for the input frequency. The modes that are generated for each model have been identified, which will generate a resonant peak with a given quality factor. We compared some modes, evaluating the shift of the resonance frequency in relation to the contamination change of the diesel EN590. According to the resonant perturbation theory, the

presence of a dielectric sample inside the cavity causes a shift of the resonant frequency and a variation of the Q-factor. Numerical eigenmode simulations of the stand-alone cavity, i.e. without coupling elements, are carried out to analyze the electromagnetic behavior of the resonator when a capillary is filled with different mixtures.

5.3.1 Design

Also, in this case two prototypes were made. They were initially evaluated as empty and air-filled cylindrical cavities and, subsequently, a capillary leaving the cavity was considered for the entry and exit of the flow of mixtures. Prototype 1 is a cylindrical cavity 35 mm high and 30 mm in diameter. The thickness is 1 mm. Prototype 2 is a cylindrical cavity 40 mm high and 50 mm in diameter. The thickness is the same. Two types of capillaries were chosen, the first cylindrical, with an internal diameter of 3 mm and a thickness of 1 mm and the second curved with an external square section with a side of 5 mm, while the side of the internal section is 3 mm. It was decided to adopt a curved capillary to increase the ability to identify small variations in the concentration of water. The cavity is in copper while the capillary in PTFE. Figure 5.23 describes the two prototypes and the solutions adopted with the two capillaries.

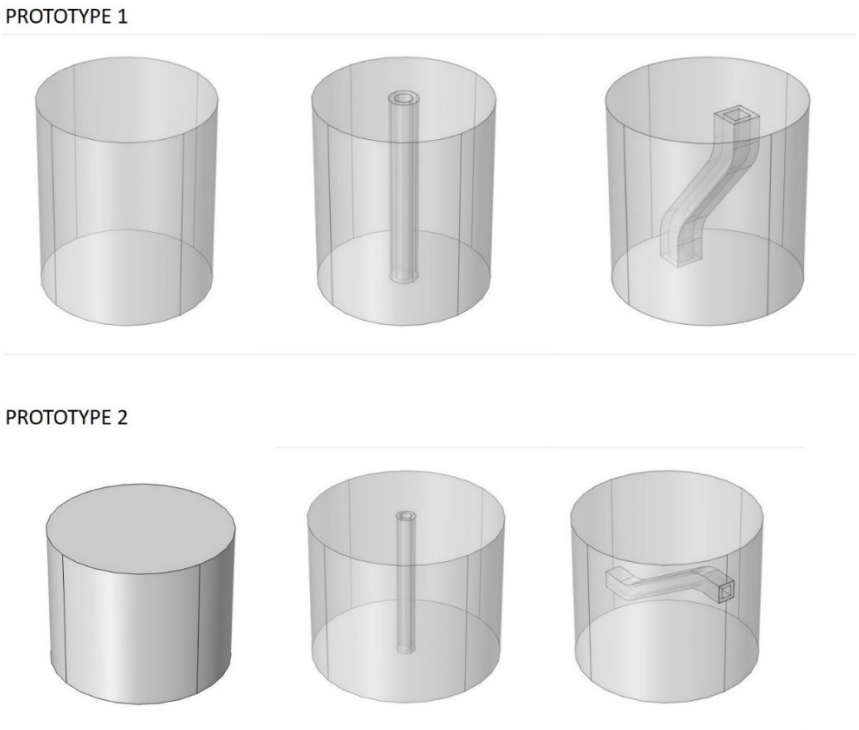

Figure 5.23. Prototypes of the Resonant Cavity.

Resonant modes were found for each prototype by comparing three software: Mathworks MATLAB, Wolfram Mathematica and Comsol.

An impedance boundary condition has been imposed to find propagation modes. So, in this first phase, devoted to determining the modes, there is no electrical coupling.

5.3.2 Propagation Modes with Matlab

It has been used a simple script, reported in figure 5.24, to derive the propagation modes, using the Bessel functions and the geometric dimensions of the cavity. Tables 5.5 and 5.6 show the resonance frequencies of the modes found for the two prototypes.

```
'The following computes the resonance frequencies of Cylindrical Cavity.
Assuming cavity filled by air dielectric (epsilon_r=1)'
r=input('Radii of the Cylindrical Cavity (in [mm])=');
h=input('Height of the Cylindrical Cavity (in [mm])=');
k=300/(2*pi);
f1=k*sqrt((2.405/r)^2+(pi/h)^2)*1000;
f2=k*sqrt((3.832/r)^2+(pi/h)^2)*1000;
f4=k*sqrt((1.841/r)^2+(pi/h)^2)*1000;
f5=k*(1.841/r)*1000;
format short g
sprintf('TM 011 : f[Mhz]=%f \n TE 011 : f[MHz]=%f \n TM 111 : f[MHz]=%f \n TE 111 : f[MHz]=%f \n TE
110 : f[MHz]=%f',f1,f2,f2,f4,f5)
```

Figure 5.24. MATLAB Script for Determining Resonance Frequencies.

PROTOTYPE 1	
	Resonant Frequency [MHz]
TM011	8773,355849
TE011	12928,63653
TM111	12928,63653
TE111	7260,023636
TE110	5860,085005

Table 5.5. Resonant Frequencies of Prototype 1.

PROTOTYPE 2	
	Resonant Frequency [MHz]
TM011	5929,594702
TE011	8223,388987
TM111	8223,388987
TE111	5140,536417
TE110	3516,051003

Table 5.6. Resonant Frequencies of Prototype 2.

5.3.3 Propagation Modes with Mathematica

An electromagnetic wave can be confined inside a space surrounded by conducting walls, which is called a cavity. Let's consider a cylindrical cavity with inner radius *R* and height *d*. There are two possible wave modes: transverse electric (TE) and transverse magnetic (TM). Separation of variables leads to harmonic solutions to the wave equation (from Maxwell's equations) thanks to Bessel function of the first kind. The possible electromagnetic resonances can be classified as TE_{mnp} or TM_{mnp}, which completely determine the electromagnetic fields E and H in the cavity. Resonance states show localization of energy density in the cylindrical cavity. In Figures 5.25 and 5.26, the

propagation modes and the respective resonance frequencies for both prototypes are reported. The results obtained with Mathematica confirm the ones obtained with MATLAB. The comparison between multiple software was necessary because, being the variation of water concentration very small, it is useful to have a comparison between values with different orders of magnitude in decimals.

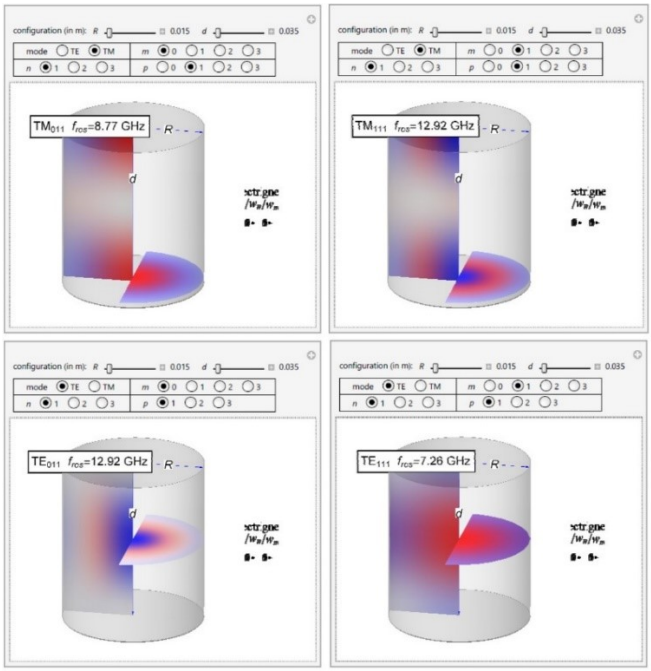

Figure 5.25. Resonant Frequencies of Prototype 1

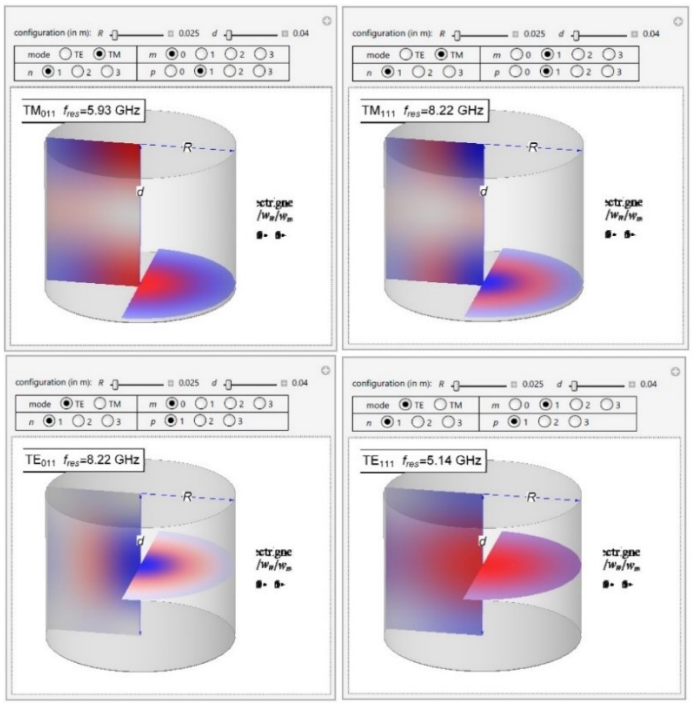

Figure 5.26. Resonant Frequencies of Prototype 2

5.3.4 Propagation Modes with Comsol

COMSOL simulation package was used to analyze the eigenfrequency inside the cavity resonator and its associated mode. The fundamental mode enables the propagation of the wave strongly across the sample and yields a high sensitivity measurement of samples. This mode will generate a resonant peak with a quality factor Q. A high Q indicates a sharp resonant peak that will be more readily analysed and improve the accuracy of the sensor. In Comsol the eigenfrequency method was used to find resonance modes. In linear algebra, every linear transformation between finite-dimensional vector spaces can be given by a matrix. For many applications, the eigenfrequency f is a more interesting quantity than the eigenvalue λ. They are often related since, equation 5.7:

$$f = \frac{i\lambda}{2\pi} \tag{5.7}$$

The eigenvalue solver algorithm leads to the generalized eigenvalue system, equation 5.8:

$$(\lambda - \lambda_0)^2 EU - (\lambda - \lambda_0)DU + KU + N^T \Lambda = 0 \tag{5.8}$$

The factor λ denotes the eigenvalue. The quadratic eigenvalue problem is solved by reformulating it as a linear eigenvalue problem.

5.3.4.1 Prototype 1

Tables 5.7 and 5.8 show the values of the resonance frequency and the Q-factor for the theoretical model and for the experimental model. Moreover, in figure 5.27, it is shown how the propagation modes, according to the resonance frequency, vary with the concentration of water. There are very low variations. In the graphs it is not possible to appreciate the variation on the vertical axis, because the values differ by four decimal orders of magnitude. These values are most noticeable in the tables.

Resonant Frequency		Theoretical Model			Experimental Model		
			TM111 TE011			TM111 TE011	
Straight Capillary		TM011		TE111	TM011		TE111
Air	1	8,77E+09	1,29E+10	7,26E+09	8,77E+09	1,29E+10	7,26E+09
0	2	8,42E+09	1,28E+10	7,11E+09	8,43E+09	1,28E+10	7,11E+09
50	3	7,94E+09	1,28E+10	7,05E+09	8,43E+09	1,28E+10	7,11E+09
100	4	7,49E+09	1,27E+10	7,02E+09	8,43E+09	1,28E+10	7,11E+09
150	5	7,09E+09	1,26E+10	7,01E+09	8,43E+09	1,28E+10	7,11E+09
200	6	7E+09	1,23E+10	6,76E+09	8,43E+09	1,28E+10	7,11E+09
250	7	7E+09	1,2E+10	6,49E+09	8,43E+09	1,28E+10	7,11E+09
			TM111 TE011			TM111 TE011	
Bend Capillary		TM011		TE111	TM011		TE111
Air	1	8,77E+09	1,29E+10	7,26E+09	8,77E+09	1,29E+10	7,26E+09
0	2	8,02E+09	1,2E+10	6,69E+09	8,02E+09	1,2E+10	6,69E+09
50	3	7,67E+09	1,19E+10	6,62E+09	8,02E+09	1,2E+10	6,69E+09
100	4	7,27E+09	1,18E+10	6,6E+09	8,02E+09	1,2E+10	6,69E+09
150	5	6,87E+09	1,17E+10	6,56E+09	8,02E+09	1,2E+10	6,69E+09
200	6	6,57E+09	1,15E+10	6,52E+09	8,02E+09	1,2E+10	6,69E+09
250	7	6,27E+09	1,14E+10	6,49E+09		1,2E+10	6,69E+09

Table 5.7. Resonant frequencies of Prototype 1

Q-Factor		Theoretical Model			Experimental Model		
			TM111 TE011			TM111 TE011	
Straigth Capillary		TM011		TE111	TM011		TE111
Air	1	11182,0	13935,6	12605,4	11182,0	13935,6	12605,4
0	2	4449,5	8744,5	11050,3	569,3	8744,5	3810,5
50	3	523,7	4709,9	4541,7	569,3	4709,9	3810,8
100	4	194,0	3732,6	1782,8	569,4	3732,6	3811,1
150	5	108,6	3160,4	759,1	569,5	3160,4	3811,4
200	6	2699,9	74,1	122,7	569,5	74,1	3811,7
250	7	2290,0	56,5	114,9	569,6	56,5	3812,0
			TM111 TE011			TM111 TE011	
Bend Capillary		TM011		TE111	TM011		TE111
Air	1	11182,0	13935,6	12605,4	11182,0	13935,6	12605,4
0	2	5536,6	8744,5	14177,1	808,2	1587,4	2315,1
50	3	620,1	4709,9	4270,7	808,3	1587,6	2315,4
100	4	194,3	3732,6	1800,7	808,3	1587,8	2315,6
150	5	100,3	3160,4	446,2	808,4	1587,9	2315,8
200	6	2117,9	74,1	201,8	808,5	1588,1	2316,0
250	7	87,5	56,5	113,7	808,6	1588,2	2316,3

Table 5.8. Q-factor of Prototype 1.

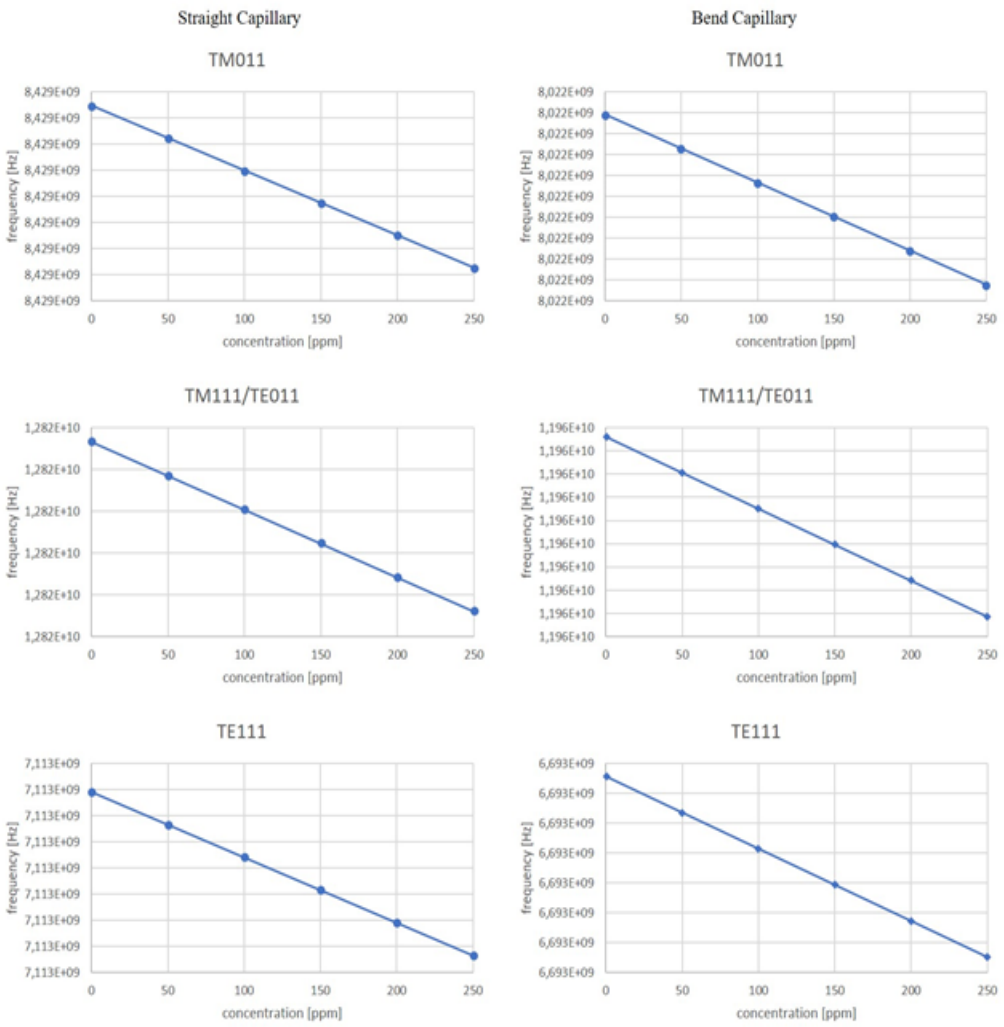

Figure 5.27. Variation of the Resonance Frequency when the Concentration of the Water Changes for the Prototype 1.

5.3.4.2 Prototype 2

Tables 5.7 and 5.8 show the values of the resonance frequency and the Q-factor for the theoretical model and for the experimental model. Moreover, in figure 5.28, it is highlighted how the modes of propagation, as a function of the resonance frequency. vary with the concentration of water. Again, the variations are very low. In the graphs it is not possible to appreciate the variation on the vertical axis, because the values differ by four decimal orders of magnitude. These values are most noticeable in the tables.

Resonant Frequency		Theoretical Model			Experimental Model		
			TM111 TE011			TM111 TE011	
Straight Capillary		TM011		TE111	TM011		TE111
Air	1	5,14E+09	5,93E+09	8,22E+09	5,14E+09	5,93E+09	8,22E+09
0	2	5,1E+09	5,86E+09	8,2E+09	5,1E+09	5,86E+09	8,2E+09
50	3	5,08E+09	5,76E+09	8,18E+09	5,1E+09	5,86E+09	8,2E+09
200	4	5,07E+09	5,43E+09	7,75E+09	5,1E+09	5,86E+09	8,2E+09
500	5	5,07E+09	6,65E+09	7,5E+09	5,1E+09	5,86E+09	8,2E+09
			TM111 TE011			TM111 TE011	
Bend Capillary		TM011		TE111	TM011		TE111
Air	1	5,14E+09	5,93E+09	8,22E+09	5,14E+09	5,93E+09	8,22E+09
0	2	5,65E+09	6,62E+09	7,81E+09	5,65E+09	6,62E+09	7,81E+09
50	3	5,62E+09	6,6E+09	7,74E+09	5,65E+09	6,62E+09	7,81E+09
200	4	5,44E+09	6,59E+09	7,4E+09	5,65E+09	6,62E+09	7,81E+09
500	5	5,71E+09	6,57E+09	7,61E+09	5,65E+09	6,62E+09	7,81E+09

Table 5.9. Resonant frequencies of Prototype 2.

Q-Factor		Theoretical Model			Experimental Model		
			TM111 TE011			TM111 TE011	
Straigth Capillary		TM011		TE111	TM011		TE111
Air	1	17307,5	12819,5	14921,5	17307,5	12819,5	14921,5
0	2	13670,8	8500,2	13893,6	3919,9	15103,1	7057,4
50	3	9320,0	1594,9	8450,1	3920,3	10163,5	7057,8
200	4	6547,2	164,9	72,8	3921,3	4730,8	7059,0
500	5	3446,7	45,0	58,0	3923,2	960,7	7061,5
			TM111 TE011			TM111 TE011	
Bend Capillary		TM011		TE111	TM011		TE111
Air	1	17307,5	12819,5	14921,5	17307,5	12819,5	14921,5
0	2	11290,9	1791,2	10852,5	4404,1	5745,0	2472,2
50	3	4494,1	1791,4	6330,9	4404,4	5745,4	2472,5
200	4	140,8	1791,9	178,3	4405,3	5746,6	2473,1
500	5	445,6	1792,9	261,3	4407,2	5749,2	2474,5

Table 5.10. Q-factor of Prototype 2.

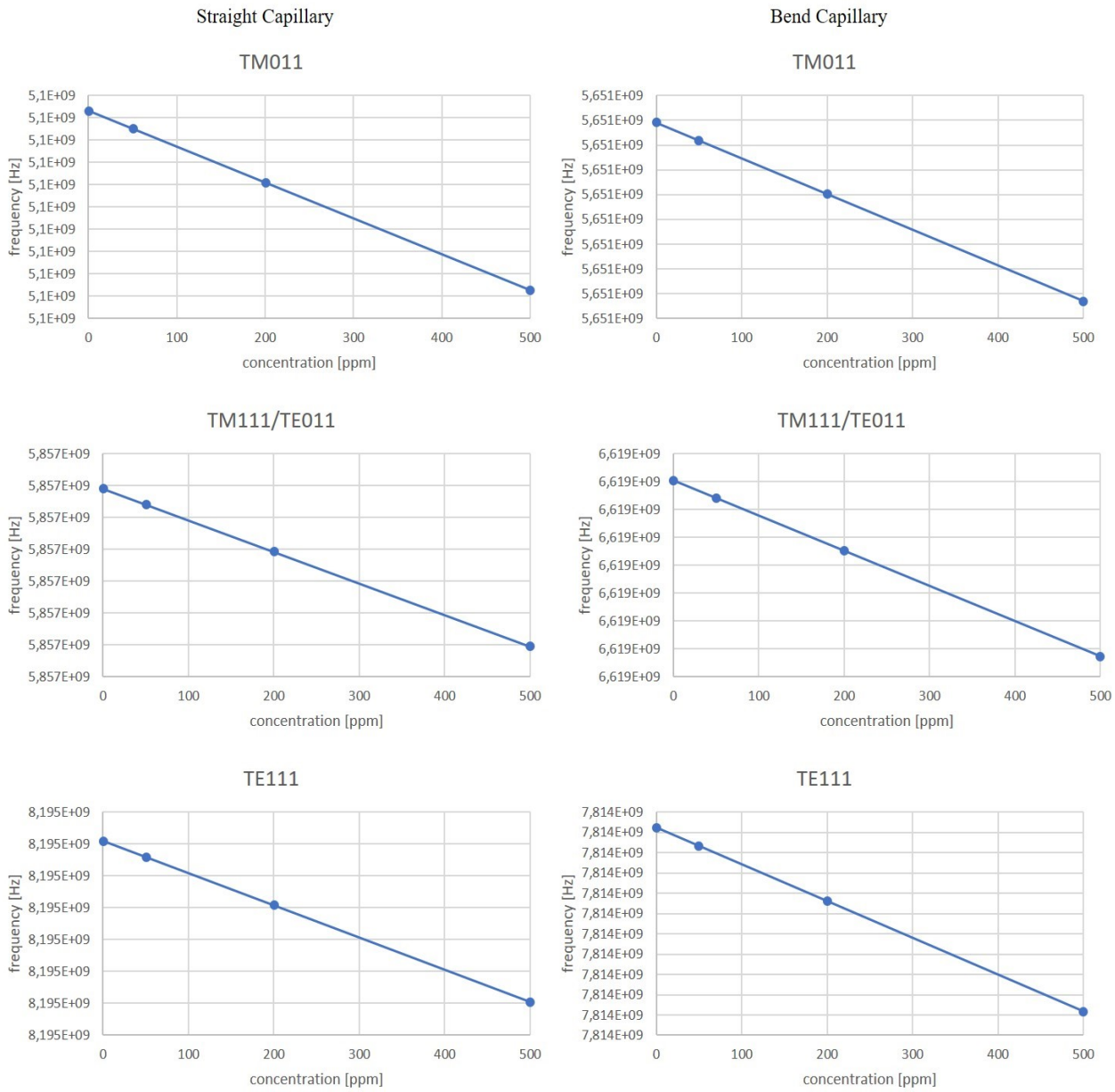

Figure 5.28. Variation of The Resonance Frequency when the Concentration of the Water Changes for the Prototype 2.

5.3.5 Design of the Coupling Structure

The most relevant resonant modes can be excited and measured by placing probes on the cavity. A transmission-type configuration is adopted for coupling the cavity to the external circuit. The device has two ports (port 1 and 2) and is coupled to 50 Ω cables via coaxial probes that are introduced in the structure through the holes drilled in the bottom wall. The coaxial probes are identical and model commercial N-type connectors. Their copper conductors have inner and outer radii of 1.2 and 6 mm,

respectively, and Teflon is in between. The physics adopted in this simulation is the same as the one used for determining propagation modes, with the difference that the ports are obviously excited.

5.3.5.1 Prototype 1

The coupling is inserted halfway up the height of the cavity. The length of the probe in the cavity is 3 mm while the diameter of the simulated dielectric is 1 mm (Fig. 5.29).

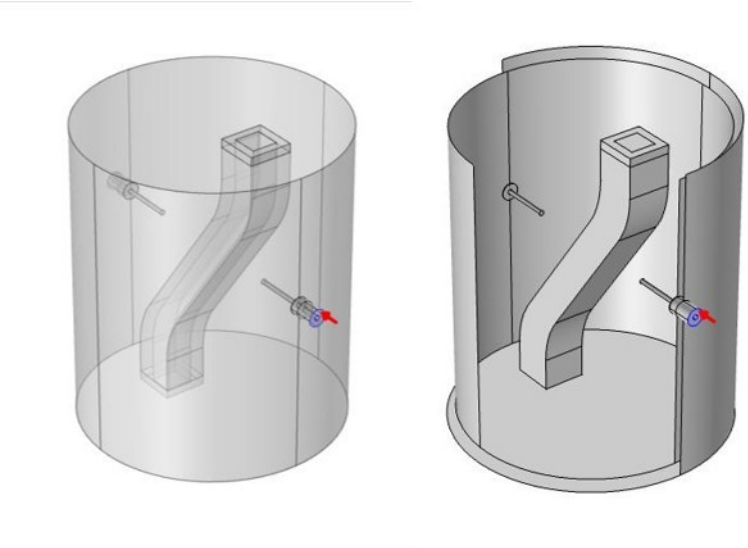

Figure 5.29. Coupling of Prototype 1.

In Figure 5.30, the reflection coefficient defines a good coupling highlighted by the frequency peaks, in which the cavity resonates.

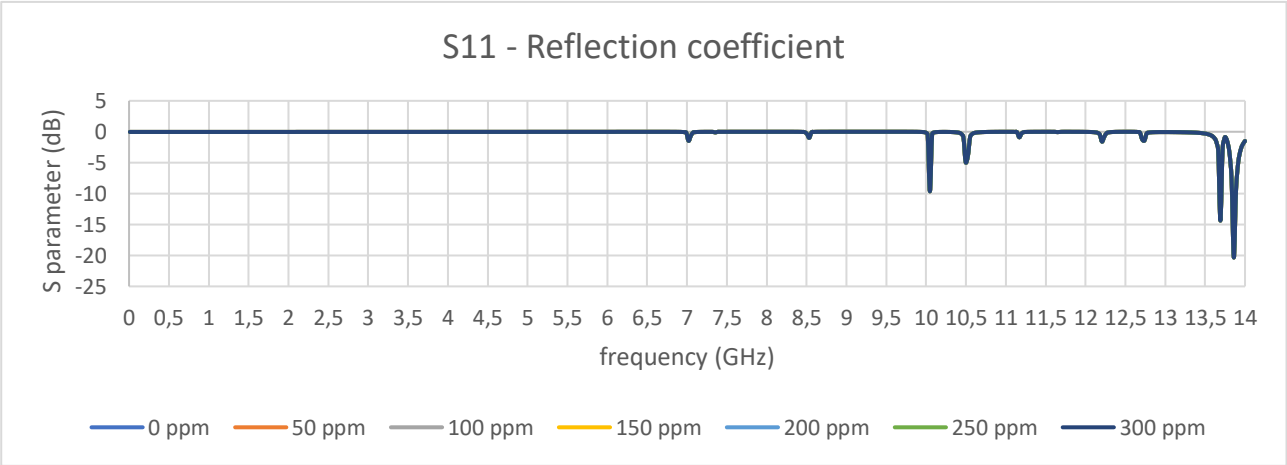

Figure 5.30. Reflection Coefficient of Prototype 1.

5.3.5.2 Prototype 2

The coupling is inserted 15 mm from the center of the top plate. The length of the probe in the cavity is 3 mm while the diameter of the simulated dielectric is 1 mm (Fig. 5.31).

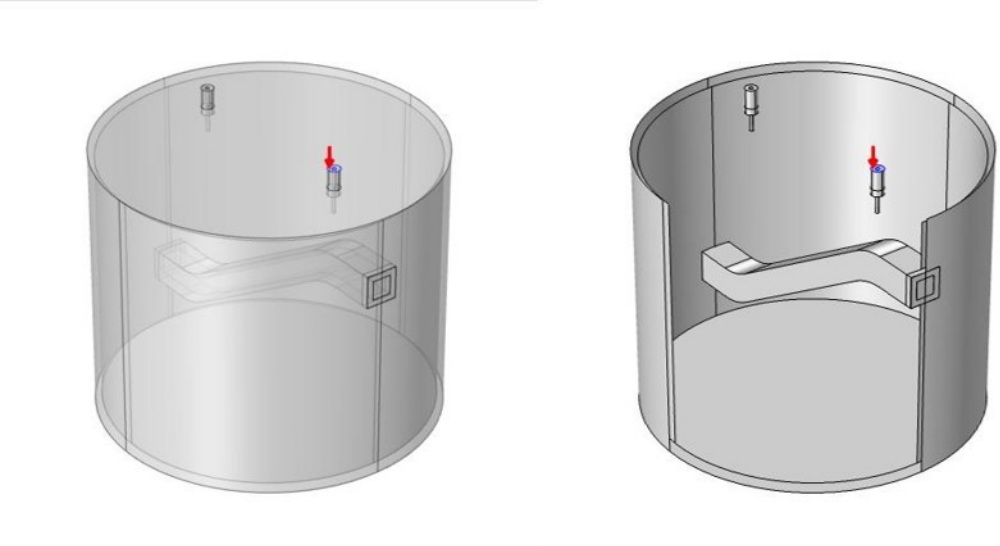

Figure 5.31. Coupling of Prototype 2.

In Figure 5.32, the reflection coefficient defines a good coupling highlighted by the frequency peaks, in which the cavity resonates.

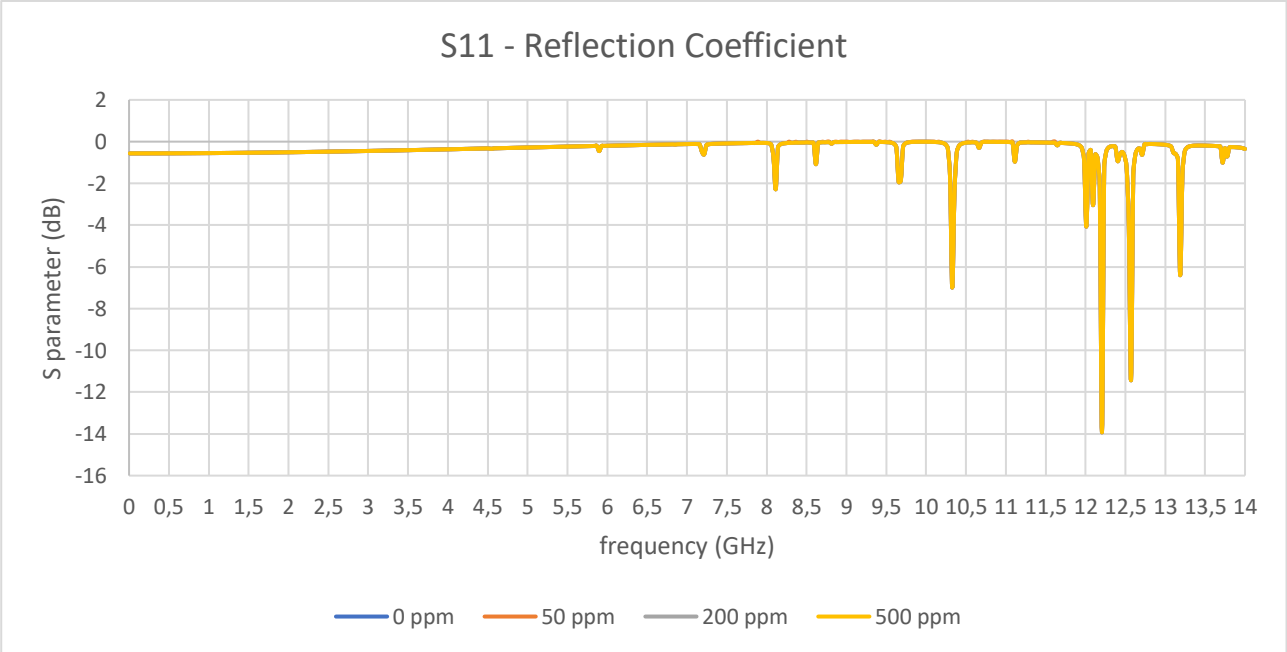

Figure 5.32. Reflection Coefficient of Prototype 2.

5.4 Re-Entrant Cavity

The cavity has the same capillary as the previous cavities, having a length equal to the length of the cavity and an internal diameter of 3 mm with a thickness of 2 mm. The coaxial is 15 mm away from the center. The internal cylinder has the following dimensions: height 80 mm and diameter 30 mm. The cavity has a diameter of 60 mm and a height of 150 mm. The dielectric of the coaxial is PTFE while the cavity is made of copper (Fig. 5.33).

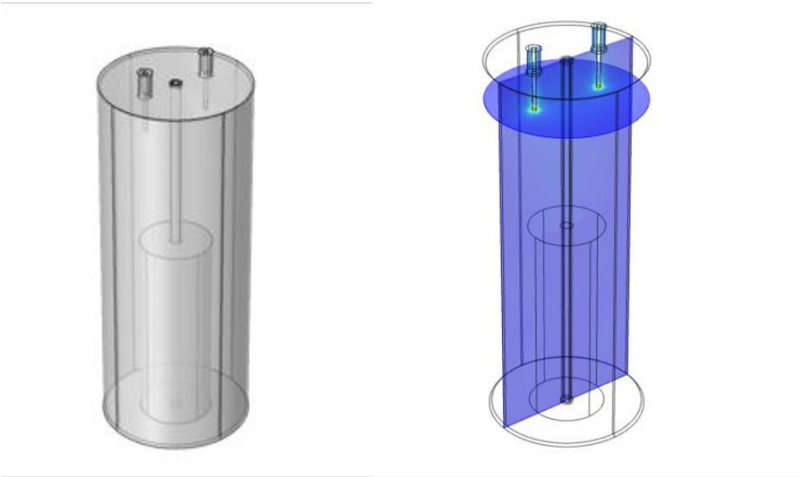

Figure 5.33. Re-Entrant Cavity.

Figure 5.34 shows the reflection coefficient of the Re-Entrant Cavity. Four frequency peaks are noted.

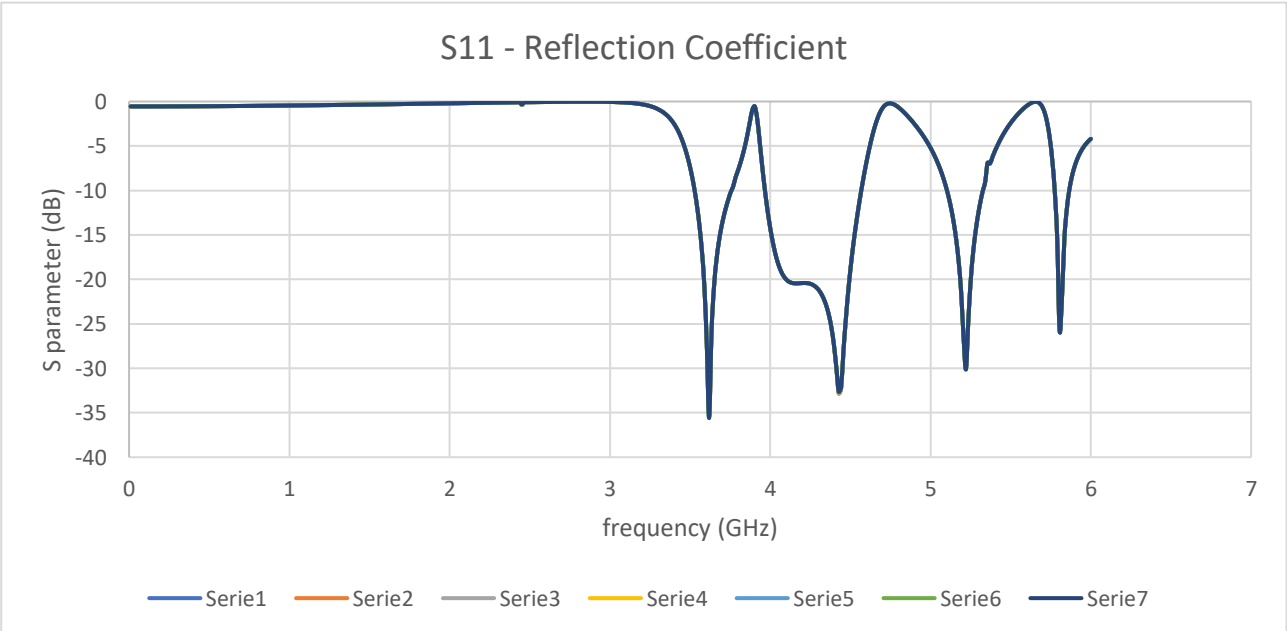

Figure 5.34. Coefficiente di Riflessione della Re-Entrant Cavity.

Also shown in figure 5.35, this solution highlights very small variations. Only in the 4.4-4.45 GHz range there is a frequency difference of 0.716 dB between 0 and 200 ppm.

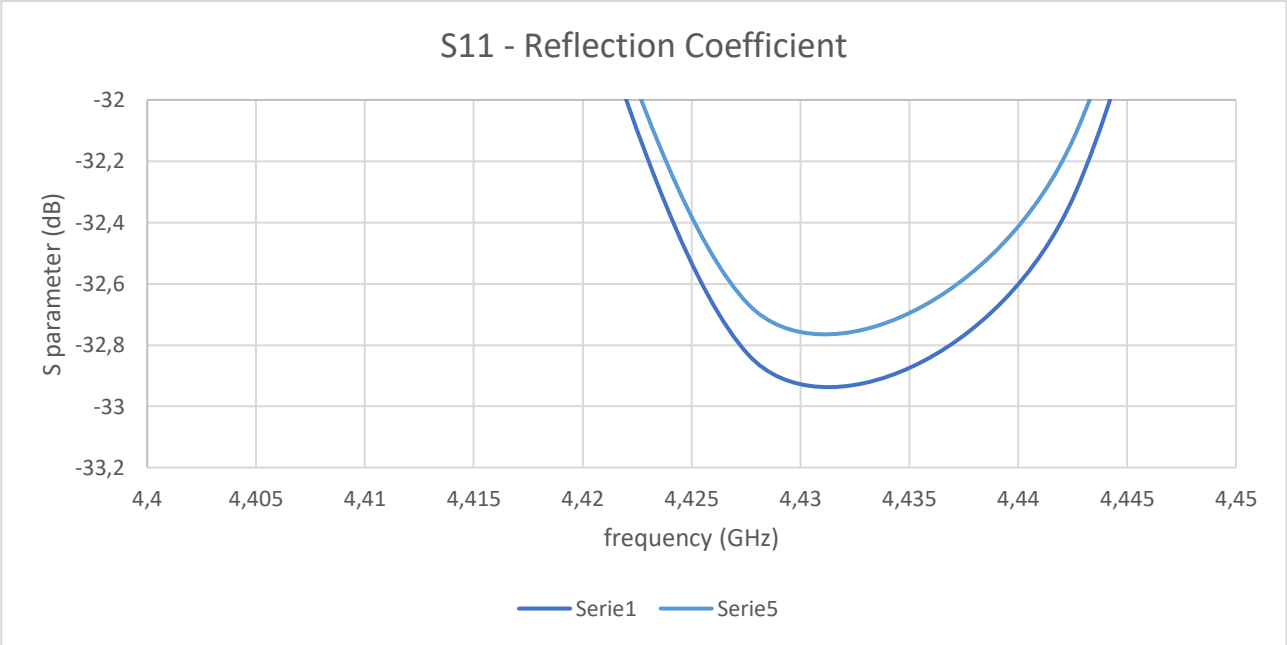

Figure 5.35. Variation of Resonance Frequency between 0 and 200 ppm.

5.5 Comparison between the Simulated Models for Water Detection

The calibration curve of the transmission line has encouraging results for the construction of the sensor. It is clear that the sensitivity of the sensor depends exclusively on the diameter of the core. Even if other parameters vary, external diameter of the shield, flow velocity and outlet pressure, the sensitivity does not change. Therefore it is believed that the sensor manufacturing is suitable for the indended purpose at Bosch.

In contrast, the resonant cavity show the variation of water concentration is so small that the variation in resonance frequency is not easily detectable. In Re-Entrant Cavities, a very small difference in resonant frequency can be detected only in a frequency peak.

5.6 Debris Sensor

The sensor was designed according to the principle of differential electromagnetic induction. The electromagnetic coil comprised two reverse winding exciting coils and one induction coil. Copper is the material used for the wire and in the simulation. The model is surrounding with air (relative magnetic permeability is 1). Materials used for the particles is copper and iron, to compare ferrous and non-ferrous behaviour.

The relative magnetic permeability of copper is 0.9999, of iron is 4000. The minimum size of the particle that the sensor must identify is approximately 200 micrometres. The coils have 5 turns and 3 layers. The length of wire for each coil is 500 mm. The length of the reel is 4 mm and they are separated by grooves with a length of 2 mm. The length of the sensor body is 50 mm with the internal radius of 1.2 mm and a thickness of 1 mm. With the multi-winding coil COMSOL function, the characteristic parameters of the coil are incorporated in a circular crown. To simulate the system, an excitation sinusoidal current of amplitude 0.1 A and a frequency of 250 Hz is assumed. The physics of magnetic fields are coupled to the electrical circuits thanks to the functions present in COMSOL, called cir.IvsU. Figures 5.36 and 5.37 show the CADs of the sensor body inside the spherical domain of the air. Current of amplitude 0.1 A and a frequency of 250 Hz are assumed.

Figure 5.36. Three-Dimensional Model with Air.

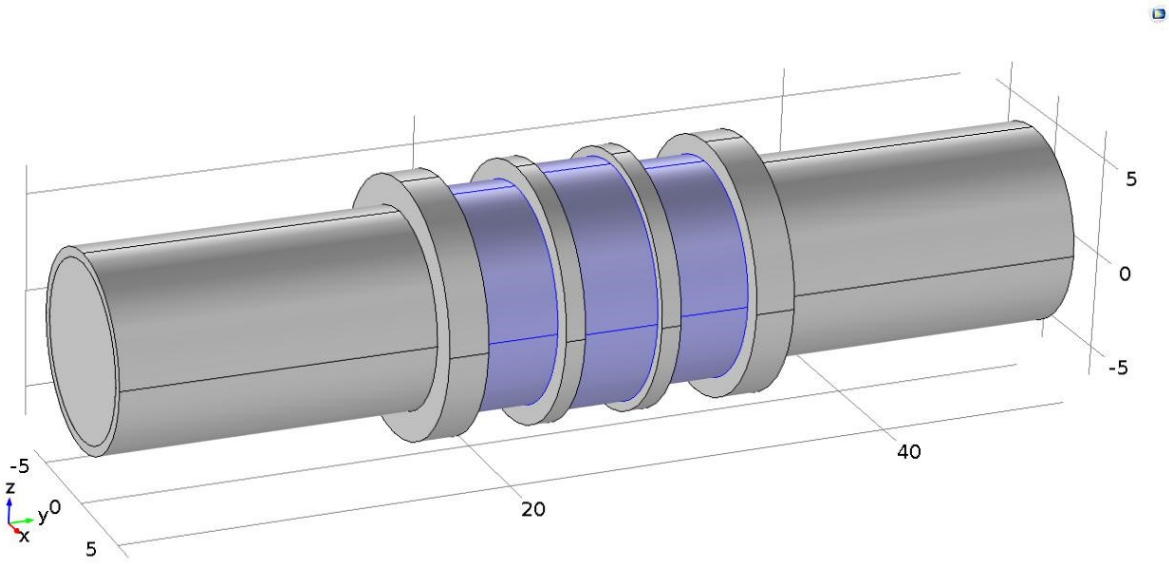

Figure 5.37. Three-Dimensional Model.

The mesh consists of 57275 volume elements and 12148 surface elements (Fig. 5.38).

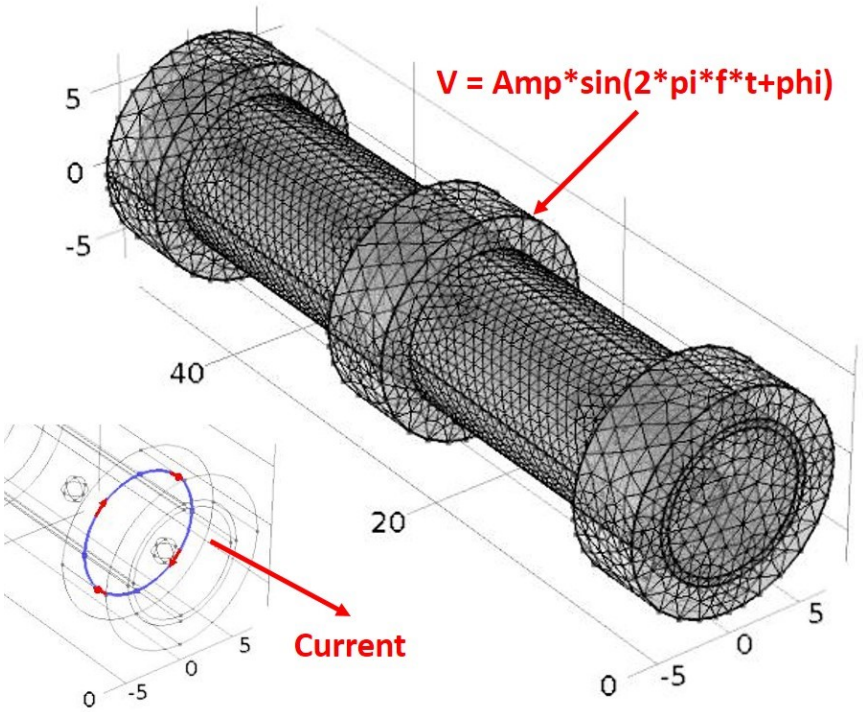

Figure 5.38. Mesh of Model.

Figure 5.39 shows the qualitative validation of the physical principle. Note the perturbation of the magnetic field induced by the ferrous particle. Moreover, in Fig. 5.40, it is highlighted the different magnetic induction between a ferrous and a non-ferrous particle. The simulations show a qualitative

result whereby a non-ferrous particle causes a variation in the magnetic field of 0.004 Tesla while a ferrous particle determines a variation of 0.011 Tesla.

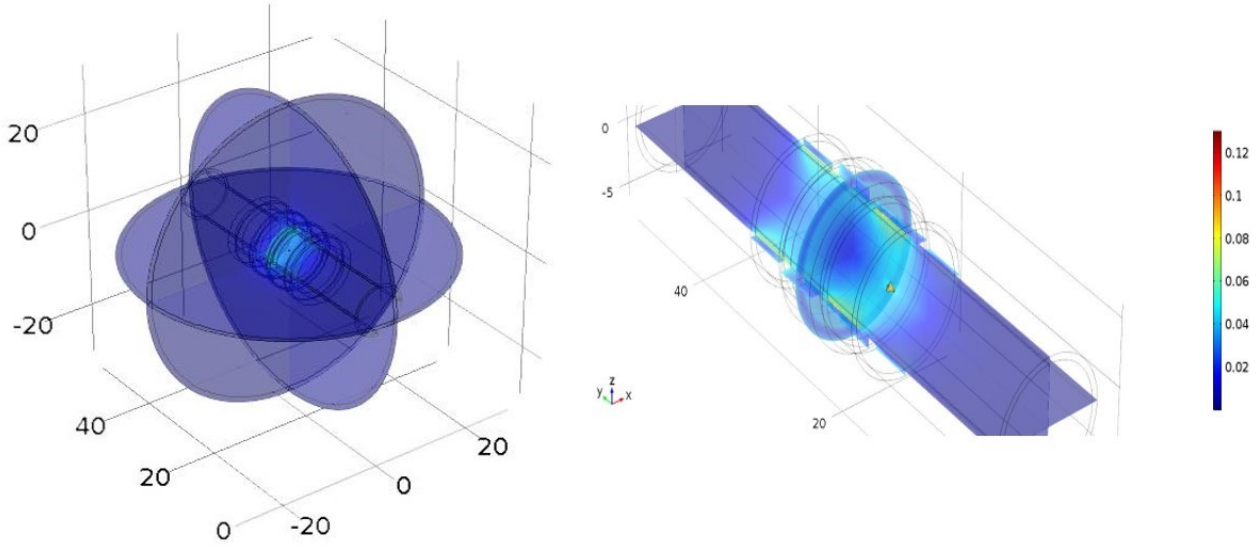

Figure 5.39. Perturbation of Magnetic Field.

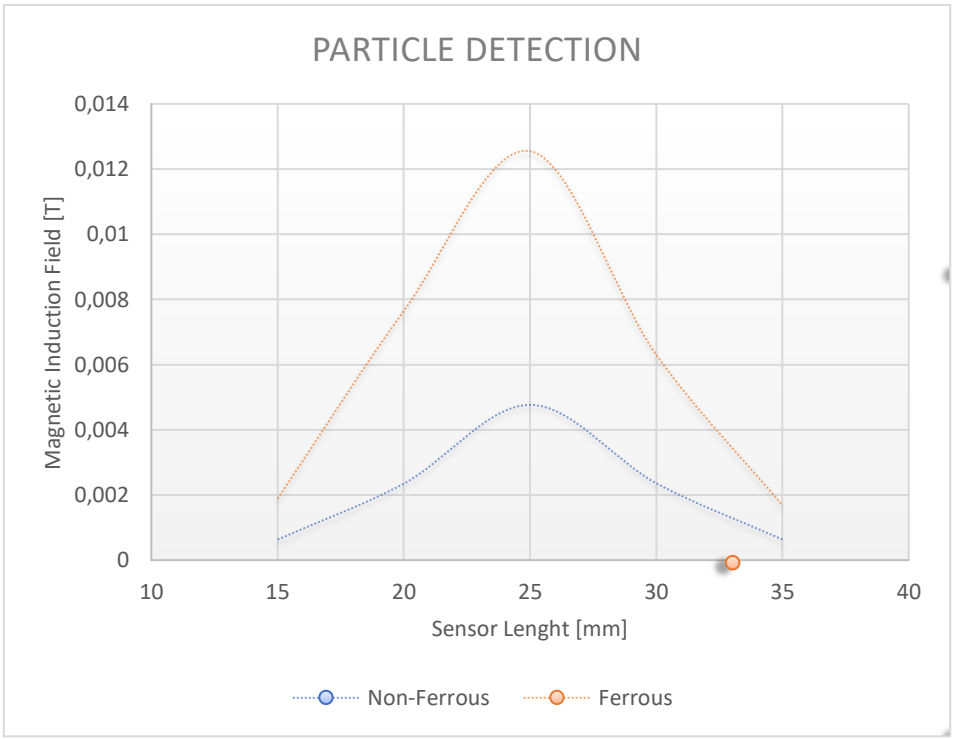

Figure 5.40. Different e between Ferrous and Non-Ferrous Particles.

In the graph in figure 5.41, the voltage variation along the direction of the detection coil (about 25 mm) is evident when the particle passes through the sensor, highlighting a peak when the particle is

positioned in the detection area. The peak of tension has very low and hardly individual values. The only solution would be to amplify the signal.

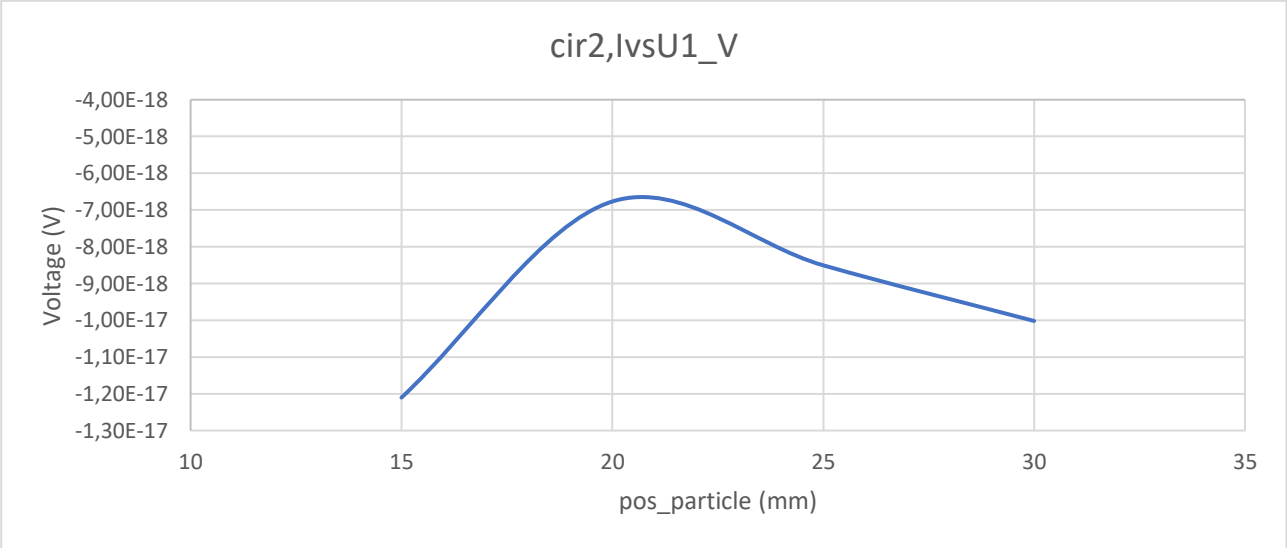

Figure 5.41. Voltage variation with Coupling of the Circuit Electric.

5.7 Sensor Allocation

Finally, we improved the sensor connection to the diesel fuel system through two sleeves, as shown (Fig. 5.42).

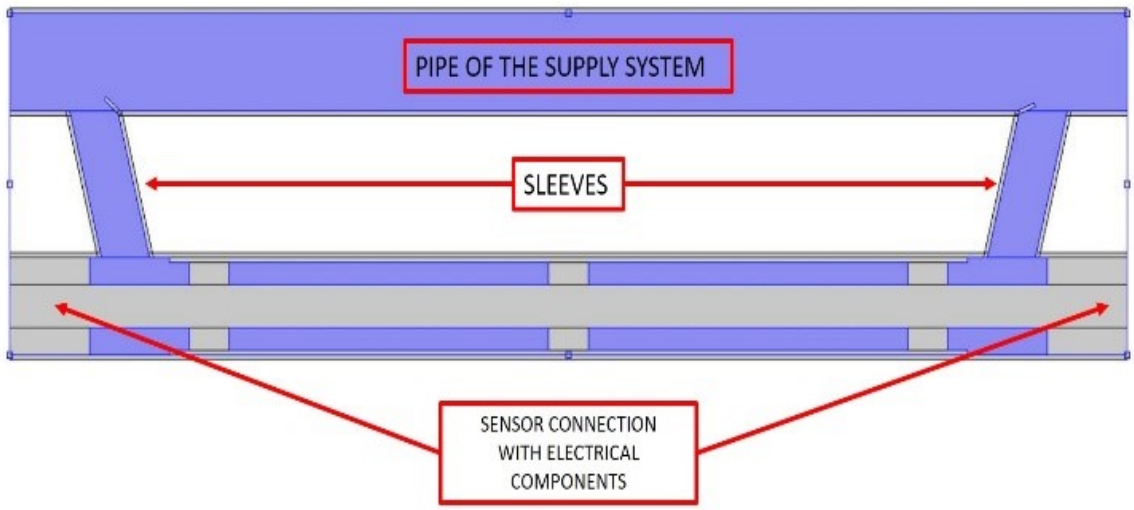

Figure 5.42. Final Configuration: Installing the Sensor in the Engine Fuel System.

The sleeves permit to separate electrical input and output ports from fluid ones. In this way electrical ports remain on a straight line, avoiding bending of the core with consequent reduction of signal reflections and losses. The sleeves may be welded to the pipe of the supply system, equipped with additional holes. In particular, it is obtained that if flaps, suitably oriented, are used, there is a flow entering the sensor at a lower speed and therefore the stress, which the flow can generate to the core in its input, is reduced, while at the output, a flap oriented in the opposite direction, minimizes pressure drop losses caused by the presence of the sensor opening. The losses considered in the design take into account both the losses distributed along the sensor as well as the ones concentrated on inlets, edges and variations in the flow passage section. Through the simulations, we estimate that in the improved design these losses are at a level of about 1000 Pa, which is considered acceptable. Full details of velocity field and pressure field, generated by the presence of guide vanes, are shown in figures 5.43 and 5.44.

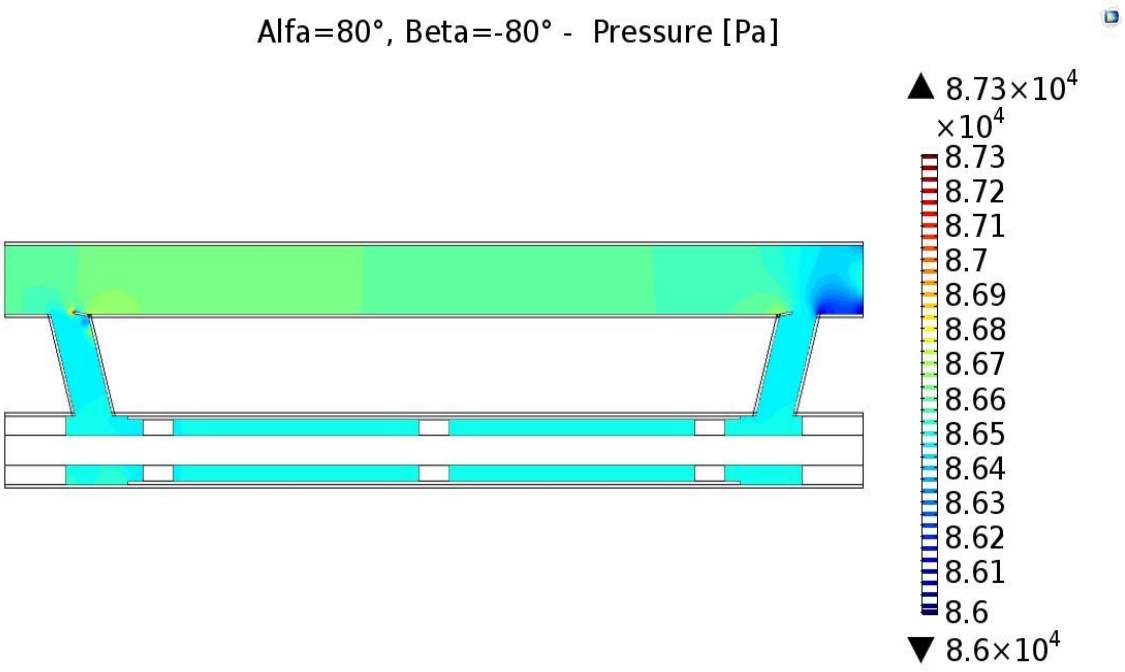

Figure 5.43. Pressure Field in the Final Configuration.

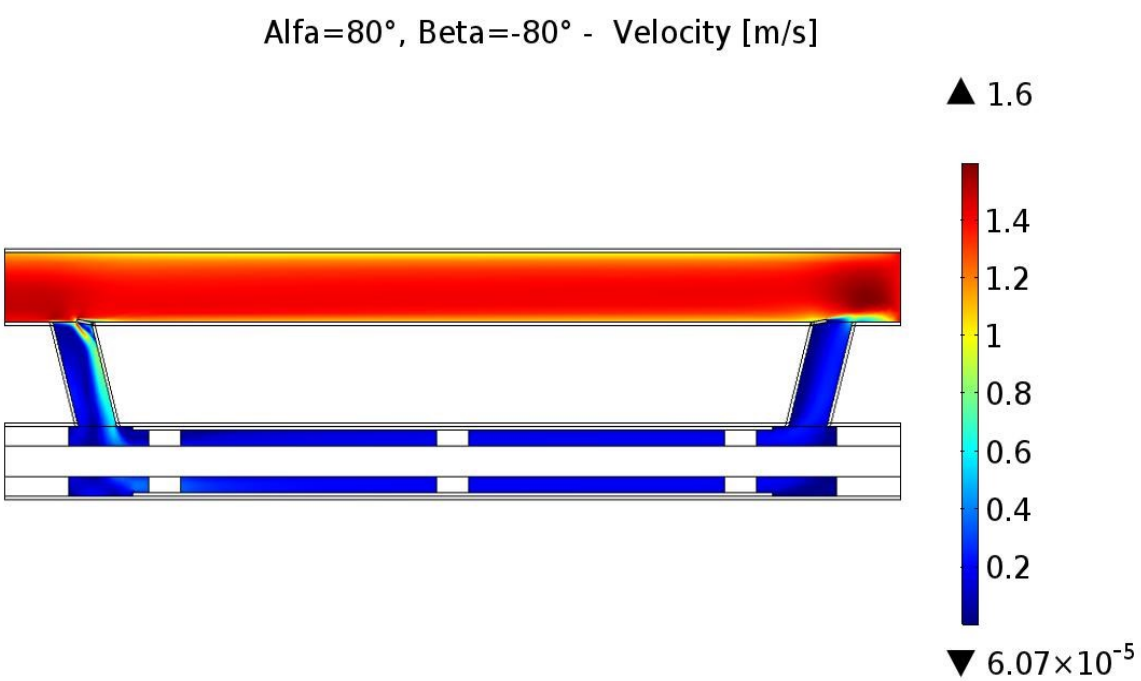

Fig. 5.44. Velocity Field in the Final Configuration.

In figure 5.45 the user iterface to be implemented in ECU. When the admissible water value, associated with the measured sensor parameter, is exceeded, the error will be suitably signaled.

Figure 5.45. User Interface For Diesel Quality Control.

CHAPTER 6

Sono tutti in gara e rallento, fino a stare fuori dal tempo
Superare il concetto stesso di superamento mi fa stare bene

Ti Fa Stare Bene – Caparezza

"Mathematical reasoning may be regarded rather schematically as the exercise of a combination of two facilities, which we may call intuition and ingenuity."

Alan Turing

EXPERIMENTAL SET-UP

In this chapter are presented the prototypes of the designs described in the previous chapter. To characterize the prototypes, the VNA described in chapter 3, was used after the calibration procedure shown in figure 6.1. The calibration was carried out as described in chapter three, i.e. through the fully calibrated 2 port procedure A data point is a sample of data representing a measurement at a single stimulus value. You can specify the number of data points that the analyzer measures across a sweep. The analyzer sweep time changes proportionally with the number of points. In our work, the number points are 201.

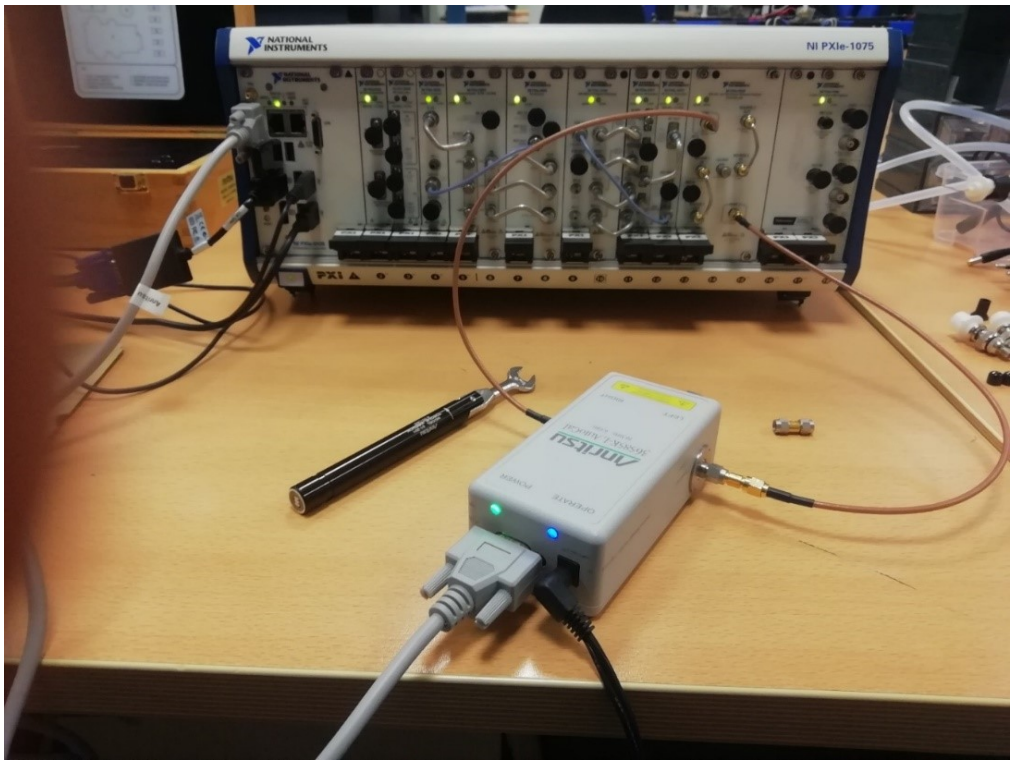

Figure 6.1. Calibration of VNA.

6.1 Manufacturing of Water Sensor

The capillaries for the resonant cavities, shown in figure 6.2, and the connectors for the electronic connection of the sensors, figure 6.3, have been created by using a 3D printer. PLA was used as the material. The capillaries were printed horizontally to ensure print uniformity at the radial level. The Roboze One has an electro-galvanized printing surface heated up to 100 ° C, to allow adhesion and hold even on very long prints. The print bed is removable. This allows the removal of the piece with extreme ease and in total safety. The resolution is 25 microns. With these characteristics it was possible to print the connectors, adapting them to the dimensions of the sensors. In this way, in addition to the electronic connection made in safety, part of the connector itself is used to bind the core and the probes of the sensors.

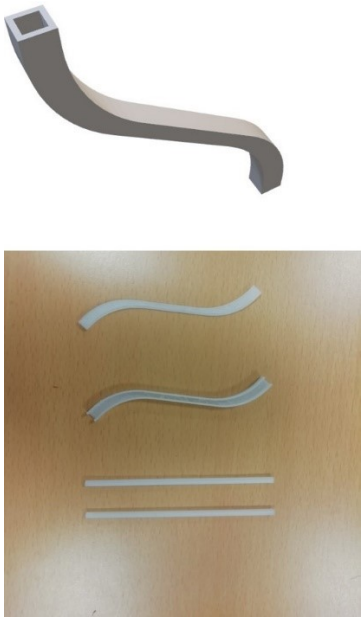

Figure 6.2. Capillary of the Resonant Cavity

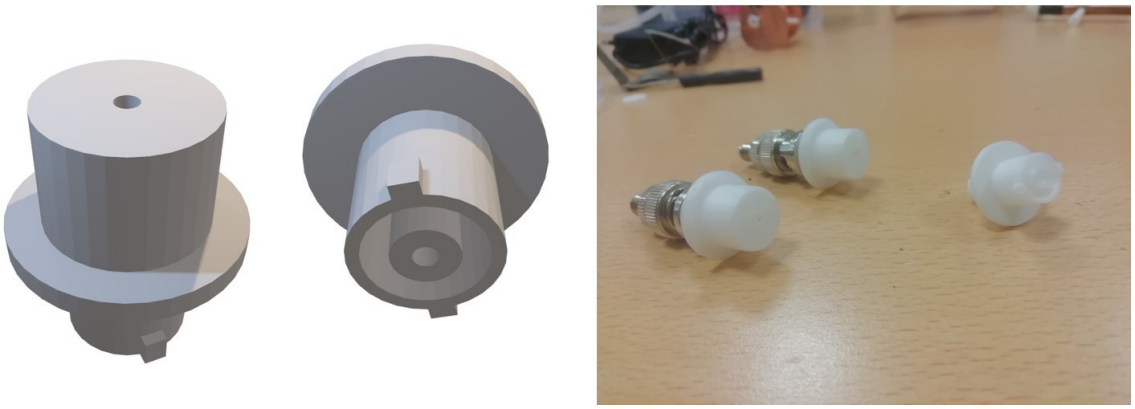

Figure 6.3. Connector for Connection to the VNA.

The copper part that defines the sensors was cut and drilled according to the specifications described in the previous chapter (Fig. 6.4-6.5). The copper tubes are cut, both sides, to have the length defined in the modeled prototypes. The cut section was filed with sandpaper and the whole piece of copper cleaned with alcohol and left to dry for a few days. Finally, two holes were drilled for the passage of the diesel.

The pumping system of the diesel-water mixtures is guaranteed by a submersible pump, with a 12 V DC electrical motor with a power of 4.8 W. The maximum flow rate is 220 L/h. The tube in which the flow will circulate is a flexible PVC silicone hose with an internal diameter of 6 mm and a thickness of 2 mm (Fig. 6.6).

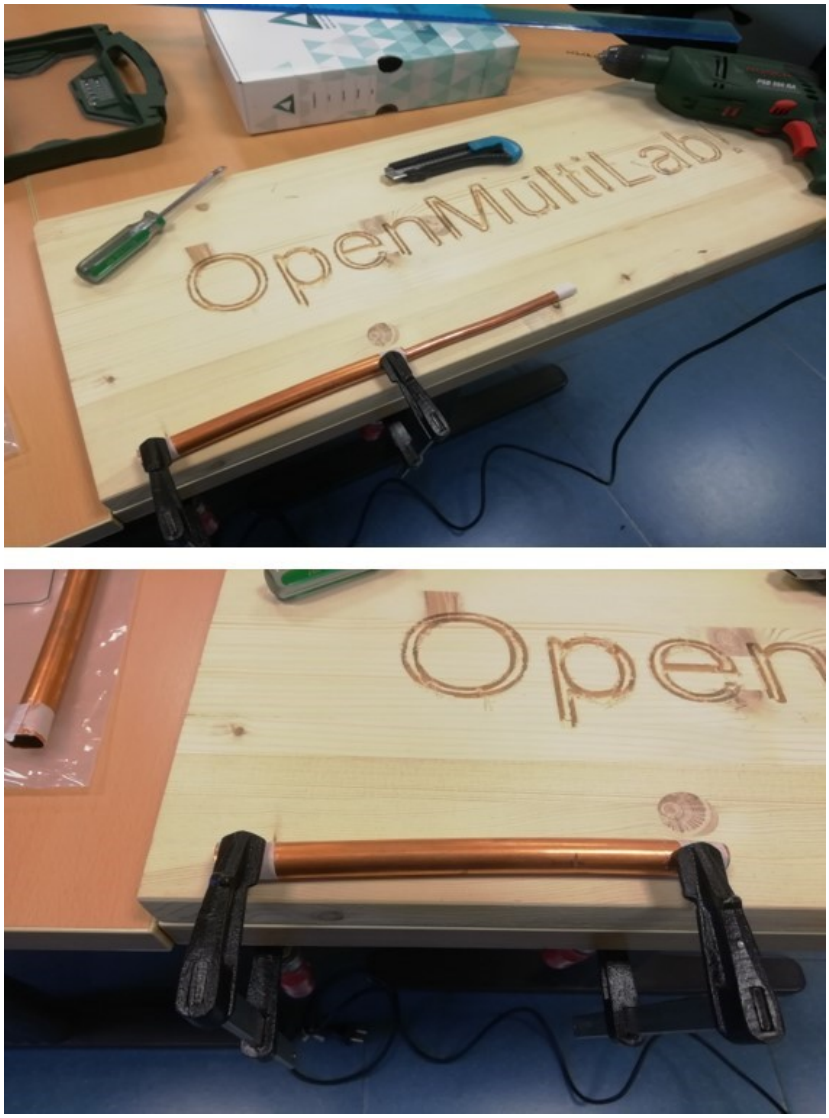

Figure 6.4. Copper Cutting.

Figure 6.5. Copper Drilling.

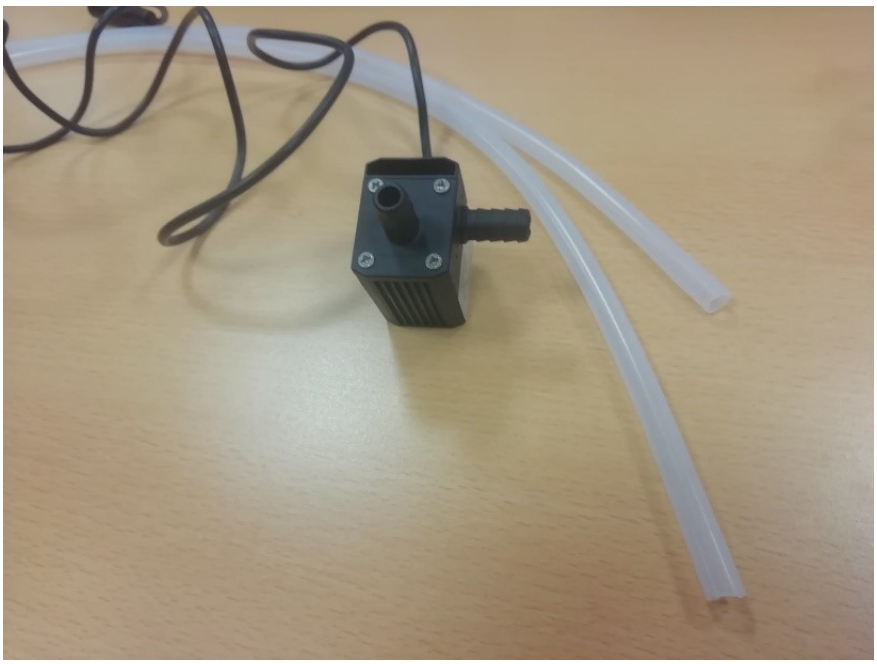

Figure 6.6 Feed Pump.

6.2 Transmission Line – Prototype 1

Prototype 1 has a length of 200 mm. The external diameter of the shield is 9.5 mm with a thickness of 1 mm while the core diameter is 1.2 mm. The flow inlet hole is positioned at 3 mm from the end while the outlet hole about at 4 mm from the end. Dimensions have been agreed by Bosch for the installation of the sensor on the pump supply line. The flow inlet hole is 4 mm in diameter (Fig. 6.7).

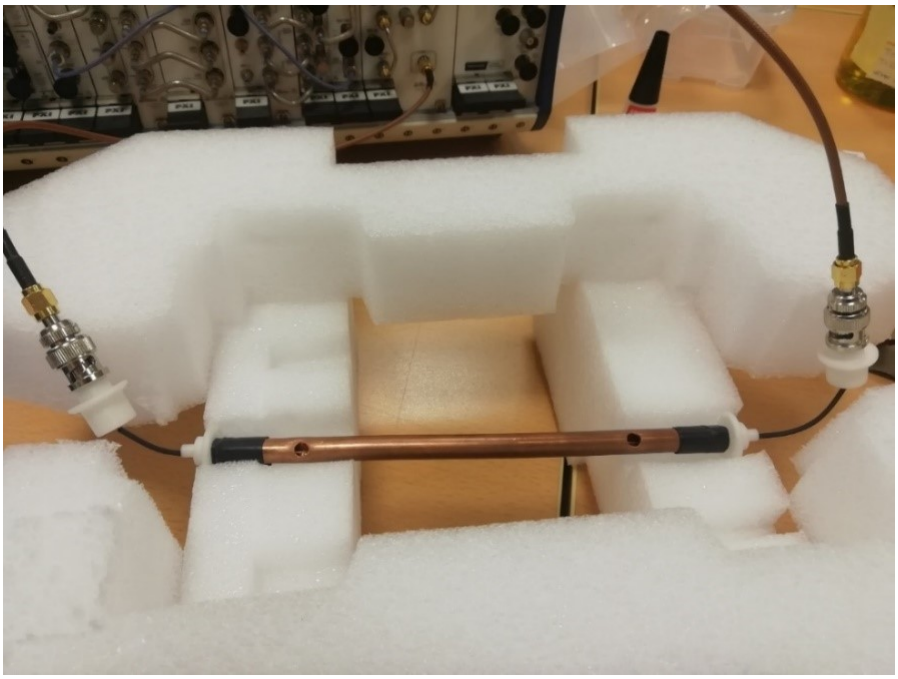

Figure 6.7. Transmission Line: Prototype 1.

With that configuration, we are unable to identify an attenuation at 200 ppm. Only when we reach a value of 1000 ppm does the VNA register an attenuation (like shows in figure 6.8).

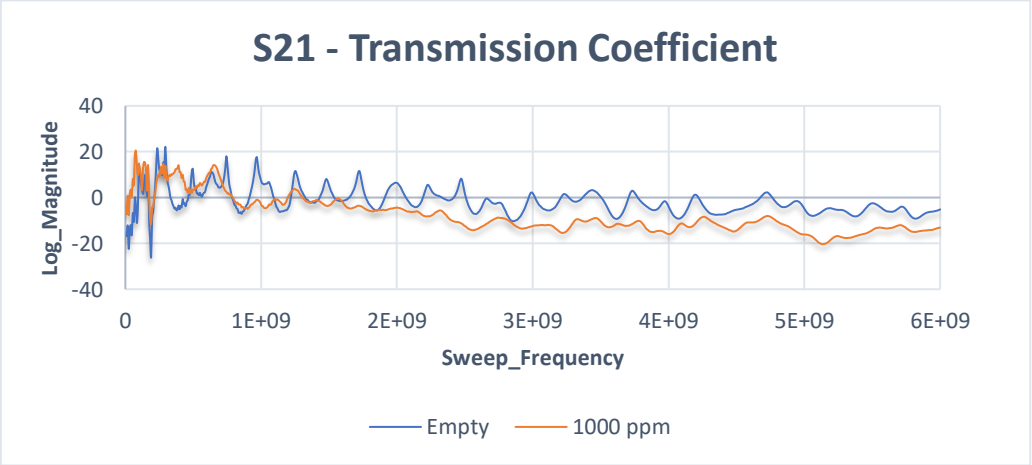

Figure 6.8. Transmission Coefficient of the Prototype 1.

6.3 Transmission Line – Prototype 2

Prototype 2 has a length of 250 mm. The external diameter of the shield is 16 mm with a thickness of 1 mm while the core diameter is 1.2 mm. The flow inlet hole is positioned at 4 mm from the end while the outlet hole at about 4 mm from the end. Also, for this prototype, dimensions have been agreed by Bosch. The diameter of the passage hole of the diesel is 8 mm (Fig. 6.9).

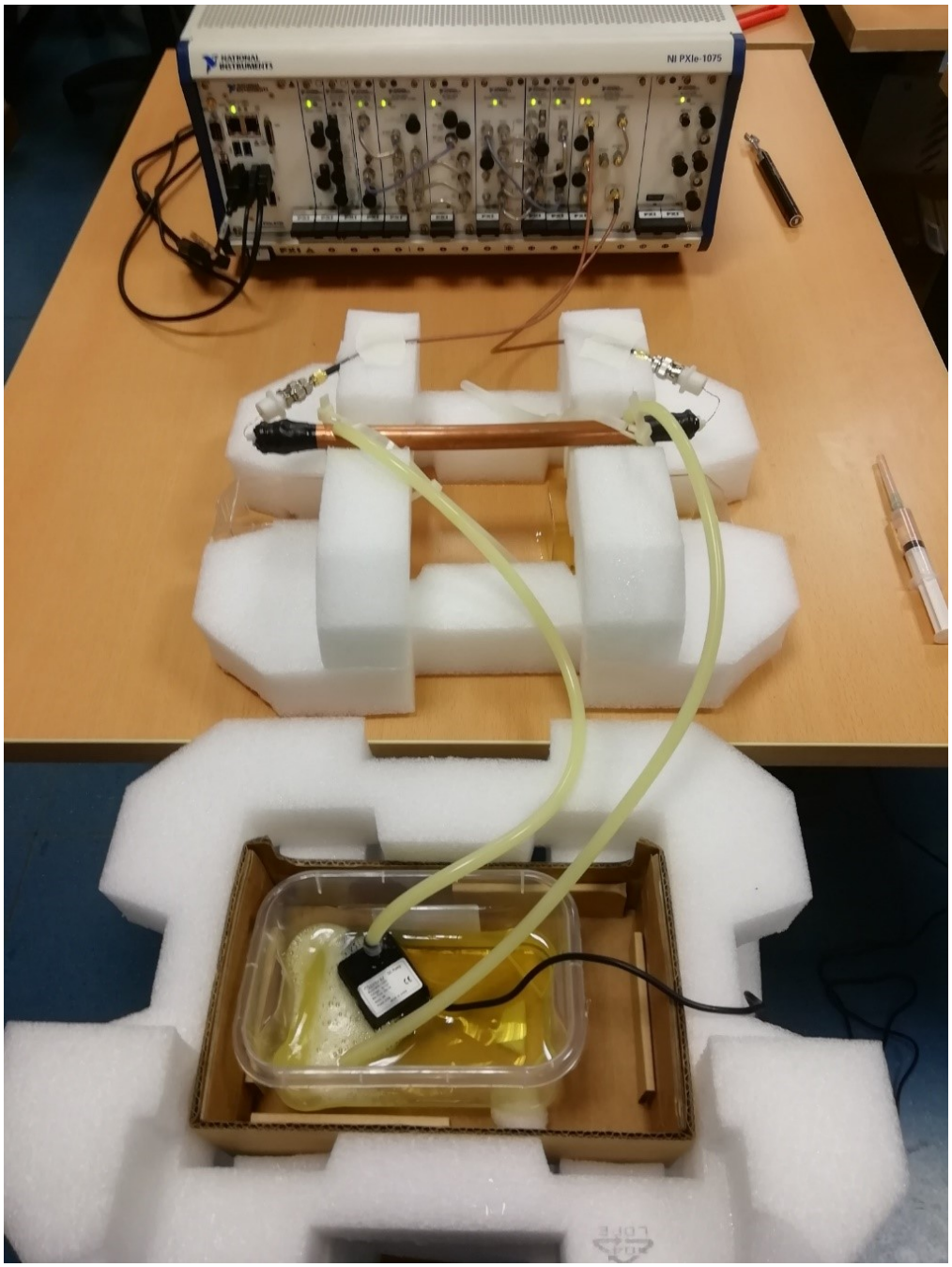

Figure 6.9. Transmission Line: Prototype 2.

In figure 6.10 the attenuation coefficient is reported while in figure 6.11 is the calibration curve at a frequency value equal to about 2.5 GHz. The attenuation variation between 50 and 200 ppm is approximately 0.4248 dB.

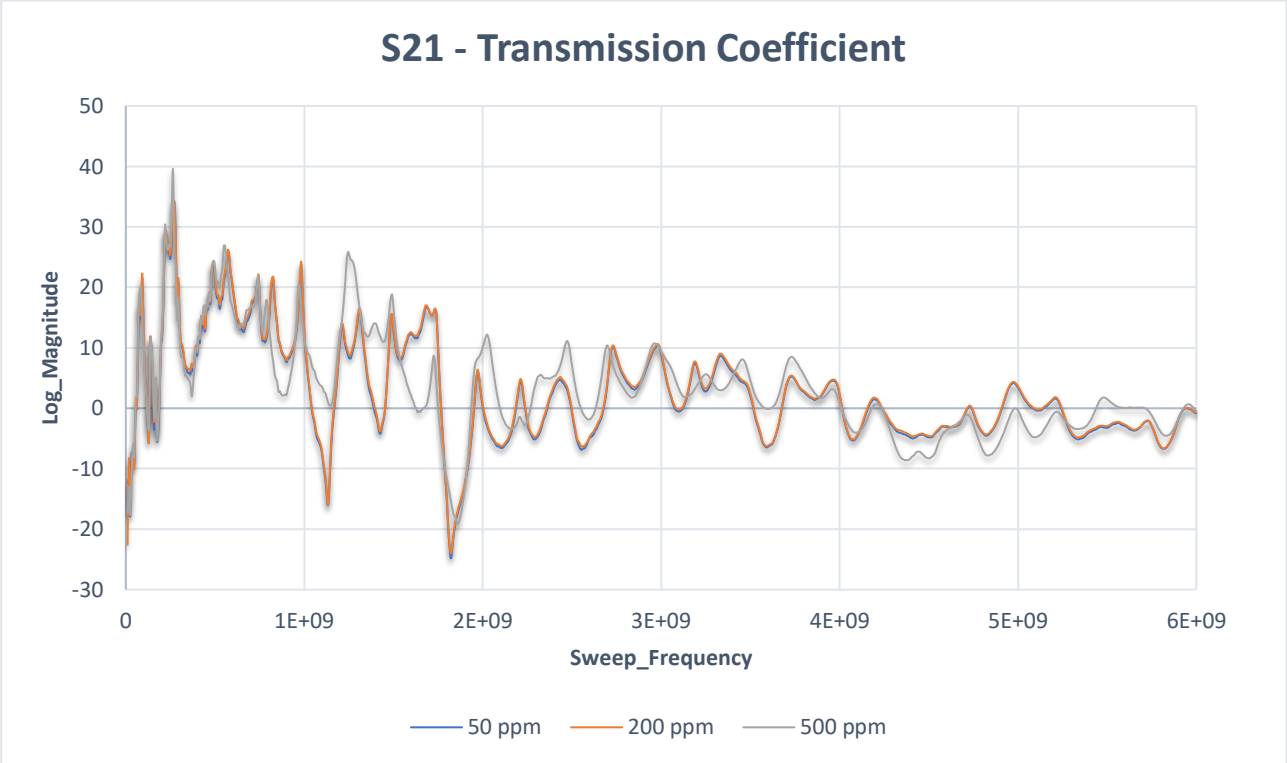

Figure 6.10. Transmission Coefficient of the Prototype 2.

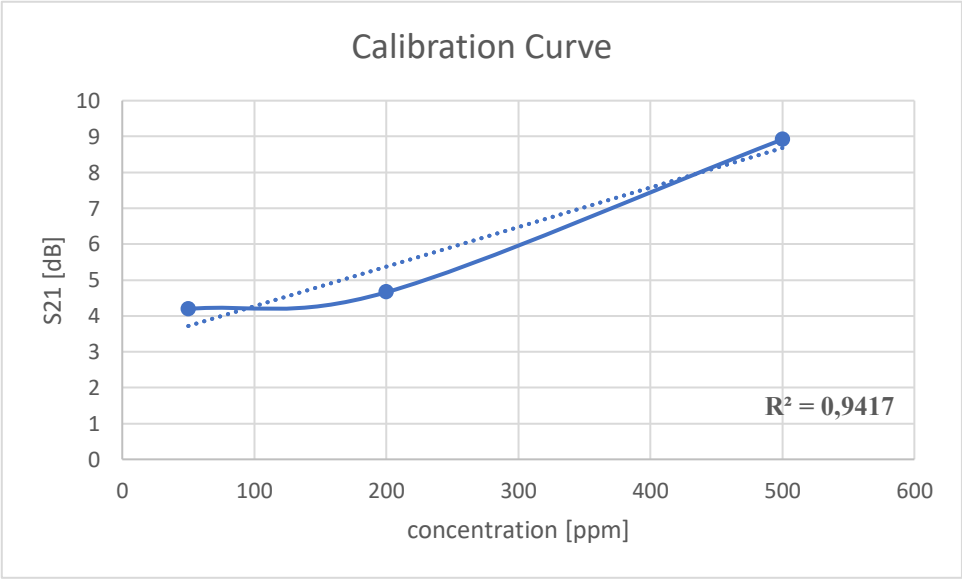

Figure 6.11. Calibration Curve Prototype 2.

6.4 Resonant Cavity – Prototype 1

Prototype 1 is a cylindrical cavity 35 mm high and 30 mm in diameter. The thickness is 1 mm. (Fig. 6.12).

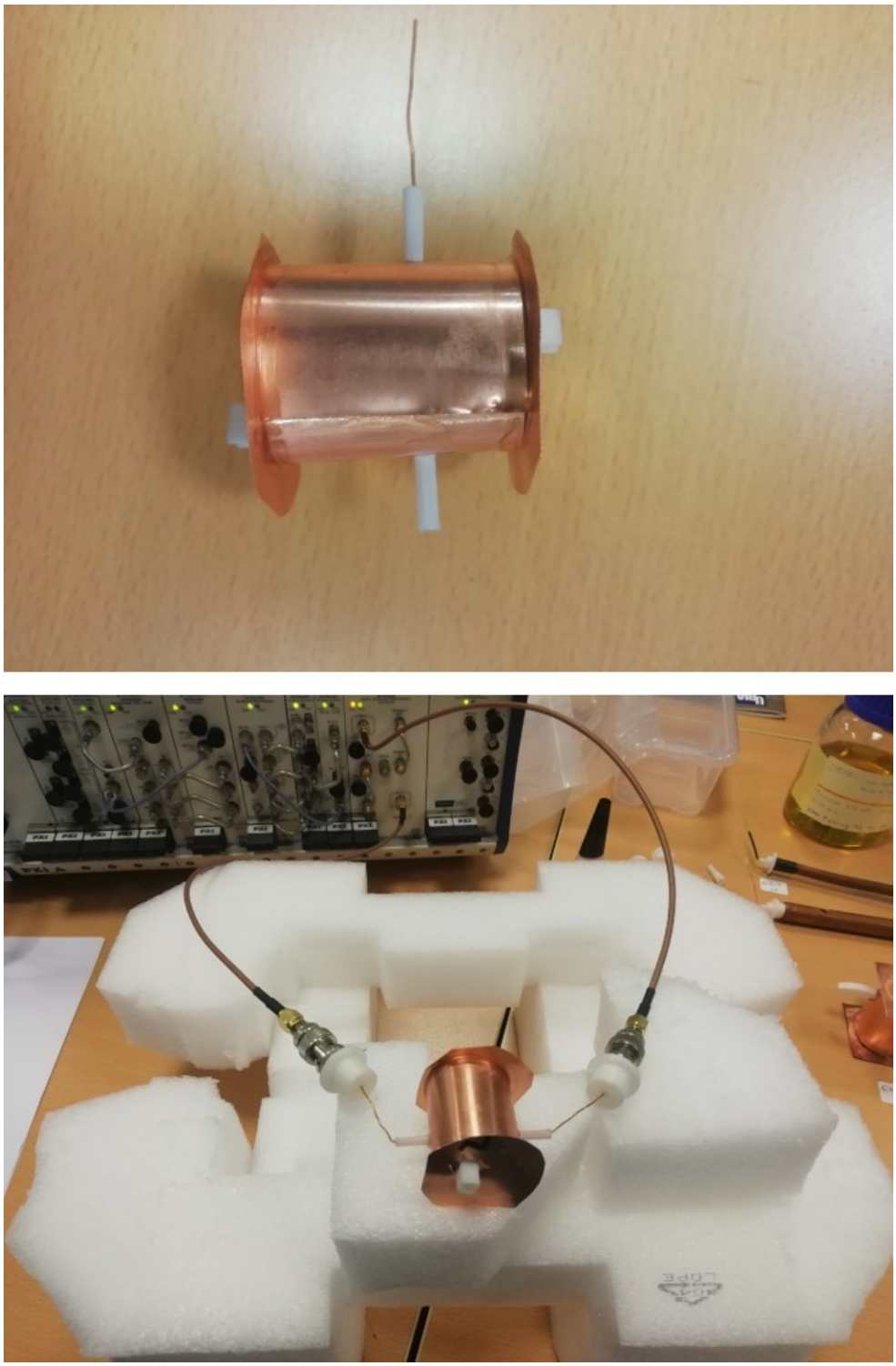

Figure 6.12. Resonant Cavity: Prototype 1.

Figure 6.13 shows the reflection coefficient, which highlights frequency shifts in the range close to 1 GHz, 3 GHz and about 4.7 GHz.

Figure 6.13. Reflection Coefficient of the Prototype 1.

Table 6.1 shows the determination coefficients of the resonance frequency and of the attenuation for the most evident peaks.

	0 (EMPTY)	50	200	R^2
Frequency [GHz]	9,3845	9,3845	9,459	***0,9423***
S11 [dB]	-20,225343	-20,579	-13,1206	***0,9212***
Frequency [GHz]	2,97505	2,97505	2,9675	***0,9423***
S11 [dB]	-21,052143	-21,052	-20,5113237	***0,9423***
Frequency [GHz]	4,7121	4,7121	4,704	***0,9423***
S11 [dB]	-19,2643	-19,264	-16,928	***0,9423***

Table 6.1. Determination Coefficients of Prototype 1.

6.5 Resonant Cavity – Prototype 2

Prototype 2 is a cylindrical cavity 40 mm high and 50 mm in diameter. The thickness is the same of prototype 1 (Fig. 6.14).

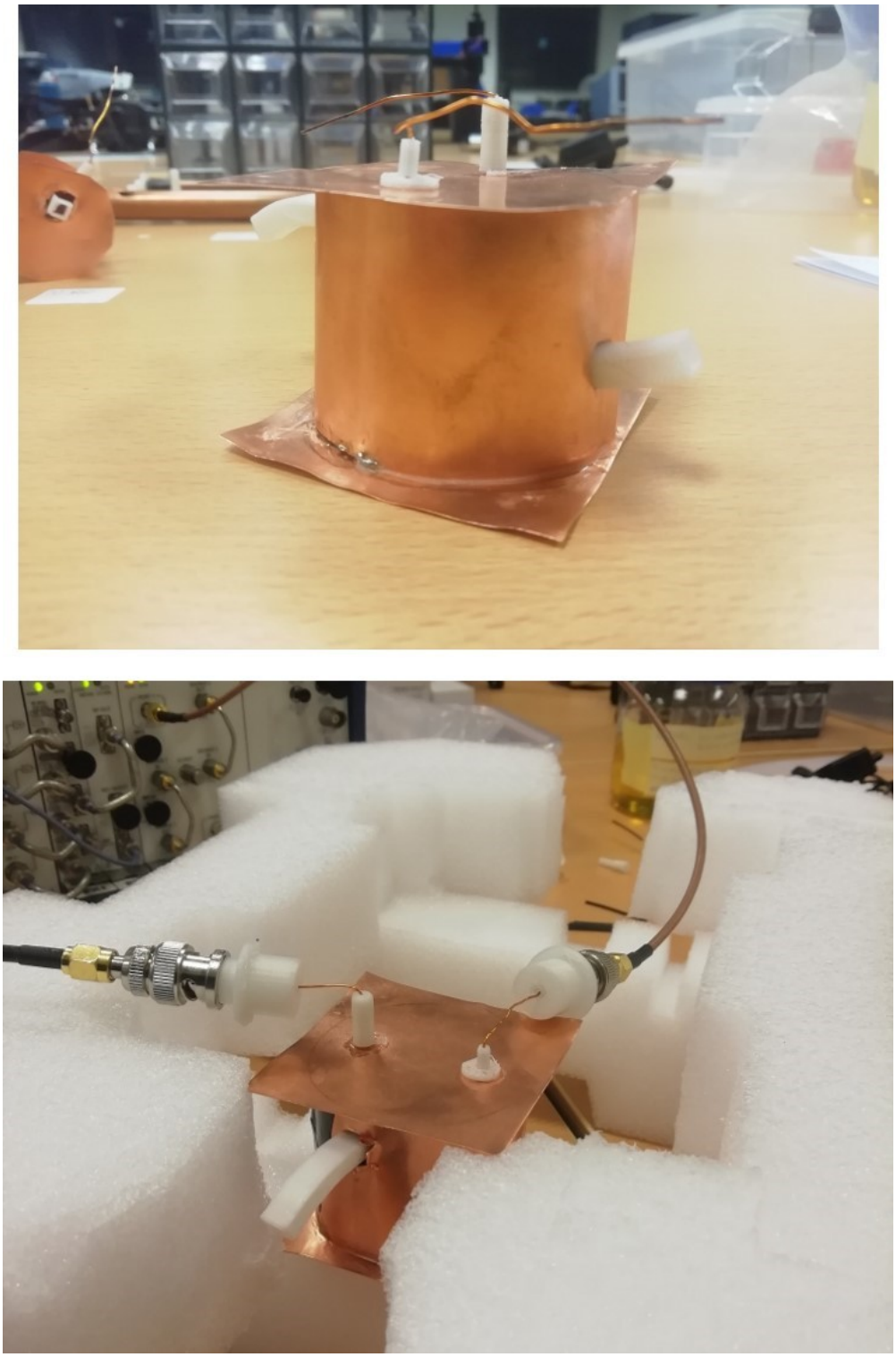

Figure 6.14. Resonant Cavity: Prototype 2.

Figure 6.15 shows the reflection coefficient, in which frequency shifts in the range close to 2.8 GHz, 4 GHz and about 6 GHz are highlighted.

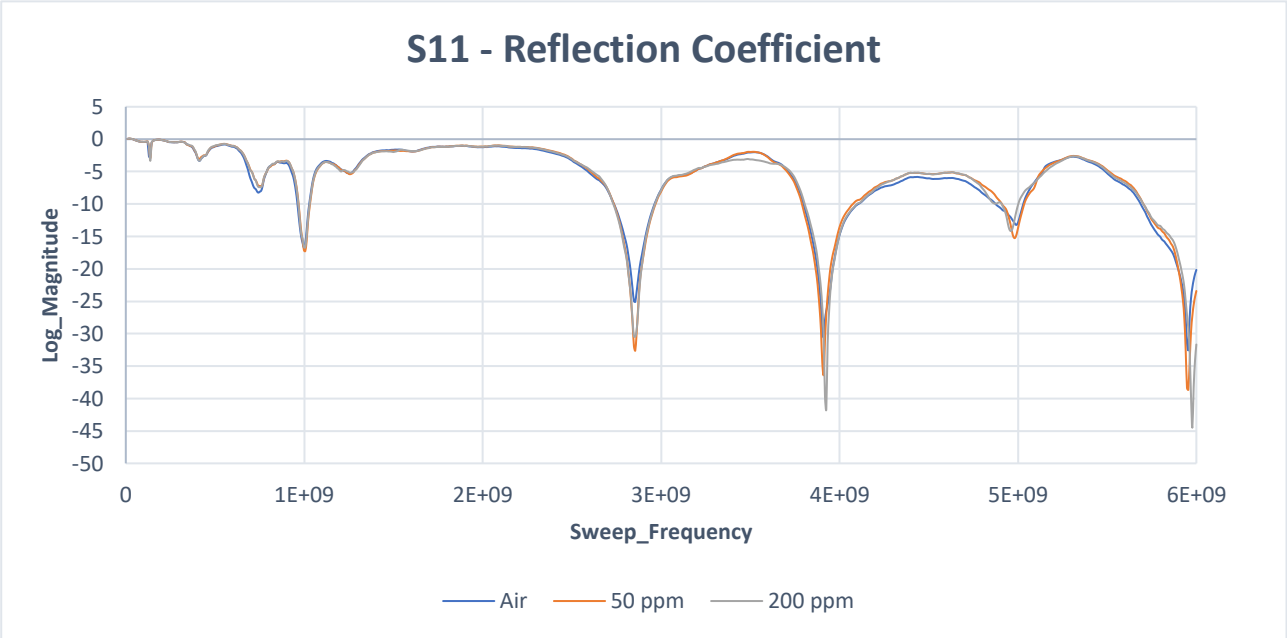

Figure 6.15. Reflection Coefficient of the Prototype 2.

Table 6.2 shows the determination coefficients of the resonance frequency and of the attenuation for the most evident peaks.

	0 (EMPTY)	50	200	R2
Frequency [GHz]	2,852	2,855	2,85525	***0,5499***
S11 [dB]	-25,08	-30,48	-32,4078	***0,7285***
Frequency [GHz]	3,91	3,91098	3,925	***0,9665***
S11 [dB]	-30,5523	-36,333	-41,6497	***0,9097***
Frequency [GHz]	5,955	5,955	5,977	***0,9423***
S11 [dB]	-32,46	-38,649	-44,499	***0,9142***

Table 6.2. Determination Coefficients of Prototype 2.

6.6 Re-Entrant Cavity

The internal cylinder has the following dimensions: height 80 mm and diameter 30 mm. The cavity has a diameter of 60 mm and a height of 150 mm. The dielectric of the coaxial is PTFE while the cavity is made of copper (Fig. 6.16).

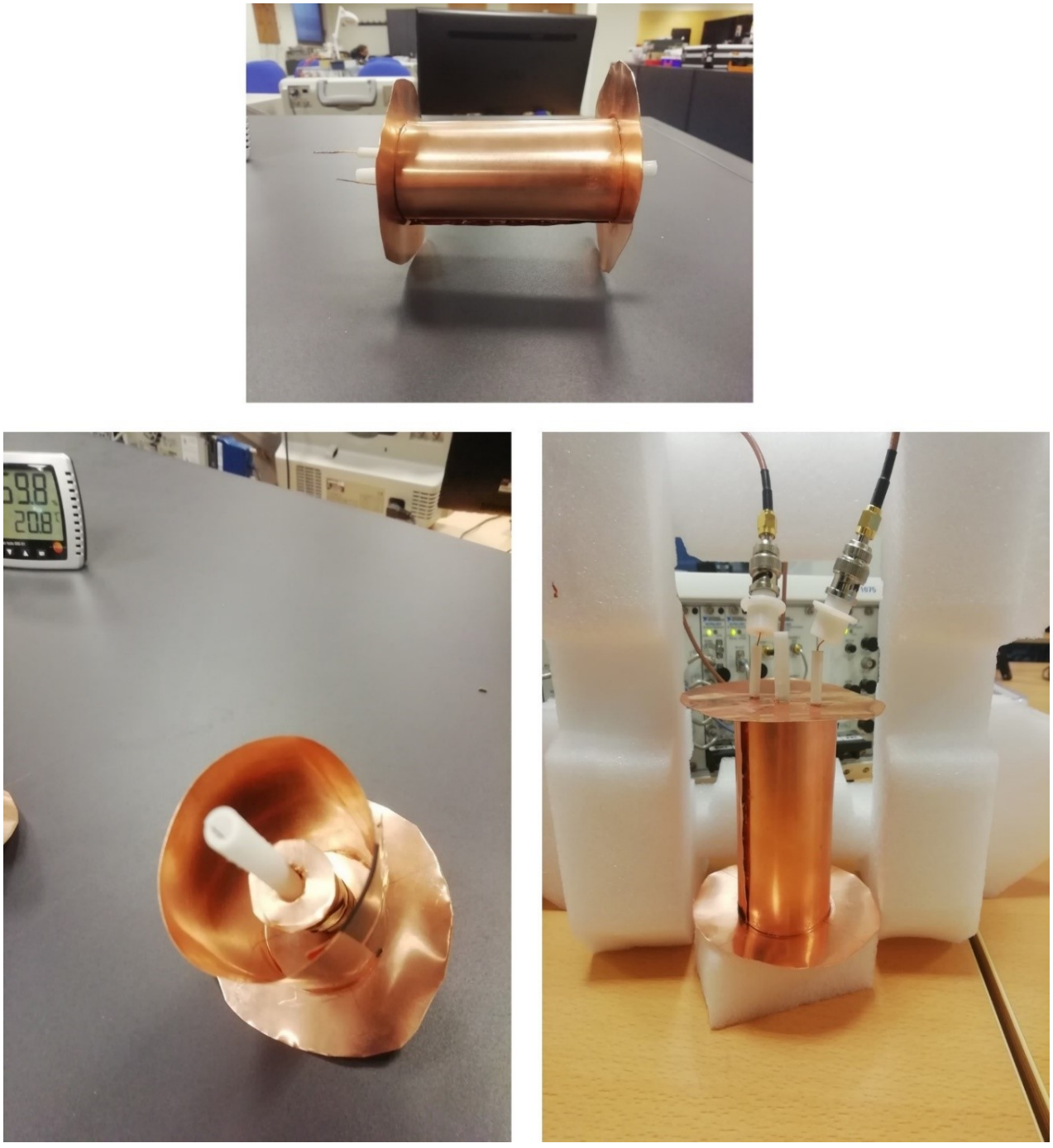

Figure 6.16. Re-Entrant Cavity.

Figure 6.17 shows the reflection coefficient, in which frequency shifts are highlighted in different areas of the graph.

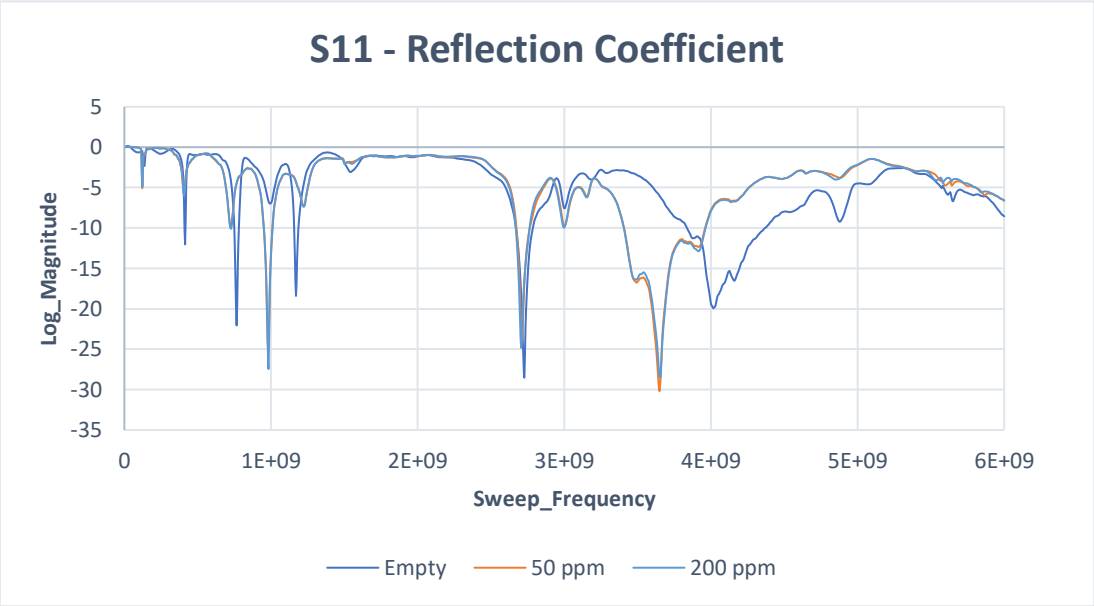

Figure 6.17. Reflection Coefficient of the Re-Entrant Cavity.

Between 3 and 4.5 GHz, there is too much variation, caused by an error in the measurement. Therefore, we consider the peaks below 1 GHz, focusing on the ones with the greatest attenuation and on the peak between 2.7 and 3 GHz. Table 6.3 are reported the determination coefficients of these resonance frequency and of the attenuation.

	0 (Empty)	**50**	**200**	**R2**
frequency [GHz]	0,9908	0,9908	0,98337	***0,9423***
S11 [dB]	-6,9637	-25,02034	-27,348	***0,5848***
frequency [GHz]	0,766	0,728	0,728	***0,4808***
S11 [dB]	-22,06	-9,8093	-10,07149	***0,4621***
frequency [GHz]	2,727	2,713	2,705	***0,8207***
S11 [dB]	-28,429	-24,04	-24,824	***0,3169***

Table 6.3. Determination Coefficients of Re-Entrant Cavity.

6.7 Debris Sensor Manufacturing and Testing

The sensor body was first made in CAD and then 3D printed at the OpenMultiLab laboratory of the Polytechnic of Bari, using a RobozeOne printer (Fig. 6.18).

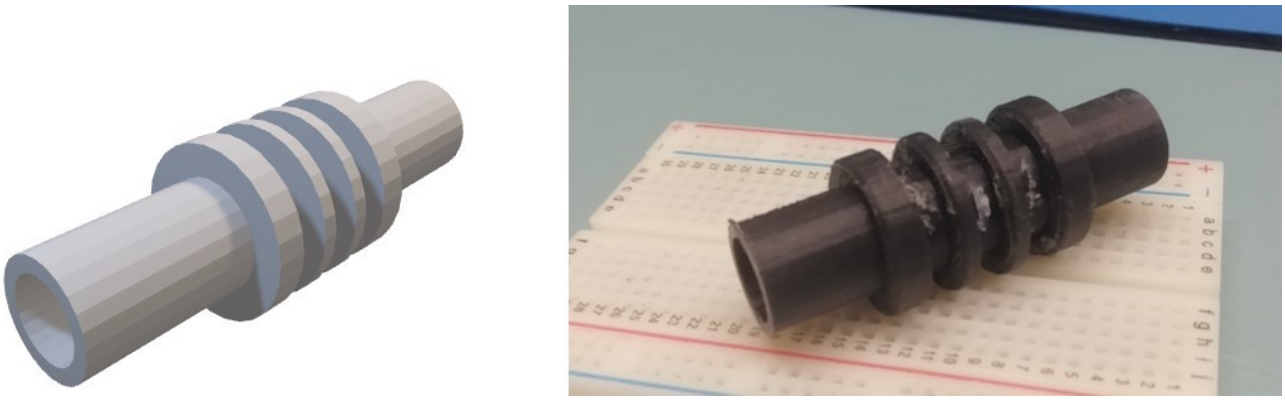

Figure 6.18. Sensor Body

.

For the creation of the coils, copper wire (0.6 mm diameter) was used, wrapped around the sensor body thanks to the use of a small capstan, also 3D printed (Fig. 6.19).

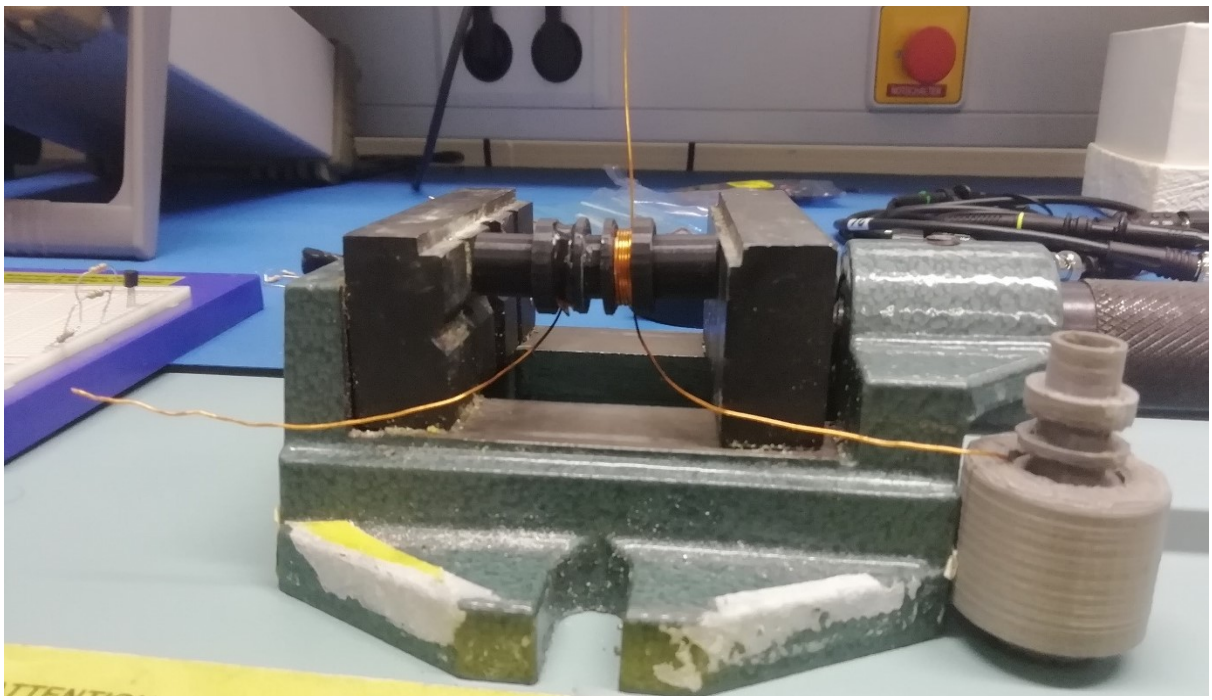

Figure 6.19. Coils Realization.

The measurement set-up provides a system that connects a wire, on which particles of different sizes are connected and run through the sensor (Fig. 6.20). A function generator is used to excite the two external coils, while an oscilloscope and a multimeter are connected to the detection coil to measure the voltage variation induced by the perturbation that the ferrous particle generates during its passage (Fig 6.21).

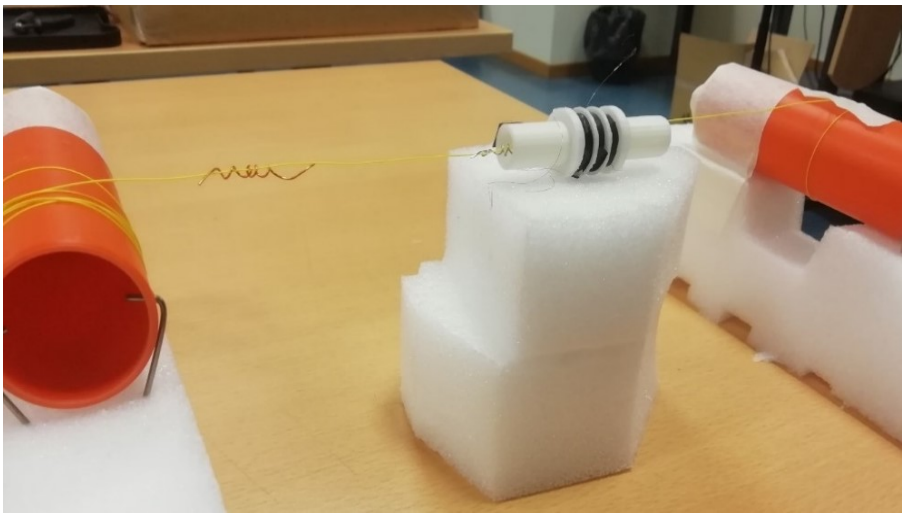

Figure 6.20. Measurement Set-up.

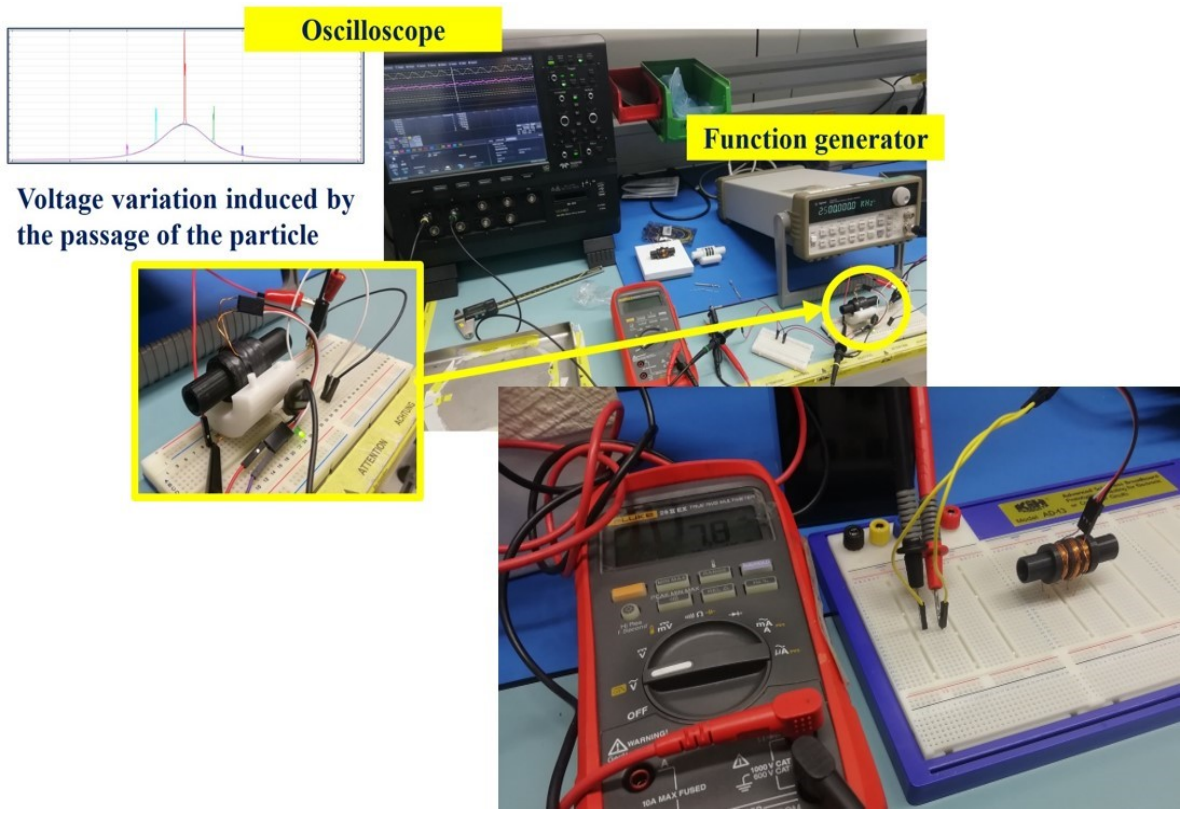

Figure 6.21. Measurement set-up for Detection.

Qualitatively the measuring principle works. However, it is unable to identify the minimum required size. The particle diameters evaluated are 0.5 mm, 2 mm and 4 mm respectively. Therefore, the minimum detectable size is equal to a sphere with a radius of 250 micrometers.

Table 6.4 shows the variation of tension values induced by the passage of the particle, as it approaches the detection zone. If the excitation frequency increases, the voltage variation increases and therefore the sensor becomes more sensitive.

		Tension [mV]		
	Diameter	**Far (15 mm)**	**Close (5 mm)**	**Detection Zone**
f = 250 Hz	P1 = 4mm	0,031	0,121	0,153
	P2 = 2 mm	0,023	0,073	0,091
	P3 = 0,5 mm	0,018	0,054	0,066
f = 500 Hz	P1 = 4mm	0,056	0,233	0,293
	P2 = 2 mm	0,037	0,142	0,178
	P3 = 0,5 mm	0,028	0,102	0,128
f = 1000 Hz	P1 = 4mm	0,096	0,426	0,537
	P2 = 2 mm	0,064	0,272	0,342
	P3 = 0,5 mm	0,049	0,201	0,251

Table 6.4. Voltage Variation in the Detection Zone

Finally, housing was designed, and 3D printed to protect the sensor body and isolate the electrical connections through holes, like shows in figure 6.22.

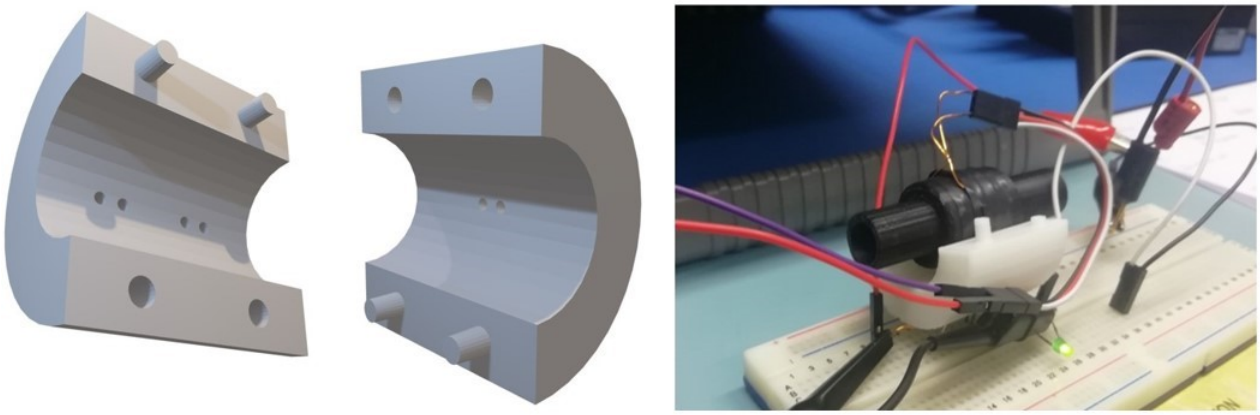

Figure 6.22. Housing of Sensor

6.8 Conclusion

In the first prototype of the transmission line, we are unable to identify an attenuation at 200 ppm. Only when we reach a value of 1000 ppm does the VNA register an attenuation.

In the second prototype, an attenuation of about 7 dB at 200 ppm can be recorded. The resonant cavities have good R2 values, but the shift of the resonance frequencies is very small, as well as the attenuation of the reflection signal. The same is true for the Re-Entrant cavity, except for a frequency value, in which the attenuation varies between 50 to 200 ppm of about 2 dB.

Therefore, with the data elaborated in this thesis, the optimal choice concerns the transmission line.

The sensor structure has been geometrically verified and ensures insertion into the fuel system where Bosch provides an intelligent sensor system for diesel quality. For a particle with a diameter equal to 0.5 mm, and a sensor excitation frequency of 1000 Hz, a variation is detected of about 0.200 mV at the passage of the particle while at the frequency of 250 Hz, the variation is about 0.042 mV. If frequency increases (1000 Hz), sensitivity reach 0.2 mV.

CONCLUSIONS

Ricorda il tuo sesto senso è quello di colpa
E tutti ne approfittano almeno una volta
Perciò va bene l'apertura verso gli altri
Ma all'entrata mettici almeno una porta
Difenditi e difendi la cultura
Non scendendo in piazza
Ma scendendo in piazza per andare a cinema o a teatro
…
Non è vero che è inutile il tuo diploma
Inutile è discutere di glutei nel perizoma
…
Perdi colpi, va così
Ma già migliora, la tua memoria, con un click

Migliora la tua Memoria con un Click – Caparezza

This thesis describes the work inherent in the development of a diesel quality sensor. The work is carried out within an industrial doctorate in partnership with Bosch and aims to constantly monitor the quality of the fuel used in most heavy vehicles, but not only. The reason that drives Bosch to this type of measurement is the deterioration of the diesel fuel pump due to the use of poor-quality fuel. The objective is the prototyping of an in-line detection system, that is placed on the pipelines for the distribution of diesel, in the pre-feeding system, next to the tank.

Fuel control is a part of the maintenance operations aimed at extending the life of the engine and is necessary because the developments in diesel, aimed at greater protection of the environment, have led to greater use of biofuels that have physical and chemical properties other than conventional fuels. The analysis of fluids guarantees the optimization of vehicle performance, the prevention of breakdowns, the reduction of emissions and prevents damage to the common rail technology or at least extends its operating life. The problem of dirty diesel has never been completely solved, but only improved with the common rail considering that, the operating pressures are such that the diesel must be of high quality.

Hence, water content is to be considered as an important parameter of diesel fuel, however it represents one of the most common contaminants found in all types of fuels, not only diesel. The main effects of water contamination are to be seen on the injection elements (fuel pipes, fuel pumps, injectors) that are exposed to corrosion and thus on lower combustion quality. Water corrosion will occur only if water is in free form. Fuel properties, like viscosity or density will change when mixed with dissolved water. In general, water causes reduction of lubricating properties, wear and corrosion of fuel system, motor power reduction and growth of bacteria. EN 590 standard allows a concentration of 200 mg/kg of water contamination, which has been proven to be the maximum possible level on most of the markets.

The techniques used today to determine the quantity of water are the centrifugal methods and the coulometric titration method of Karl Fischer, which are laboratory techniques. For in-line fuel monitoring, the most promising measurement techniques are resonant cavity dielectric technology, spectroscopic techniques (UV-Vis, NIR, FT-IR, fluorescence and Raman), interdigitated capacitive sensing technology, ultrasonic and microwave technology. The creation of an automatic system for the optimal management of automotive engines represents a priority topic in the panorama of international industrial research. Vehicle performance depends not only on engine quality but also on fuel characteristics. In this perspective, the on-line measurement of the physical and chemical properties of the fuel and the use of additional functions are essential to face a very competitive

market. The use, for that purpose, of optical or microwave technologies seems to be the right way to create a low-cost, precise and real-time measurement detection system.

The innovative feature is the ability to exploit the diesel as an element that flows inside the sensor itself and, during its passage, measure microwave attenuation, in real-time, thank an easy and low-cost sensor.

The parameter we measured to characterize the amount of water in diesel is the permittivity. For the preliminary simulations, a very simple mathematical model was chosen to express the dielectric constant of the analyte as a function of the water concentration. Remembering that the dielectric constant varies with the amount of water and therefore the impedance of the cable also varies.

Subsequently it has been described the procedure to achieve some diesel samples of known quantities of water. These samples will first be characterized through laboratory techniques (off-line), to define an empirical relationship that quantifies the change in the dielectric constant of diesel as the water concentration changes.

Analytical chemistry techniques were used to make the mixtures of known quantities of water, starting from a quantity of diesel that has been preliminarily analyzed at a qualitative level, to have a starting point from which to define the water-diesel mixtures.

Characterization of contaminants is developed following two methods. Optical techniques with the use of the spectrophotometer and microwave techniques with the aid of a probe.

In the first case, can be seen from the absorption spectra, how optical techniques are not useful for the characterization of water-diesel mixtures. First of all, for the small quantities of contaminant, which make the preparation and cleaning of the samples difficult. Despite the repetition of the measurement, from the calibration curves it can be seen that the determination coefficient does not exceed a value of 0.3, however they have been highlighted by the characteristic peaks. However, the small quantities of water are confused with each other, without the possibility of distinguishing them progressively. So, optical technique has a low sensitivity.

Instead, the characterization through the probe and the VNA provided encouraging data which were confirmed by comparison with the mathematical models present in the literature. The coefficient of determination of the calibration curves are close to 0.9. Thanks to this characterization, an empirical relationship has been obtained with which the sensors proposed in the following work have been modeled.

The sensor is designed for the automotive field, with the aim of monitoring the quality of the diesel in real time. The sensor is expected to be housed in the pipes of the power supply system. The innovative aspect of this sensor is the ability to exploit the diesel as an element that flows inside the sensor itself and, during its passage, measure microwave attenuation. In this way, the presence of water can be detected and, if the system is appropriately sized, conditioned and calibrated, water content can be measured. A transmission measurement method has been chosen as it appears the simplest and most economic technique, because of the availability of very low-cost integrated circuits for the generation of the stimulus signal, and the use of a simple sensor with an envelope threshold detector for the measurement of the attenuated signal, which can be part of a small and low power embedded system. The signal attenuation can be evaluated through the scattering parameter S_{21} (forward voltage gain, or transmission coefficient), which is the ratio between outgoing wave amplitude at output port 2 and ingoing wave amplitude at input port 1, assuming load impedance matching at port 2. A threshold detector may be useful, in particular, to provide an alert around a programmable level of the signal output. The most suitable guiding structure is certainly the coaxial one that guarantees the maximum fringing of the EM field in the analyte and, consequently, the maximum sensitivity.

Two solutions for contaminant detection through permittivity measurement have been designed and modeled: the first based on the theory of the transmission line and the second on resonant cavities. In the first case the parameter to be evaluated is the power signal while in the second case the resonance frequency shift and the reduction of the quality factor are measured. Dielectric constant measurements can provide information about critical design parameters for many electronic applications. In the first case the power attenuation of the stimulus signal is evaluated while in the second case the theory of resonant perturbation is exploited. For a resonator with a given EM field, when a part of this varies, due to the introduction of a sample, its resonant frequency changes while the quality factor is reduced. From them, we can refer to the dielectric properties of the sample.

For each approach, the variation in the concentration of contaminant (water) in the diesel was analyzed with a mathematical model and was studied the geometric sweep of the critical parameters.

Electromagnetic simulations were carried out using the COMSOL Multiphysics software aimed at validating the physical measurement principle. In particular, different frequency values were explored, the variation in the concentration of contaminant (water) in the diesel, through a mathematical model, and the geometric sweep of the critical dimensional parameters of the analyzed structures.

The various models have also been validated at the fluid dynamic and mechanical level.

The calibration curve of the transmission line has encouraging results for the construction of the sensor. It is clear that the sensitivity of the sensor depends exclusively on the diameter of the core. The attenuation increases for larger radii. Even if other parameters vary, external diameter of the shield, flow velocity and outlet pressure, the sensitivity does not change. Therefore it is believed that the sensor manufacturing is suitable for the indended purpose at Bosch. The increase of the frequency of the stimulus signal, with the same radius, sensitivity increases. Hence sensor detectivity may be tuned. This can be useful because, although the standards set a maximum limit of water, this limit will vary according to the geographical area of origin of the diesel. On a fluid dynamic level, assuming an input speed of the flow of 2 m/s, it occurs that if the radius of the internal diameter of shield increases, the output velocity of the flow decreases, thus reducing the stress of the flow on the core. (maximize the stiffness and rigidity if the core of the transmission line). It is evident that the maximum pressure decreases when radius increases. However, its value is in the order of magnitude of millibars (very low).
In contrast, the resonant cavity show the variation of water concentration is so small that the variation in resonance frequency is hard to detect, also with bended capillary, where the sensitivity is slightly higher. In Re-Entrant Cavities, a very small, however greater than the classical resonant cavities, difference in resonant frequency can be detected just in a frequency peak.
The calibration curve of the transmission line has encouraging results for the construction of the sensor. The sensitivity of the sensor depends exclusively on the diameter of the core.

After validation, in terms of simulation, the prototypes were made. Two prototypes based on the logic of transmission lines, two resonant cavities and a re-entrant cavity. In the first prototype of the transmission line, we are unable to identify an attenuation at 200 ppm. Only when we reach a value of 1000 ppm does the VNA register an attenuation. In the second prototype, an attenuation of about 0.45 dB at 200 ppm can be recorded. At f = 2.54 GHz the sensitivity is 4.6 mdB/ppm while at f =1.8219 GHz the sensitivity is 5.45 mdB/ppm. The determination coefficient is, for both, major of 0.99.

The resonant cavities have good R^2 values, but the shift of the resonance frequencies is very small, as well as the attenuation of the reflection signal. In prototype 1, the maximum shift reach is 8.1 MHz at f = 4.7121 GHz, while the maximum attenuation is 8.1 dB, at same frequency. In prototype 2, the maximum shift reach is 21.04 MHz at f = 5.955 GHz, while the maximum attenuation is 22 dB, at same frequency.

Similar results are obtained in the Re-Entrant cavity. The maximum shift is reached at f = 2.727 GHz and it is 22 MHz while the maximum attenuation is 28.384 dB at f = 0.9908 GHz.

Therefore, with the data elaborated in this thesis, the optimal choice concerns the transmission line, to comply with all the constraints imposed by the company and the problem in it.

Finally, at Bosch's request, a sensor was created to monitor the solid particles created by the wear of the diesel passage in the fuel pump because wear in one of the main reasons that cause mechanical equipment failures, and numerous wear particles are produced during the device running process. In the simulation, the qualitative analyze is realized. When the ferrous particle passes through the sensor, there is a variation of 0.011 Tesla. When the nonferrous particle passes through the sensor, there is a variation of 0.004 Tesla. During the experimental step, we define a minimum identifiable particle, about 250 μm and we verified that is the frequency increases, the sensitivity greater. In fact, when f = 250 Hz, the voltage attenuation is 0.042 mV while if f = 1000 Hz, the voltage attenuation is 0.2 mV.

The realization of these two sensors enters into the ***future goals*** of hybridizing the vehicle, through an in-line system of sensors, based on intelligent control, in order to improve the quality of combustion, reduce emissions and increase the life of the fuel system components.

A further possible and interesting development is the integration of the two types of sensors by exploiting the possibility of detecting the presence of residual particles directly with high frequency methods, sensitive to permittivity. In this regard, in consideration of the frequency range useful for sensitivity purposes, one could think of adopting more compact, remotely controllable and economical systems such as portable VNAs. Finally, the experimental activity could be extended, trying to describe the impact of some setting parameters, such as fuel mass flow, fuel temperature because during this work, I used the data provided by Bosch. This represent a further step towards the application of the device.

APPENDIX A

PHYSICAL PRINCIPLES OF LABORATORY INSTRUMENTS

A.1 Scattering Parameters

To characterize radio frequency networks [MHz GHz], which cannot be represented with circuit models with concentrated parameters, the parameters are introduced. measurement and design problems. These parameters are useful in the analysis of microwave devices, as they are easier to measure and use at high frequencies than other types of parameters.

Based on the theory of transmission lines, it is possible to define parameters suitable for characterizing networks at high frequencies: S parameters. The two-port linear networks, described in figure A.1, are characterized by several equivalent circuit parameters, such as the transfer matrix, the impedance matrix, the admittance matrix and the scattering matrix.

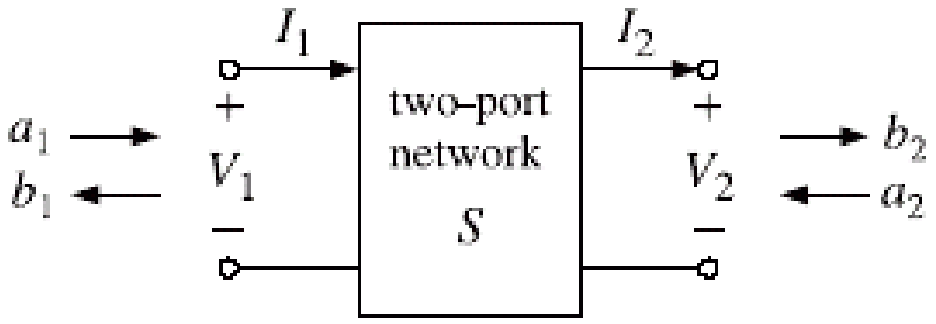

Figure A.1: Two-port Network.

The transfer matrix (eq.A.1) binds the voltage and current at port 1 to those of port 2, while the impedance matrix (eq. A.2) provides the link between the two voltages V_1 and V_2 to the two currents I_1 and I_2:

$$\begin{bmatrix} V_1 \\ I_1 \end{bmatrix} = \begin{bmatrix} A & B \\ C & D \end{bmatrix} \begin{bmatrix} V_2 \\ I_2 \end{bmatrix} \quad \text{(A.1)}$$

$$\begin{bmatrix} V_1 \\ V_2 \end{bmatrix} = \begin{bmatrix} Z_{11} & Z_{12} \\ Z_{21} & Z_{22} \end{bmatrix} \begin{bmatrix} I_1 \\ -I_2 \end{bmatrix} \quad \text{(A.2)}$$

The admittance matrix is simply the inverse of the impedance matrix; the scattering matrix (eq. A.3) links the outgoing waves b_1 and b_2 to the incoming waves a_1 and a_2 which affect the two ports:

$$\begin{bmatrix} b_1 \\ b_2 \end{bmatrix} = \begin{bmatrix} S_{11} & S_{12} \\ S_{21} & S_{22} \end{bmatrix} \begin{bmatrix} a_1 \\ a_2 \end{bmatrix} \quad \text{(A.3)}$$

The elements S_{11}, S_{12}, S_{21} and S_{22} of the matrix go under the name of scattering parameters or S parameters; the parameters S_{11}, S_{22} have the meaning of reflection coefficients while those S_{12} and S_{21} represent the transmission coefficients. The variables a_1, b_1 at port 1 and a_2 b_2 at port 2 are defined in terms of voltage V_1, V_2 and current I_1, I_2 and of characteristic impedance Z_0 generally assumed with a value of 50 Ω.

Scattering parameters or S-parameters describe the electrical properties and performance of RF electrical components or network of components when undergoing various steady state electrical signal stimuli. They are unitless complex numbers, having both magnitude and phase, and are related to familiar measurements such as gain, loss, and reflection coefficient. Scatter Parameters, also called S-parameters, belong to the group to two-port parameters used in two-port theory. Like the Y or Z parameter, they describe the performance of a two-port completely. Different to Y and Z, however, they relate to the traveling waves that are scattered or reflected when a network is inserted into a transmission line of a certain characteristic impedance Z_L. Therefore, S-parameters can be compared to reflection and through pass of a pair of spectacles. S-parameters are important in microwave design because they are easier to measure and to work with at high frequencies than other kinds of two-port parameters. They are conceptually simple, analytically convenient and capable of providing detailed insight into a measurement and modeling problem. However, it must keep in mind that -like all other two-port parameters, S-parameters are linear by default. I.e. they represent the linear behavior of the two-port. S_{11} and S_{21} are determined by measuring the magnitude and phase of the incident, reflected

and transmitted signals when the output is terminated in a perfect Zo load. This condition guarantees that a2 is zero. S_{11} is equivalent to the input complex reflection coefficient or impedance of the DUT, and S21 is the forward complex transmission coefficient.

Likewise, by placing the source at port 2 and terminating port 1 in a perfect load (making a1 zero), S_{22} and S_{12} measurements can be made. S_{22} is equivalent to the output complex reflection coefficient or output impedance of the DUT, and S_{12} is the reverse complex transmission coefficient. The accuracy of S-parameter measurements depends greatly on how good a termination we apply to the port not being stimulated. Anything other than a perfect load will result in a1 or a2 not being zero (which violates the definition for S-parameters). When the DUT is connected to the test ports of a network analyzer and we don't account for imperfect test port match, we have not done a very good job satisfying the condition of a perfect termination. For this reason, two-port error correction, which corrects for source and load match, is very important for accurate S-parameter measurements. The magnitude of S_{11} and S_{22} is always less than 1. Otherwise, it would represent a negative ohmic value. On the other hand, the magnitude of S_{21} (transfer characteristics) respectively S_{12} (reverse) can exceed the value of 1 in the case of active amplification. Also, S_{21} and S_{12} can be positive and negative. If they are negative, there is a phase shift. The numbering convention for S-parameters is that the first number following the S is the port at which energy emerges, and the second number is the port at which energy enters. So S_{21} is a measure of power emerging from Port 2 as a result of applying an RF stimulus to Port 1.

Generally, the calculation of the dielectric parameters is performed by measuring the S-parameters of the network under examination [61]. S-Parameters are used because they are relatively easy to obtain at high frequencies and measure voltage traveling waves with a vector network analyzer. Enough they don't need shorts/opens which can cause active devices to oscillate or self-destruct and can compute H, Y, or Z parameters from S-parameters if desired. Finally, they can easily import and use S-parameter files in our electronic-simulation.

A.2 Network Analyzers

The network analyzer is a very complex tool capable of measuring the parameters characterizing a network, active or passive, quickly and accurately. The network analyzer can be seen as a set of equipment which, through an appropriate connection, allows to carry out a multiplicity of measures. They fall into two main categories: scalars and vectors. The scalar analyzer measures and shows on

the display only the amplitude of the signal being analyzed according to the frequency; the vector analyzer measures and shows both amplitude and phase of the signal. The latter feature allows the vector analyzer to display the parameters not only in a linear scale but also in a complex form, for example through the Smith chart. The vector analyzer can also measure and show the Scattering parameters at the same time as it continuously scans its two input ports. Instrument suitable for characterizing the signal in a circuit; the characterization of the signal can be of two types: linear (a signal with one tone at the input to the circuit, and a single tone at the output to the same), or with multiple tones. To perform a linear characterization, it is necessary to use the network analyzer. When it comes to radiofrequency, there are several issues: vector measurements will certainly be needed since quantities in module and phase must be measured; when we talk about high frequencies, such as radio frequencies, the structure we are dealing with is distributed: we have voltages and currents that depend substantially on the position we are in. It does not make sense to measure voltages or currents: what would be measured would be the quantities at the gates, but a few millimeters later something completely different would be measured, frustrating the sense of measurement.

A measurement of the reflection from and/or transmission through a material along with knowledge of its physical dimensions provides the information to characterize the permittivity and permeability of the material. A vector network analyzer consists of a signal source, a receiver and a display. The source launches a signal at a single frequency to the material under test. The receiver is tuned to that frequency to detect the reflected and transmitted signals from the material. The measured response produces the magnitude and phase data at that frequency. The source is then stepped to the next frequency and the measurement is repeated to display the reflection and transmission measurement response as a function of frequency. Simple components and connecting wires that perform well at low frequencies behave differently at high frequencies. At microwave frequencies wavelengths become small compared to the physical dimensions of the devices such that two closely spaced points can have a significant phase difference. Low frequency lumped-circuit element techniques must be replaced by transmission line theory to analyze the behavior of devices at higher frequencies. Additional high frequency effects such as radiation loss, dielectric loss and capacitive coupling make microwave circuits more complex and expensive. It is time consuming and costly to try to design a perfect microwave network analyzer. Instead, a measurement calibration is used to eliminate the systematic (stable and repeatable) measurement errors caused by the imperfections of the system. Random errors due to noise, drift, or the environment (temperature, humidity, pressure) cannot be removed with a measurement calibration. This makes a microwave measurement susceptible to errors from small changes in the measurement system. These errors can be minimized by adopting good

measurement practices, such as visually inspecting all connectors for dirt or damage and by minimizing any physical movement of the test port cables after a calibration. A VNA contains both a source, used to generate a known stimulus signal, and a set of receivers, used to determine changes to this stimulus caused by the device-under-test or DUT. The scheme is represented in figure A.2.

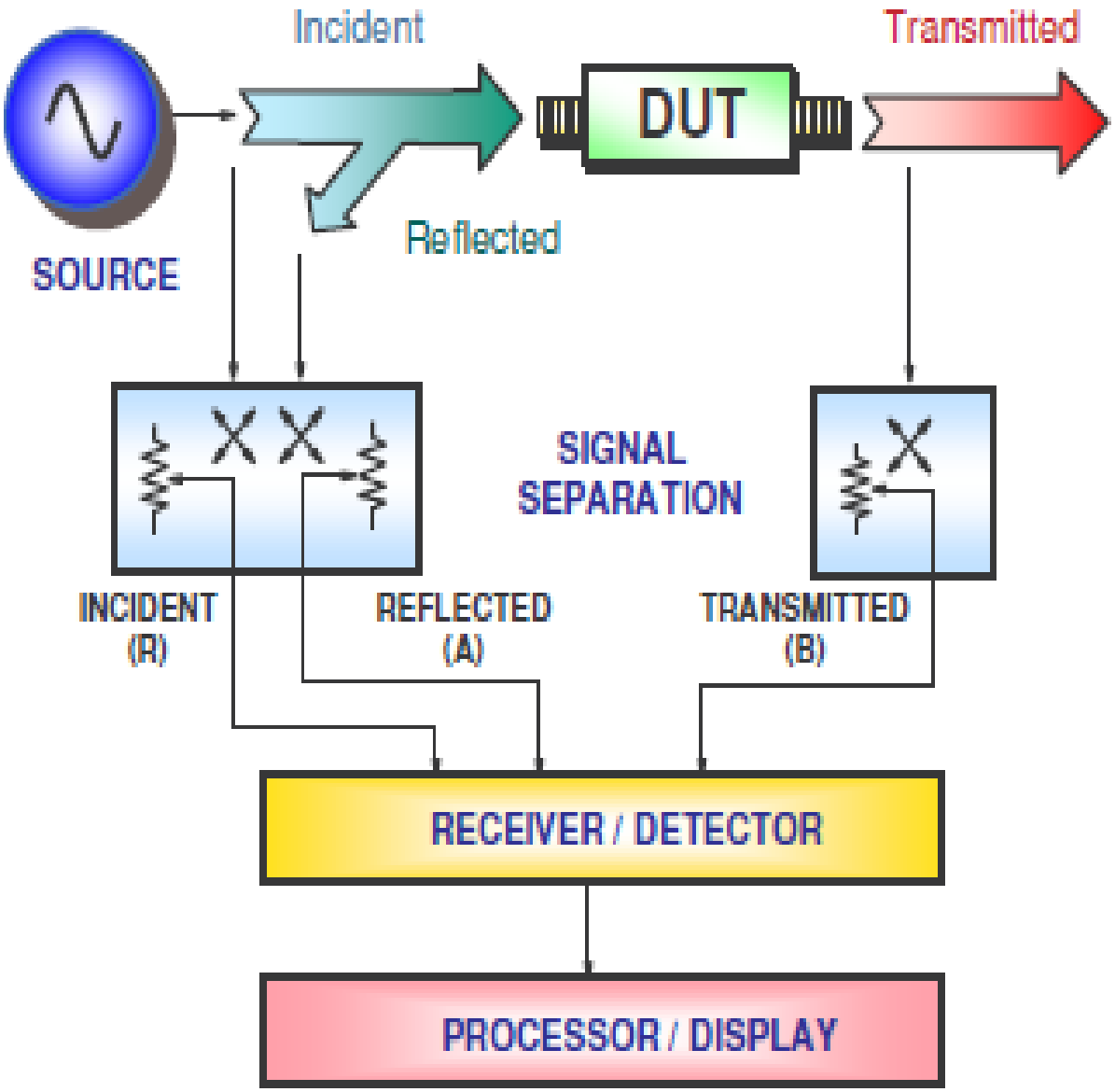

Figure A.2. Scheme of Network Analyzer.

For the characterization of the contaminants, in the laboratory, a Vector Network Analyzer can be used to measure transmitted and reflected waves, from which the scattering parameters are subsequently processed to obtain complex permittivity [62, 63, 64, 65, 66, 67].

A.3 Configuring the VNA

Before discussing calibration further, and some of the alternatives available, it is important to first gain a clear understanding of any VNA setup issues as they will affect calibration performance. In almost all cases, the VNA settings are used during calibration. Therefore, setting up the VNA as desired beforehand can be especially helpful. The settings of interest are:

1. Frequency Start, Stop and Number of Points: These settings are obvious. Segmented sweep must also be setup in advance if a more custom frequency list is desired.

2. IF Bandwidth and Averaging - These parameters control the digital filtering and post-processing that determine the effective noise floor, amount of trace noise and, in some special cases, immunity to interfering signals. The trade-off for improved noise performance is slower sweep speed.

3. Point-by-Point versus Sweep-by-Sweep Averaging: Point-by-point averaging incurs additional measurements at each given frequency point and increases sweep time roughly proportionally. Because the additional measurements are taken at once, the effect is like the proportional change in IFBW. An additional benefit is that the displayed data is fully optimized during the first sweep. Sweep-by-sweep averaging acquires additional measurements on subsequent sweeps. The result is a gradual shift in trace amplitude. Before extracting data, the VNA user must verify that a fully corrected sweep has occurred. Sweep-by-sweep averaging is a rolling average, so the time it takes to fully stabilize from a sudden DUT change is roughly proportional to the average count. Consequently, it offers an alternate way to improve lower-frequency variations.

4. Power: Port power is somewhat less critical due to the excellent linearity of the receivers, but any step-attenuator settings must be selected before calibration. Changing the step-attenuator settings alters the RF match in the measurement paths as well as in the insertion loss thus. Therefore, changing them will invalidate the calibration.

An important aspect of test-set power level is the consideration of dynamic range. Setting the port power to the maximum level before receiver compression provides the widest possible signal-to-noise floor ratio and thus dynamic range. Be sure to perform this setting before beginning calibration.

A.4 NI PXIe-5632 VNA

For the activities carried out in this research work, the PXIe-5632 [68] will be used, the architecture of which is shown in figure A.3 while the specifications in figure A.4.

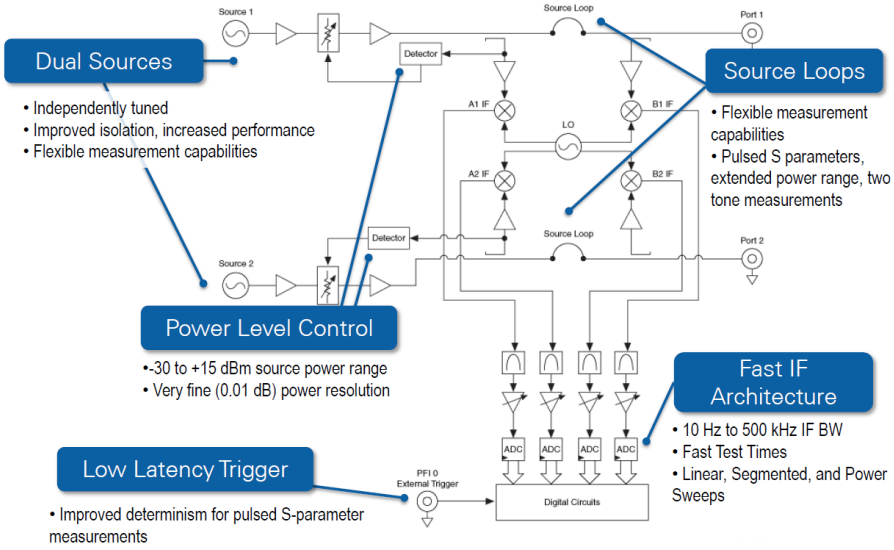

Figure A.3. NI PXIe-5632 VNA Architecture.

Specifications	NI PXIe-5632
Frequency Range	300 kHz to 8.5 GHz
Architecture	2-port, full S-parameters PXI Express, 3 slots
Power Range	-30 to +15 dBm, 0.01 dB steps
IF Bandwidth	10 Hz to 500 kHz
Dynamic Range	>110 dB (115 dB typ) below 6 GHz >105 dB (110 dB typ) below 8 GHz
Measurement Time	<65 µsec/pt (100 kHz IFBW) Forward or Reverse S-parameters
Number of Points	20,001

Figure A.4. Specification of the NI PXIe-5632.

An automatic system has been developed for reading the outputs of the radio frequency sensors using LabVIEW to control the VNA NI-PXIe-5632 in order to monitor in real time the scattering parameters characterizing in the microwave circuit. Figure A.5 shows the scheme in LabVIEW. Laboratory Virtual Instrument Engineering Workbench (LabVIEW) is a system-design platform and development environment for a visual programming language from National Instruments. I want to see the attenuation in the transmission line due to the presence of water.

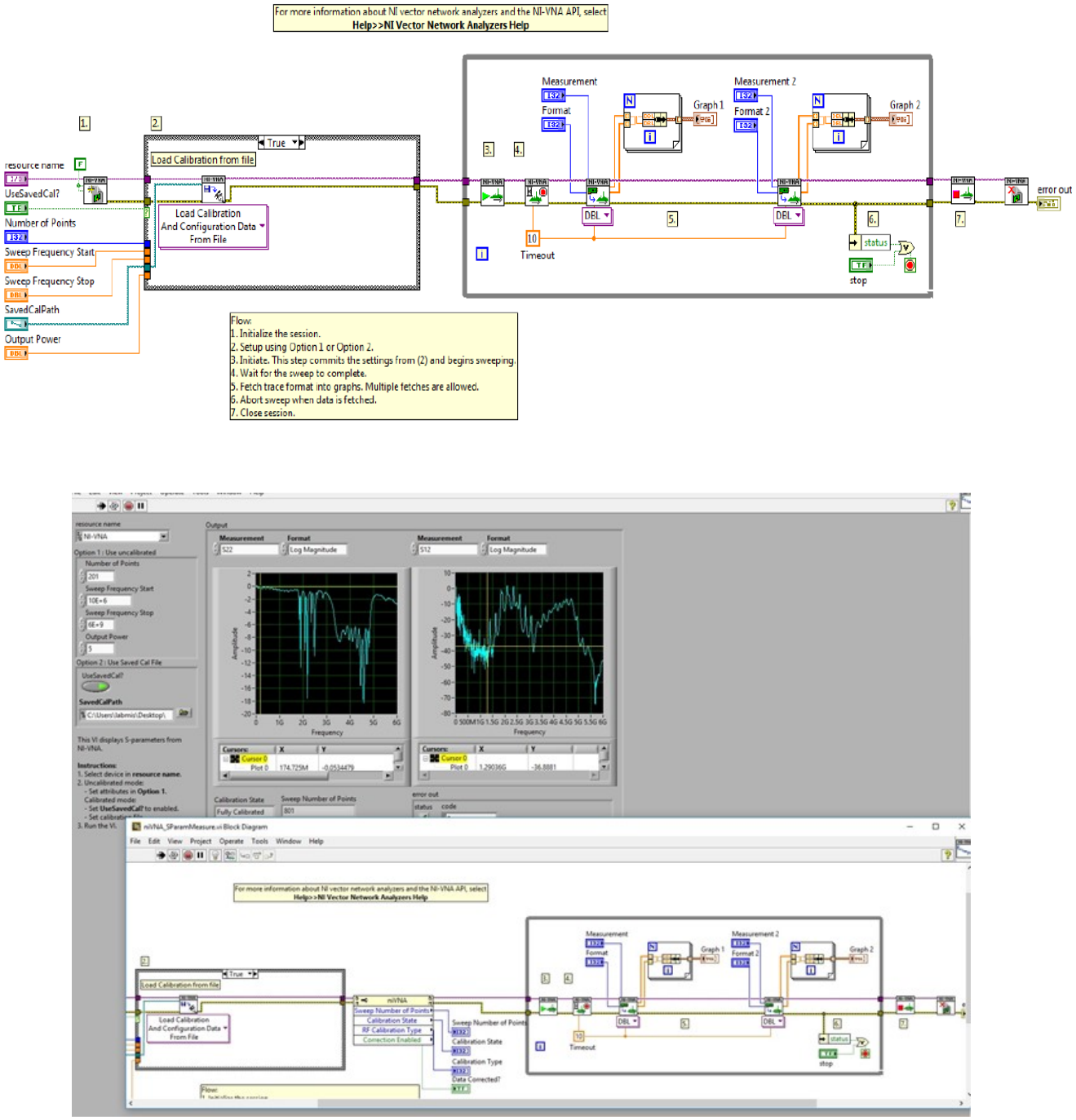

Figure A.5. niVNA_SParamMeasure.vi.

A.5 Automatic Calibration (AutoCal)

SOLT (Short, Open, Load, Thru)) calibration is one of the most common VNA calibration methodologies. It uses a well-defined short circuit, open circuit and load (with characteristic impedance, usually 50 or 75 ohms). There are several types of calibrations, defined by what ports are involved and what level of correction is accomplished. These calibration types include Full 2-Port. This is the most used and most complete calibration involving two ports. All four S-parameters (S_{11}, S_{12}, S_{21}, and S_{22}) are fully corrected. The advantages are that it is simple, redundant standards and not band limited but requires very well-defined standards and has lower accuracy at high frequency. In contrast to the mechanical standards approach to calibration, automatic calibration modules can be used to simplify the calibration method.

Automatic calibration techniques, such as those performed by the AutoCal modules available from Anritsu, are often the preferred method for calibrating VNAs. AutoCal provides VNA users with the ability to quickly calibrate the network analyzer with the simple push of a button. The AutoCal module incorporates extremely accurate, repeatable solid-state switches to select a variety of impedance standards from just one connection between the VNA and a calibrator module. Calibrations employing AutoCal modules are consistent, repeatable and provide better accuracy than traditional broadband-termination, 12-term calibrations. In addition, automatic calibrations are much faster than with traditional calibration kits. Precision AutoCal module requires only two connections, while a mechanical calibration kit requires 7 to 9 connections for a typical calibration.

The basic concept in Precision AutoCal is the transfer of known calibration parameters from a traceable VNA to measure the calibration standards within the Precision AutoCal module, a process referred to as Precision AutoCal characterization. A calibrated VNA (using a traceable calibration kit) measures the S-parameter data of each impedance standard throughout the calibrator module's frequency range. The accuracy of the calibrated VNA is thereby transferred to the Precision AutoCal module. The stability and repeatability of the Precision AutoCal impedance standards provides excellent automatic calibrations over a defined time frame [69].

Very high calibration accuracy is maintained through the use of certain principles:

- The use of many impedance and transmission states covering as wide a range as possible across the Smith chart.
- The creation of very stable states that are further enhanced with a constant-temperature thermal platform inside the module.

- The use of very reliable and repeatable solid-state switching constructed to provide a great variety of state impedances for better calibration stability.

A.5.1 Calibration Kit

The calibration kits contain all of the precision components and tools required to calibrate an Anritsu (Figure A.6).

Figure A.6. Calibration Kit.

Anritsu and other vendors provide calibration kits for a variety of algorithms and circumstances. In all cases, certain information must be provided to the VNA in order to complete the calibration. The nature of that information varies by kit and application. These kits are all based on SOLT and require that data describing all of the reflection standards (provided by the factory) be loaded into the VNA on a serial number basis. Typically, these calibration kits are loaded using the Cal Kit/AutoCal utility menu.

References

[1] G. Ferrari, Motori a Combustione Interna, Società Editrice Esculapio, 2016.

[2] C. Duca, *Fuel Quality Sensor for HD Engines,* Master of Science Thesis, KTH Industrial Engineering and Management, Machine Design, 2014.

[3] C. Chevron, *Diesel Fuels Technical Review,* Global Marketing, 2007.

[4] C. S. Hsu, «Diesel Fuels Analysis,» *Encyclopedia of Analytical Chemistry,* pp. 1-9, 2006.

[5] *EN 590:2004 - Automotive Fuels. Diesel. Requirements and Test Methods,* Standard, European Committee for Standardization, 2004.

[6] *ISO 12937:2000 - Petruleum Products - Determination of Water - Coulometric Karl Fischer Titration Method,* Standard, International Organization for Standardization, 2000.

[7] J. Scheider, *Fuel Composition and Quality Sensing for Diesel Engines,* Urban-Champaign: Thesis for the Degree of Master od Science in Mechanical Engineering in the Graduate College of the University of Illinois , 2011.

[8] «Fuel Regulation,» [Online]. Available: http://www.diesalnet.com/standard.

[9] A. Gonzalez, J. Olazagoitia e J. Vinolas, «A Low-Cost Data Acquisition System for Automobile Dynamics Applications,» *Sensors,* vol. 18, n. 2, pp. 1-20, 2018.

[10] L. Yang, S. Zhang, Y. Wu, Q. Chen, T. Niu, X. Huang, S. Zhang, L. Zhang, Y. Zhou e J. Hao, «Evaluating Real-World C02 and NOX Emissions for Public Transit Buses using a Remote Wireless On-Board Diagnostic (OBD) Approach,» *Environmental Pollution,* vol. 218, pp. 453-462, 2016.

[11] G. Andria, F. Attivissimo, A. D. Nisio, A. Lanzolla e A. Pellegrino, «Development of an Automotive Data Acquisition Platform for Analysis of Driving Behavior,» *Measurement,* vol. 93, pp. 278-287, 2016.

[12] J. Mare, «Dynamic Loading Systems for Ground Testing of High-Speed Aerospace Actuators,» *Aircraft Engineering and Aerospace Technology,* vol. 78, n. 4, pp. 275-282, 2006.

[13] D. Filatov, A. Friedrich e A. Devyatkin, «Parameters Identification of Thrust Generation Subsystem for Small Unmanned Aerial Vehicles,» in *IEEE International Conference on Control in Technical Systems (CTS)*, St. Petersburg, 2017.

[14] G. D. Angelis, M. B. E. Dati e F. Leccese, «Development on Aerospace Composite Structures Investigation using Thermography and Shearography in Comparison to Traditional NDT Methods,» in *IEEE Metrology for Aerospace (MetroAeroSpace)*, Benevento, 2015.

[15] F. Adamo, G. Andria, A. D. Nisio, C. C. Carducci, A. Lay-Ekuakille, G. Mattencini e M. Spadavecchia, «Designing and Prototyping a Sensors Head for Test and Certification of UAV Components,» *International Journal on Smart Sensing and Intelligent System,* vol. 10, n. 3, pp. 646-672, 2017.

[16] F. Adamo, G. Andria, A. D. Nisio, G. C. Carducci, A. Lanzolla e G. Mattencini, «Development and Characterization of a Measurement Instrument System for UAV Components Testing,» in *IEEE International Workshop on Metrology for Aerospace (MetroAeroSpace)*, Padua, 2017.

[17] K. Loizou e E. Koutroulis, «Water Level Sensing: State of the Art Review and Performance Evaluation of a Low-Cost Measurement System,» *Measurement,* vol. 89, pp. 204-214, 2016.

[18] M. Ciaciotta, «A First Study on Prognostic System for Electric Engines based on Envelope Analysis,» in *IEEE Metrology for Aerospace (MetroAeroSpace)*, Benevento, 2014.

[19] S. Rahman, M. Ismail, N. Noor e H. Bakhtiar, «Embedded Capacitor Sensor for Monitoring Corrosion of Reinforcement in Concrete,» *Journal of Engineerign Science and Technology,* vol. 7, pp. 209-218, 2012.

[20] K. Loizou, E. Koutroulis, D. Zalikas e G. Liontas, «A Low-Cost Capacitive Sensor for Water Level Monitoring in Large-Scale Storage Tanks,» *Industrial Technology (ICIT),* pp. 1416-1421, 2015.

[21] A. Agoston, C. Otsh e B. Jakoby, «Viscosity Sensors for Engine Oil Condition Monitoring - Application and Interpretation of Result,» *Sensors and Actuators A: Physical,* vol. 121, n. 2, pp. 327-332, 2005.

[22] S. Leonardi, M. Bonyani, K. Ghosh, A. Dhara, L. Lombardo, N. Donato e G. Neri, «Development of a Novel Cu (II) - Complex Modified Electrode and a Portable Electrochemical Analyzer for the Determination of Dissolved Oxygen (DO) in Water,» *Chemosensors,* vol. 4, n. 2, pp. 1-10, 2016.

[23] S. Grassini, S. Corbellini, M. Parvis, E. Angelini e F. Zucchi, «A Simple Arduino-based EIS System for in situ Corrosion Monitoring of Metallic Works of Art,» *Measurements,* vol. 114, pp. 508-514, 2018.

[24] C. Casavola, P.Pappalardi, G. Pappalettera e G. Renna, «A Fringe Projection based Approach for Corrosion Monitoring in Metals,» *Experimental Techniques,* vol. 22, pp. 1-7, 2018.

[25] Y. Martin, M. Oliveros, J. Pavon, C. Pinto e B. Cordero, «Electronic Nose based on Metal Oxide Semiconductor Sensors and Pattern Recognition Techniques: Characterisation of Vegetable Oils,» *Analytica Chimica Acta,* vol. 449, n. 1-1, pp. 69-80, 2001.

[26] M. Ciaciotta, S. Giarnetti, F. Leccese, B. Orioni, M. Oreggia, C. Pucci e S. Rametta, «Flavors Mapping by Kohonen Network Classification of Panel Tests of Extra Virgin Olive Oil,» *Measurement,* vol. 78, pp. 366-372, 2016.

[27] T. Quickenden e J. Irvin, «The Ultraviolet Absorption Spectrum of Liquid Water,» *The Journal of Chemical Physics,* vol. 72, n. 8, pp. 4416-4428, 1980.

[28] Z. Fan, O. Schroder e J. Krahl, «Analysis of Diesel Fuels/Biodiesel Blends and Identification of Biodiesel using Time-Resolved Laser-Induced Fluorescence Spectroscopy (TRLFS),» *Appl. Agric. Forestry Res.,* vol. 65, pp. 1-14, 2015.

[29] E. Arik, H. Altan e O. Esenturk, «Dielectric Properties of Diesel and Gasoline by Terahertz Spectroscopy,» *Millimeter and Terahertz Waves,* vol. 35, pp. 759-769, 2014.

[30] F. Attivissimo, C. C. Carducci, A. Lanzolla, A. Massaro e M. Vadrucci, «A Portable Optical Sensor for Sea Quality Monitoring,» *IEEE Sensors Journal,* vol. 15, n. 1, pp. 146-153, 2015.

[31] J. Milpied, M. Uhrich, B. Patissier e L. Bernasconi, «Application of Turning Fork Resonators for Engine Oil, Fuel, Biodiesel and Urea Quality Monitoring,» *SAE International Journal of Fuels and Lubrificants,* vol. 2, n. 2, pp. 45-53, 2010.

[32] J. Curcio e C. Petty, «The Near Infrared Absorption Spectrum of Liquid Water,» *JOSA,* vol. 41, pp. 302-304, 1951.

[33] M. Anderson, «Determination of Infrared Optical Constants for Single Component Hydrocarbon Fuel,» 2000.

[34] C. D. Carvalho, A. Barros, M. Lopes, F. Silva, E. Santana e F. Sinfronio, «Determination of the Composition of Biodiesel/Diesel Blends using the Dielectric Constant,» *Instrumentation Science & Technology,* vol. 44, pp. 377-385, 2016.

[35] N. Ahmadian, S. Hasan e O. Calla, «Permittivity and Backscattering Coefficient of Diesel Oil Contaminated Soil at C-Band (5.3GHz),» *International Journal of Microwave Science and Technology,* pp. 1-9, 2013.

[36] A. Sen, V. Anicich e T. Arakelian, «Dielectric Constant of Liquid Alkanes and Hydrocarbon Mixtures,» *Journal of Physics D: Applied Physics,* vol. 25, pp. 516-521, 1992.

[37] D. Rodrigues, H. Peres e W. Becari, «Ethanol Fuel Analysis by Time Domain Reflectometry,» in *Microwave & Optoelectronics Conference*, 2013.

[38] A. Cataldo, L. Tarricone, M. Vallone, F. Attivissimo e A. Trotta, «Uncertaintly Estimation in Simultaneous Measuremetns of Levels and Permittivities of Liquids using TDR Technique,» *IEEE Transactions on Instrumentation and Measurement,* vol. 57, n. 3, pp. 454-466, 2008.

[39] G. Ruvio, M. Vaselli, V. Lopresto, R. Pinto, L. Farina e M. Cavagnaro, «Comparison of different Methods for Dielectric Properties Measurements in Liquid Sample Media,» *International Journal of RF and Microwave Computer Aided Engineering,* vol. 28, pp. 1-20, 2018.

[40] M. Venkatesh e G. Raghavan, «An Overview of Dielectric Properties Measuring Techniques,» *Canadian Biosystems Engineering ,* vol. 47, pp. 15-30, 2005.

[41] S. Severo e A. D. Salles, «Non-Resonant Permittivity Measurement Methods,» *Journal of Microwave, Optoelectronics and Electromagnetic Applications,* vol. 16, n. 1, pp. 297-311, 2017.

[42] M. Klemm, J. Leenderetz, D. Gibbins, I. Craddock, A. Preece e R. Benjamin, «Microwave Radar-based Breast Cancer Detection: imaging in Inhomogeneous Breast Phantoms,» *IEEE Antennas and Wireless Propagation Letters,* vol. 8, pp. 1349-1352, 2009.

[43] E. Njoku e D. Entekhabi, «Passive Microwave Remote Sensing of Soil Moisture,» *Journal of Hydrology,* vol. 184, pp. 101-129, 1996.

[44] F. Adamo, G. Andria, O. Bottiglieri, F. Cotecchia, A. D. Nisio, D. Miccoli, F. Sollecito, M. Spadavecchia, F. Todari, A. Trotta e C. Vitone, «GeoLab, a Measurement System for the Geotechnical Characterization of Polluted Submarine Sediments,» *Measurement,* vol. 127, pp. 335-347, 2018.

[45] L. Yee, N. Hau, C. Kuan, P. Nan, L. Sheng e L. Hock, «Modelling of Microwave Elliptical and Conical Tip Sensors for in vivo Dielectric Measurements,» in *IEEE International RF and Microwave Conference (RFM)*, Kuching, 2015.

[46] G. Andria, F. Attivissimo, A. D. Nisio, A. Lanzolla, A. Maiorana, M. Mangiantini e M. Spadavecchia, «Dosimetric Characterization and Image Quality Assessment in Breast Tomosynthesis,» *IEEE Transactions on Instrumentation and Measurement,* vol. 66, n. 10, pp. 2535-2544, 2017.

[47] G. Andria, F. Attivissimo, G. Guglielmi, A. Lanzolla, A. Maiorana e M. Mangiatini, «Towards Patient Dose Optimization in Digital Radiography,» *Measurement,* vol. 79, pp. 331-338, 2016.

[48] A. Gregory e R. Clarke, «Dielectric Metrology with Coaxial Sensors,» *Measurement Science and Technology,* vol. 18, pp. 1372-1386, 2007.

[49] A. Cataldo, E. D. Benedetto, G. Cannazza, A. Masciullo, N. Giaquinto, G. D'Aucelli, N. Costantino, A. D. Leo e M. Miraglia, «Recent Advances in the TDR based Leak Detection System for Pipeline Inspection,» *Measurement,* vol. 98, pp. 347-354, 2017.

[50] J. Choi, F. Iza, H. Do, J. Lee e M. Cho, «Microwave Excited Atmospheric Pressure Microplasmas based on a Coaxial Transmission Line Resonator,» *IOP Publishing, Plasma Sources Sci. Technol.,* vol. 18, pp. 1-8, 2009.

[51] S. Ahmad, M. Charlse, D. Allal, P. Negi e V. Ojha, «Realization of 2.4 mm Coaxial Microcalorimeter System as National Standard of Microwave Power from 1 MHz to 50 GHz,» *Measurement,* vol. 116, pp. 106-113, 2018.

[52] A. Cataldo, E. D. Benedetto, G. Cannazza, E. Piuzzi e N. Giaquinto, «Embedded TDR Wire like Sensing Elements for Monitoring Applications,» *Measurement,* vol. 68, pp. 236-245, 2015.

[53] J. Sheen, W. Mao e W. Liu, «Study of Measurements Techniques of Microwave Dielectric Properties,» in *National Telecommunications Seminar* , 2009.

[54] G. Kitic e V. Crnojevic-Bengin, «A Sensor for the Measurement of the Moisture of Undisturbed Soil Samples,» *Sensors,* pp. 1693-1705, 2013.

[55] X. Li, *Design of a Cylindrical Cavity Resonator for Measurements of Electrical Properties of Dielectric Materials,* University of Gavle: Master Thesis in Electronics/Telecommunication, 2010.

[56] G. Gennarelli, S. Romeo, M. Scarfi e F. Soldovieri, «A Microwave Resonant Sensor for Concentration Measurements of Liquid Solutions,» *IEEE Sensors Journal,* vol. 13, n. 5, pp. 1857-1864, 2013.

[57] A. Mason, J. Goh, O. Korostynska, A. Al-Shamma'a, M. Field e P. Browing, «Real-Time Monitoring of Bodily Fluids using a Novel Electromagnetic Wave Sensor,» *Journal of Public Health Frontier,* vol. 2, pp. 201-206, 2013.

[58] W. W. Wenxuan, C. Aixin e J. Tiehua, «Design and Analysis of the Coaxial-fed Cavity-backed Annular Slot Antenna,» *IEEE,* pp. 528-531, 2008.

[59] H. Hamzah, A. Abduljabar, J. Lee e A. Porch, «A Compact Microwave Microfluidic Sensor using a Re-Entrant Cavity,» *Sensors,* pp. 1-12, 2018.

[60] Z. Wei, J. Huang, J. Li, G. Xu, Z. Ju, X. Liu e X. Ni, «A High-Sensitivity Microfluidic Sensor Based on a Substrate Integrated Waveguide Re-Entrant Cavity for Complex Permittivity Measurement of Liquids,» *Sensors,* pp. 1-17, 2018.

[61] M. Feulner, G. Hagen, A. Muller, D. Bruggermann e R. Moss, «In-Operation Monitoring of the Soot Load of Diesel Particulate Filteres with a Microwave Method,» *Topics in Catalysis,* vol. 56, pp. 483-488, 2013.

[62] X. Hao, L. Weijun e G. Qiulai, «A New Dual-Channel Measurement Method for Accurate Characterization of Low-Permittivity and Low-Loss Materials,» *IEEE Transactions on Instrumentation and Measurement,* pp. 1-10, 2018.

[63] A. Phungasem, K. Nuanyai, N. Puangngernmak e S. Chalermwisutkul, «Implementation of a Mobile Device for Complex Permittivity Measurement of Liquid based on Microwave Resonant Method,» *IEEE,* pp. 412-416, 2014.

[64] J. Obrzut, «General Analysis of Microwave Network Scattering Parameters for Characterization of Thin Film Materials,» *Measurement,* vol. 46, pp. 2963-2970, 2013.

[65] A. Aboutaleb, G. Chi-Tangyie, K. Huddersman e C. Oxley, «Microwave Dielectric Measurements of Fibrous Catalyst using Transmission Line Technique in the Frequency RAnge of 1-4 GHz,» *Microwave and Optical Technology ,* vol. 56, pp. 2671-2676, 2014.

[66] R. Ismail, H. Al-Mattarneh, M. Nuruddin, N. Shafiq e M. Dahim, «Dielectric Dispersion Characteristics of Unsaturated Sand Contaminated by Diesel,» *Journal of Material Sciences & Engineering,* pp. 1-6, 2017.

[67] S. Zeng, A. Trontz, W. Zhu, H. Xiao e J. Dong, «A Metal-Ceramic Coaxial Cable Fabry-Perot Microwave Interferometer for Monitoring Fluid Dielectric Constant,» *Sensors and Actuators,* pp. 1-7, 2017.

[68] *SPECIFICATIONS PXIe-5632 8.5 GHz Vector Network Analyze,* National Instruments, 2018.

[69] *Understanding VNA Calibration,* Anritsu Company, 2012.

[70] V. Komarov, S. Wang e J. Tang, «Permittivity and Measurements,» *Encyclopedia of RF and Microwave Engineering,* 2005.

[71] *Dielectric Theory - Basic of Measuring the Dielectric Properties of Materials,* Keysight Technologies.

[72] J. Wang e T. Schmugge, «An Empirical Model for the Complex Dielectric Permittivity of Soils as a Function of Water Content,» *IEEE Transactions on Geoscience and Remote Sensing,* vol. 18, n. 4, pp. 288-295, 1980.

[73] M. Pereira e C. Pereira, «Computational Method for Calculating the Effective Permittivity of Complex Mixtures,» *Journal of Microwave Power and Electromagnetic Energy,* vol. 49, n. 2, pp. 85-99, 2016.

[74] C. Park, A. Behrendt, E. LeDrew e V. Wulfmeyer, «New Approach for Calculating the Effective Dielectric Constant of the Moist Soil for Microwaves,» *Remote Sensing,* pp. 1-30, 2017.

[75] M. Brown, «Dielectrics,» *Encyclopedia of Physics, Springer,* vol. 17, 1956.

[76] M. Ansoult, L. D. Backer e M. Declercq, «Statistical Relationship between Apparent Dielectric Constant and Water Content in Porous Media,» *Soil Sci. Soc. Am. J.,* vol. 49, pp. 47-50, 1984.

[77] M. Dobson, F. Ulaby, M. Hallikainen e M. Elrayes, «Microwave Dielectric Behavior of Wet Soil. Dielectric Mixing Models,» *IEEE Trans. Geosci. Remote Sens.,* vol. 23, pp. 35-46, 1985.

[78] K. Karkkainen, A. Sihvola e K. Nikoskinen, «Effective Permittivity of Mixture: Numerical Validation by the FDTD Method,» *IEEE Transactions on Geoscience and Remote Sensing,* vol. 38, n. 3, pp. 1303-1308, 2000.

[79] C. Bottcher, Theory of Electric Polarization, Amsterdam: Elsevier, 1952.

[80] O. Wiener, *LeipzigerBerichte,* vol. 62, 1910.

[81] C. Pearce, «The Permittivity of Two-Phase Mixture,» *Brit. J. Appl. Phys.,* vol. 6, pp. 358-361, 1955.

[82] J. Birchak, C. Gardner, J. Hipp e J. Victor, «High Dielectric Constant Microwave Probes for Sensing Soil Moisture,» *Proc. IEEE,* vol. 62, pp. 93-98, 1974.

[83] K. Wagner, «Explanation of the Dielectric After-Effects based on Maxwell's Idea,» *Arch. Elektrochem.,* vol. 3, pp. 371-387, 1914.

[84] D. Bruggeman, «Berechnung Verschiedener Physikallischer Konstanten von Heterogenen Substanzen,» *Ann. Phys. (Leipzig),* vol. 100, pp. 199-212, 1935.

[85] M. Khardly e W. Jackson, «Properties of Artificial Dielectrics Comprising Arrays of Conducting Elements,» *Proc. Inst. Elec. Eng.,* vol. 1953, pp. 199-212, 100.

[86] S. Nerping e A. Chudnovskii, «Physics of the Soil,» in *Israel Program for Scientific Translations*, Jerusalem, 1970.

[87] L. Rayleigh, «On the Influences of Obstacles Arranged in Rectangular Order on the Properties of a Medium,» *Phil. Mag.,* vol. 34, pp. 481-502, 1892.

[88] W. Rothwell, «Complex Permittivity of Conductor-Dielectric Mixtures,» *IEEE Trans. Microwave Theory Tech.,* vol. 19, pp. 413-414, 1971.

[89] G. Poe, A. Stogryn e A. Edgerton, *Determination of Soil Moisture Content using Microwave Radiometry,* Microwave Div., El Monte: Final Rep. 1648FR-1, DOC Contract 0-35239, Aerojet General Corp., 1971.

[90] F. Attivissimo, A. D. Nisio, G. D'aucelli, S. Camporeale e P. Pappalardi, «Design of a Microwave Sensor for Fuel Quality Monitoring,» in *IEEE Interntational Workshop on Metrology for Aerospace*, Rome, 2018.

[91] G. Andria, F. Attivissimo, A. d. Nisio, A. Trotta, S. Camporeale e P. Pappalardi, «Design of a Microwave Sensor for Measurement of Water in Fuel Contamination,» *Measurement,* vol. 136, pp. 74-81, 2019.

[92] A. D. Nisio, T. D. Noia, C. Carducci e M. Spadavecchia, «High Dynamic Range Power Consumption Measurement in Microcontroller-Based Applications,» *IEEE Transactions on Instrumentation and Measurement,* vol. 65, n. 9, pp. 1986-1976, 2016.

[93] HUBBER+SUHNER, *RF CONNECTOR GUIDE. Understanding Connector Technology,* 2007.

[94] M. Ashby, Materials Selection in Mechanical Design, Butterworth-Heinemann, 1999.

[95] B. Liu, F. Zhang, D. Li e J. Yang, «Research on the Influence of Excitation Frequency on the Sensitivity in Metal Debris Detection with Inductor Sensor,» *Advances in Mechanical Engineering,* 2014.

[96] R. Jia, B. Ma, C. Zheng, L. Wang, Q. Du e K. Wang, «Improvement of Sensitivity and Detectability of the Three-Coil Wear Debris Detection Sensor using LC Resonance Method and Modified Lock-In Amplifier,» *Preprints,* 2017.

[97] H. Jiang, P. Gao e W. Zhao, «Simulation Research on Detection Sensor of Metal Wear Particle in Oil Fluid,» in *International Conference on Electrical, Mechanical and Industrial Engineering* , 2016.

[98] R. Jia, B. Ma, C. Zheng, L. Wang, X. Ba, Q. Du e K. Wang, «Magnetic Properties of Ferromagnetic Particles under Alternating Magnetic Fields: Focus on Particle Detection Sensor Applications,» *Sensors,* vol. 18, pp. 1-17, 2018.

[99] Z. Yunbo e G. Yuhai, «Research of the On-Line System for Detecting Metal Particles in Oil,» in *IEEE International Conference on Electronic Measurement & Instruments (ICEMI)*, 2017.

[100] C. Li, J. Peng e M. Liang, «Enhancement of the Wear Particle Monitoring Capability of Oil Debris Sensors Using a Maximal Overlap Discrete Wavelet Transform with Optimal Decomposition Depth,» *Sensors,* pp. 6207-6228, 2014.

La borsa di dottorato è stata cofinanziata con risorse del
Programma Operativo Nazionale Ricerca e Innovazione 2014-2020 (CCI 2014IT16M2OP005),
Fondo Sociale Europeo, Azione I.1 “Dottorati Innovativi con caratterizzazione Industriale”

UNIONE EUROPEA
Fondo Sociale Europeo